



SAPIENZA
UNIVERSITÀ DI ROMA

Facoltà di Scienze Matematiche Fisiche e Naturali
Dipartimento di Chimica

Dottorato in Scienze Chimiche XXIX ciclo

Studio di Miscele Multicomponente di Liquidi Ionici e Composti Molecolari

Study on multicomponent mixtures of Ionic Liquids and Molecular Compounds

Candidato
Alessandro Mariani

Relatore
Prof. Ruggero Caminiti

*This is a story about magic and where it goes and,
perhaps more importantly, where it comes from and why,
although it doesn't pretend to answer all or any of these questions.
It may, however, help to explain why Gandalf never got married and why Merlin was a man.
Because this is also a story about sex, although probably not in the athletic, tumbling,
count-the-legs-and-divide-by-two sense unless the characters get totally beyond the author's
control. They might.*

(Sir Terry Pratchett)

Index

*The universe was full of ignorance all around
and the scientist panned through it
like a prospector crouched over a mountain stream,
looking for the gold of knowledge among the gravel of unreason,
the sand of uncertainty
and the little whiskery eight-legged swimming things of superstition.
("Witches Abroad" – Sir Terry Pratchett)*

Introduction	
A brief history	I
Genesis	I
First Generation Ionic Liquids	3
Second Generation Ionic Liquids	4
Third Generation Ionic Liquids	5
Fourth Generation Ionic Liquids	6
Classification	6
Aprotic Ionic Liquids	7
Protic Ionic Liquids	7
Remarkable Properties Overview	8
Brief applications overview	11
Mixtures	13
Aim of the project	14
References	14
Chapter I: Techniques	
X-ray Diffraction	17
Principles	17
In home Instrument	21
Synchrotron Radiation	23
Molecular Dynamics simulations	25
Definition	25
Critical Issues	29
Effect of Dielectric Constant	30
NMR DOSY	32
Principles	32

Redlich-Kister fitting	34
References	35
Chapter II: Ionic Liquids Structure	
Nanoscale segregation	36
Ionic Liquids used	38
Ethylammonium Nitrate	38
Propyl/Butyl-ammonium Nitrate	43
Effect of Pressure	47
Contextualization	52
Summary	53
References	55
Chapter III: Homogenous Binary Systems	
From Neat Compounds to Mixtures	59
Similia Similibus Solventur	61
Results	62
EAN+DMSO	62
EAN+Ethylene Glycol	69
EAN+2-Amino-1-Ethanol	78
EAN+2-Methoxy-1-Ethanol	84
Contextualization	90
Summary	92
References	93
Chapter IV: Unusual Binary Systems	
Micelles, clusters, or...?	98
Janus Compounds	99
EAN+methanol	99
EAN+acetonitrile	109
Symmetric Compounds	121
EAN+1,2-dimethoxy ethane and EAN+1,4-diaminobutane	121
Contextualization	129
Summary	132
References	132
Chapter V: Conclusions	
Final considerations	136
Appendix A: Materials	143

Introduction



*“We are trying to unravel the Mighty Infinite
using a language which was designed to tell one another
where the fresh fruit was.”
(Sir Terry Pratchett)*

I. A brief history

I.1. Genesis

Ionic Liquids (henceforth referred in this manuscript as ILs) are likely one of the hottest topics in modern chemistry, as this is a fast growing field¹⁻¹¹. The main reason is, perhaps, their astounding flexibility in term of chemical and physical properties¹². The very origin of the Ionic Liquids history cannot be straightforwardly placed. The greatest trick is that the term “ionic liquid” as we intend it has been used for years with a series of different meaning. “Ionic Liquids” were the slags in metallurgy, the molten inorganic salts, the “low melting” alkali halide eutectic mixtures (LiCl-KCl, m.p. 355 °C), and the liquid clathrates used for coal liquefaction. We can say that the first documented (unrecognized) observation of a properly said Ionic Liquid was the Lewis acid obtained as side-product of the Friedel-Crafts reaction: the “Red Oil” (1877)¹³. At that time there was no way to determine what that substance was, and only when NMR became a routine the Red Oil was confirmed to be the theorized stable intermediate of the Friedel-Craft reactions named “Sigma complex”. For an AlCl₃ catalysed reaction, the Sigma complex has the structure

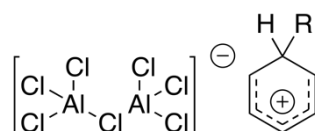


Figure a. Sigma complex from a Friedel-Crafts reaction, also known as “Red Oil”. The first synthesized Ionic Liquid.

that is with no doubt a salt in the liquid state at room temperature: here it was the first Ionic Liquid. Nevertheless, generally the dawn on ILs is considered to be 1888, when S. Gabriel and J. Weiner publish the paper “Ueber einige Abkömmlinge des Propylamins”¹⁴ or “On some derivatives of Propylamine”. In that pioneering work they reported the synthesis of Ethanolammonium Nitrate (EOAN), a salt

AlCl_3 -1-ethylpyridinium bromide will result in a liquid form at room temperature. That eutectic mixture can be used for the electrodeposition of Aluminium. This was the first milestone: Aluminium Chloride-based ILs will be heavily studied and used for the following decades filling the pages of almost every scientific journal. Now I will discuss the progress of ILs in terms of “Generations”. This approach is not linear with time (e.g. EAN -1914- is a third generation Ionic Liquid while AlCl_3 -1-ethylpyridinium bromide -1948- is a first generation one) but it can give a hint of the evolution of such compounds and how scientists systematically try to solve the intrinsic problems of a specific Ionic Liquid.

1.II. First Generation Ionic Liquids

John S. Wilkes is, without any doubt, the most important character in first generation ILs movie^{2,19}. In the 1960-1980 period the main challenge was to find a suitable molten electrolyte to be used in batteries. Until then they used cryolite (Na_3AlF_6) which has a m.p. of 1009 °C or the “low melting” (355 °C) eutectic mixture LiCl-KCl ¹. Obviously such temperatures were the cause of several issues like high energy required to reach the working temperature, find suitable materials to build the batteries that can afford such temperatures for long time, and the battery had to be almost completely isolated from the rest of the apparatus to prevent liquefactions, ignitions and any other temperature-related damage. Levin *et al.*²⁰ suggested the use of some Chloroaluminate compounds which were known to have low melting points. The first attempts were really promising (NaCl-AlCl_3 mixture has a m.p. of 175 °C) but they were still far from the nowadays definition of ionic liquid. To further lower the melting point of the substance Osteryoung proposes to use large organic, asymmetrical cations to prevent molecular packing²¹. So in 1978 the properly said ionic liquid 1-butylpyridinium chloride – aluminium chloride (BPC-AlCl_3) was developed. This is the birth date of the modern era R&D on ILs. So we are now at the point that we have a salt that is liquid at ambient conditions. Shamefully BPC-AlCl_3 1:1 mixture (*i.e.* the one that has the highest conductivity) melts at 40 °C, moreover when the molar fraction of AlCl_3 is less than 0.5 (*i.e.* basic conditions required to be a better electrolyte for batteries) the cation is easily reduced. The next challenge was, therefore, to find a better cation. A series of chemicals was produced with this logic.

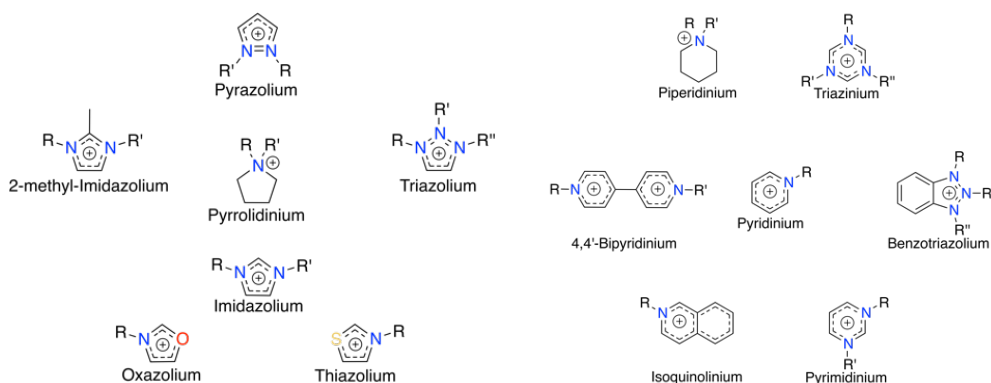


Figure c. Common cyclic cations in ionic liquids

The most promising cations were the ones of the dialkyl imidazolium family. In particular, 1-ethyl-3-methyl-imidazolium (C_2mim^+) - $AlCl_3$ is liquid in a large region of $AlCl_3$ molar fraction (0.33-0.66, thus including the high-conductive 0.5 and the basic $pH < 0.5$), and it has a reduction potential 0.9 V lower than the BPC- $AlCl_3$ ²². The best of the first generation was therefore reached in 1986, and its legacy is: large, asymmetric, charge-dispersed organic cations are the best choice to obtain a room temperature, electrochemically stable liquid salt.

I.III. Second Generation Ionic Liquids

A major drawback of chloroaluminate ILs is their extreme reactivity with oxygen and water. Moreover, the side-product of the reaction with water is HCl, not the friendliest waste you could wish. This is not a problem inside a battery, because they are sealed and no external agents may interact with the electrolyte, but it is a severe limitation in potential applications. In the early 1990s M. Zaworotko had the idea to develop some air/water stable ILs, by eliminating the chloroaluminate portion and substituting it with some inorganic anions chosen to be inert with moisture²³. Anions like $[SO_3CF_3]^-$, $[N(SO_2CF_3)_2]^-$ and the halides were taken into account to achieve open air stability along with all the advantages from the generation one ILs.

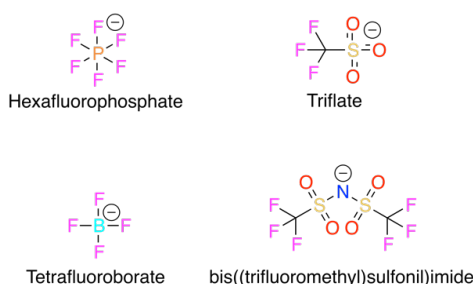


Figure d. Common fluorinated anions in ionic liquids

The great results obtained with the new chemicals gave start to a massive and enthusiastic run in ionic liquid research, and a real “golden age” for these compounds starts at the end of the century.

I.IV. Third Generation Ionic Liquids

Until now, all the research efforts on ionic liquids were focused on halogen-derivate. Of course Group VII elements are the most reliable choice when net charges need to be taken into account, but the charge stability comes with a price: environmental and animal toxicity is a major drawback of halogen-based compounds. In the last two decades the tendency of both research and industry was of find sustainable alternatives to the well-established but polluting processes and chemicals. To achieve this goal, the first years of the XXI century marked the starting of the ionic liquids golden age. Their impressive flexibility in chemical and physical properties design them as the perfect candidate to replace common organic solvents. Avoiding halogen-based anions and starting to use NO_3^- , $\text{H}_x\text{SO}_4^{(2-x)-}$, SO_3CH_3^- , HCO_2^- , $\text{CH}_3(\text{CH}_2)_x\text{CO}_2^-$, and so on. The cations used are still mainly of the family of dialkylimidazolium or quaternary ammonium/phosphonium. The enthusiasm for the new development was really outstanding: from 2000 to 2014 there was an exponential growth of the research in the ionic liquid field, passing from about 1k publications/year to over 6k publications/year. We are, anyway, still far from the “green” achievement.

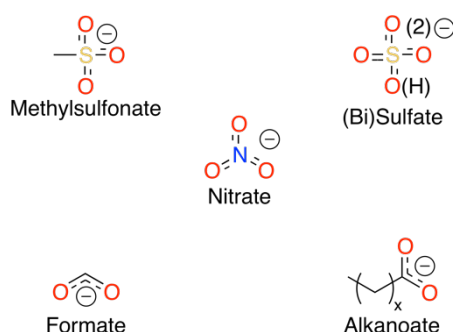


Figure e. Non fluorinated anions in ionic liquids

I.V. Fourth Generation Ionic Liquids

Finally, in the last few years, we are assisting to the developing of a biocompatible family of ionic liquids based on choline as a cation and an amino acid as anion.

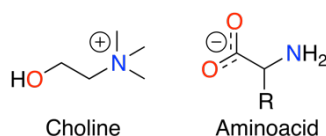


Figure f. Schematic representation of a fourth generation ionic liquid based on bio-molecules

They seem to be great alternatives to the treatment of the biomasses, cellulose extraction and even battery electrolyte. Just few work are around for now, because of the initial difficulties to find a suitable ionic pair to satisfy some fundamental characteristic such as low viscosity, thermal stability and, hopefully, low hygroscopicity. Looking closely to the ionic liquid evolution, it is possible to find traces of society evolution as well. Generation one ILs was simply designed to obtain a room temperature liquid salt, generation two started to think to find a way to make them stable to avoid waste and find new applications, generation three is the answer to environmental problems trying to have the less impact possible, generation four want to be the solution to most of the chemistry problems presenting itself as the “greener” alternative to almost any organic compound.

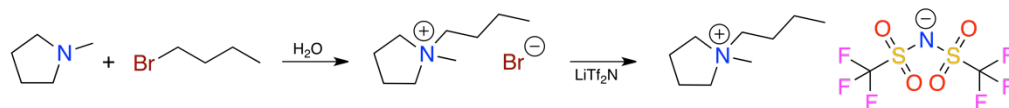
II. Classification

Amongst all the possible combination of cations and anions that leads to “salts with melting point below 100 °C”, it is possible to individuate two main classes and a number of sub-classes. They differ notably by certain point of view²⁴. The belonging to one of the main two classes is established by the origin of the ionicity of the compound. If the ions are generated by proton transfer from a Brønsted acid to a Brønsted base, so the resulting ionic liquid is a protic one. As a consequence, protic ionic liquids show the presence of one or more hydrogen atoms bonded to an electronegative atom (O or N in most cases), capable to establish extended hydrogen bonded networks.

II.1. *Aprotic Ionic Liquids*

Historically, this is the class that firstly was developed and studied. Even the first ever IL, the “Red Oil”, belongs to this family. Almost all the first and second generations ILs belongs to this class. Their precursors are mainly nitrogen-based heterocyclic compounds both aromatic or not. Imidazole is probably the most

used substrate for aprotic ionic liquids synthesis. Other widely used compounds are listed in Figure c. Their synthesis is generally relatively simple, as reported in scheme a.



Scheme a. Synthesis of an aprotic ionic liquid

II.II. Protic Ionic Liquids

Ethanolammonium Nitrate and Ethylammonium Nitrate both belong to this family. Their ability to set an extended 3D hydrogen bonded network give rise to a series of interesting properties. Moreover, they are the ideal probe to find which water property is due to hydrogen bonds and which not, because while they share a morphologically similar hydrogen bond network with water, they differ from almost every other aspects. Ammonium salts are the most representative exponents of this family, but phosphonium, sulfonium and, recently, selenonium cations can be find in literature.

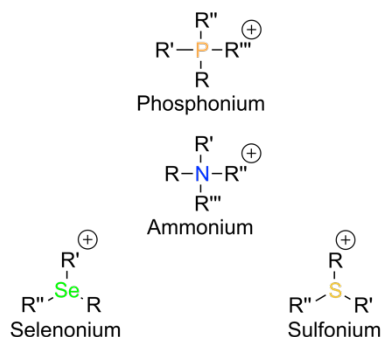
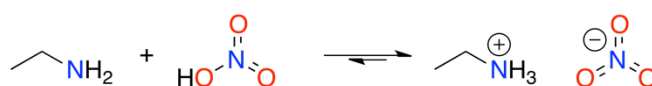


Figure g. Cations used in protic ionic liquids

Protic ILs are somewhat less stable than the aprotic ones, because their synthesis is the neutralization of a Brønsted acid and a Brønsted base (scheme b).



Scheme b. Synthesis of a protic ionic liquid

This straightforward, trivial reaction is an equilibrium one, thus heating a protic ionic liquid may lead reverse the reaction obtaining the parent compounds. This is not as bad as one may think, because one can use this property to own

advantage. In fact, while most ionic liquid has almost zero vapour pressure, its precursors have generally a low boiling points, thus enabling to distil the IL that is then resynthesized.

III. Remarkable Properties Overview

The success of ionic liquids is strongly linked to their tunable physical and chemical properties^{3,10,25,26}. Changing one of the two ions has a dramatic effect on the resulting compound. Table a shows some examples.

Cation	Anion	m.p. [°C]	Density [g/ml]	Viscosity [cP]
Na	Cl	808	1.547*	1.38*
	I	662	2.722*	1.45*
	BF₄	384	2.47*	--
	Tf₂N	257-258	--	--
	NO₃	310	1.898*	2.86*
	PF₆	200	2.369*	--
C₂mim	Cl	82-87	1.11*	62
	I	80	--	--
	BF₄	6	--	31.76
	Tf₂N	-3	1.5178	32.022
	NO₃	38	--	--
	PF₆	58-68	--	--
C₄mim	Cl	77-79	--	142*
	I	-58	1.49	1110
	BF₄	-81	1.19	219
	Tf₂N	-4	1.4342	51.223
	NO₃	36	1.1565*	165.27*
	PF₆	-6	1.37	450
C₂NH₃	Cl	107-108	1.22*	--
	I	193	--	--
	BF₄	152.4	--	--
	NO₃	13	1.216	32
C₄NH₃	BF₄	198.2	--	--
	NO₃	<15	1.10152	89.954

Table a. Melting points, densities and viscosities for some ionic liquids. * means data collected at melting point. All data were taken from NIST Ionic Liquids Database²⁷

As may be noticed, the more the ions are bulky the lower are the melting point and the viscosity, albeit it is not always true. The appeal of ionic liquids thus arises from:

- **Low melting points.** This is a truism coming from the very definition of ionic liquid. Nevertheless, it is probably the main cause of the success of these compounds. The possibility to have a molten salt at/near/below room temperature leads to a series of applications that will be discussed in section IV. As may be noticed in table a., changes in the structure have a dramatic effect on melting points.
- **Thermal stability.** Some aprotic ionic liquids are not decomposed by temperature up to $\sim 450\text{ }^{\circ}\text{C}$. The upper limit is settled by the carbon-heteroatom bond strength, which is of the order of 300 kJ mol^{-1} . On the other hand, protic ionic liquids are somewhat less stable, forming back the parent compounds upon warming over $\sim 100\text{ }^{\circ}\text{C}$.
- **Low vapour pressure.** Strong Coulombic forces between ions, prevents the vaporization of these compounds. As an example, Ethylammonium Nitrate has a vapour pressure of $\sim 1\text{ Pa}$ at $650\text{ }^{\circ}\text{C}$.
- **Wide electrochemical window.** It is defined as the range of potential within which a substance does not undergo either oxidation or reduction. Water has an electrochemical window of only 1.2 V , 1-butyl-3-methylimidazolium hexafluorophosphate 4.15 V with respect to a Pt electrode, 1-ethyl-3-methylimidazolium tetrafluoroborate and 1-butyl-1-methylpyrrolidinium bis(trifluoromethyl sulfonyl)imide of 4.10 V and 5.5 V respectively, compared to a glassy carbon electrode. Such wide electrochemical window allows the electrodeposition of metals and semiconductors at room temperature.
- **Density.** ILs are generally denser than water, with a value range spanning from ~ 1 to $\sim 1.6\text{ g ml}^{-1}$. The density is strongly dependent from cation alkyl chain length.
- **High conductivity.** As made up by free ions, they have good conductivity values, often exceeding 10 mS cm^{-1} . Even higher values can be achieved on dilution, because of the consequent viscosity drop.

- **Environmental stability.** From generation two on, ILs are almost inert in regard to air moisture and water. Nevertheless, in most cases they are hygroscopic, then one must carefully dry them before any use.
- **(Generally) low toxicity.** This aspect of ionic liquids is still a matter of discussion²⁸. We often speak of “green” ionic liquids referring only to the low volatility, implying that all the risks linked to the inhalation are avoided. However, we rarely mention their properly said toxicity. Many of them, being soluble in water, could come in contact with natural aqueous environments. Ecotoxicity studies have been made by Maginn²⁹ to determine the value of LC_{50} (lethal concentration expressed in mg/L) of two ionic liquids on *Daphnia Magna*, a cold water crustacean. The results, summarized in table b, show that both liquids are toxic almost like benzene, less than ammonia and phenol, but more toxic than acetone. Another study, done by W. Gouveia et al.³⁰ studied the toxicity of ILs composed by imidazolium, pyridinium and choline cations, with bromide and several amino-acids as anions. This study was carried out on the crustacean *Artemia Salina* (Artemiidae), component of the fauna of saline aquatic and marine ecosystems. It has been used in laboratory bio-assays to determine toxicity through the estimation of the medium lethal concentration (LC_{50}). In table b the relative (LC_{50}) values are shown. It can be seen that a marked difference appears when both the cation and the anion are derived only from biomaterials (choline and amino acids, [Ch][AA]). In those compounds the toxicity can be two orders of magnitude lower than that of the imidazolium and pyridinium based ILs: the LC_{50} of [Ch][Ala] is only 9.001 mg/L, while the one of [C₄mim][Ala] is 0.114 mg/L.

Substance	LC₅₀ [mg/l]	Reference
Acetone	30642	21
Toluene	60-313	21
Benzene	203	21
Chlorobenzene	5-86	21
Phenol	5.01	21
Ammonia	0.53	21
Chlorine	0.028	21
C₄mim PF₆	250-300	21
C₄mim BF₄	225-275	21
C₄mim Br	0.092	22
C₄mim Ala	0.114	22
C₄py Br	0.117	22
C₆py Br	0.086	22
Ch Ala	9.001	22
Ch Arg	2.896	22
Ch Cys	5.437	22
Ch Gln	6.468	22
Ch Glu	6.278	22

Table b. Toxicity of some ionic liquids

IV. Brief applications overview

Considering an estimated number of $\sim 10^{18}$ possible different ionic liquids³¹, it is simple to understand that probably there is the perfect ionic liquid for any purpose. By now, only about $1000/10^{18}$ have been studied and characterized. There is a long way. Often ILs are called “Task Specific”^{12,32}, thus indicating their flexibility and general purpose. It would take hundreds of pages to systematically present and discuss every application of such compounds^{5,10,24,33–35}, here will be reported some of them.

- **As a solvent.** Ionic liquids dissolve various organic materials, inorganic and organometallic compounds. They are able to dissolve salts, fats, proteins, polysaccharides, plastics, DNA and surfactants. This means that they can substitute the majority of volatile organic solvents for the organic and organometallic synthesis³². They also can be used in the liquid-liquid extraction. Some examples: extraction of aromatic molecules from water

or alkanes, or of alcohols from alkanes and or of butanol from aqueous fermentation broth³⁶.

- **As a medium for metals electrodeposition.** Electrochemical stability, high conductivity and high metal-salts solubility makes ILs the perfect candidates to perform electrodeposition. Moreover, all the water/metal chemistry is avoided through this route. Outstanding results are achieved for Ag, Cu, Zn/Sn, Zn, Cr and Ni deposition on brass using some Choline-based ILs.
- **As a removal agent for heavy metals.** Ionic liquids, pure or in solution, can be used to remove heavy metals. For example, the addition of 1-butyl-3-methylimidazolium hexafluorophosphate to some crown ethers leads to an improvement in the extraction of metal ions from aqueous solutions³⁷. Ionic liquids with imidazolium cation functionalized with urea, thiourea or thioether and anion PF_6^- allow to extract Hg^{2+} , Cd^{2+} or radioactive metals³². Furthermore, the possibility of increasing the hydrophobic character, by adjusting the length of the alkyl chain(s), improves the coefficient of partition between the aqueous solution containing the metal ion and the hydrophobic phase.
- **As a lubricant.** Ionic liquids are used as lubricants due to their high capacity to reduce friction, also on the treated surface they give rise to a protective thin film against wear. For example, treating two surfaces of steel with an alkylimidazolium fluorophosphate, leads to better results than that obtained using liquid paraffin containing 2% (wt/wt) of dialkyl thiophosphate of zinc³⁸.
- **As an electrolyte.** Ionic liquids are used as electrolytes in lithium batteries. For this kind of battery, an aprotic compound with an electrochemical window above the cathodic potential electrochemical Li/Li^+ is needed; the use of ionic liquids has allowed to replace the flammable and volatile organic solvents. For example, it has been demonstrated that the use of LiTf_2N in 1-ethyl-3-methylimidazolium bis(trifluoromethyl sulfonyl)imide allows to have a good performance and a low self-discharge (less than 5% after 2000 h)³⁹. Furthermore, being electrolytes, ILs may be coupled to electrodes of carbon nanotubes. In

fact, the good behaviour of carbon nanotubes with the widest electrochemical window and the low volatility of ionic liquids has suggested a new approach in building of capacitors, batteries and electromechanical actuators. Photoelectrochemical cells incorporating nanotubes and ionic liquids with improved conversion efficiency were also prepared.

- **As a catalyst.** In the context of catalysis, ionic liquids can be used as catalysts, activators and substrates for enzyme-catalysed reactions. ILs offer at the same time the advantages of a homogeneous and heterogeneous catalysis: a suitable IL can, in fact, be immiscible with the reactants and products, but it can dissolve the catalyst. The ionic nature of the IL, in addition, also gives the opportunity to control the chemistry of the reaction, or to participate or stabilize the highly polar or ionic transition state. Some examples: 1-butyl-3-methylimidazolium dicyanamide and 1-ethyl-3-methylimidazolium dicyanamide act as catalysts in acetylation of alcohols⁴⁰. There are also biocompatible microbial biotransformations, e.g. thermolysin is used in ionic liquids to synthesize the Z-aspartame, a precursor of the artificial sugar.

V. Mixtures

If we quantify how much we know on ionic liquids on the basis of the ratio “characterized ILs”/“total ILs”, then we almost know nothing. So many efforts will be needed to achieve a deep knowledge of these multi-faced compounds. To study a system, it should be as pure as possible, so in the beginning, impurities (*in primis* water) were understood to be avoided. Nevertheless, scientists love to make things harder, so the gigantic branch of ILs mixtures was created. As mentioned above, it is highly probable that there is the perfect ionic liquid for almost any purpose, the problem is find the right one. The trial-and-error process is not so convenient when a very large number of options are on the table. An alternative to module finely the ILs properties is to mix them with a co-solvent. This procedure leads to a mixture that shows the properties of both the compounds (by some extent that depends on the relative quantity of each one) and sometimes exhibit new features that were not observable before.

VI. Aim of the project

It should be clear at this point for the reader that the field of Ionic Liquids is in constant evolution, finding always new compounds with interesting and specific properties. Moreover, the binary mixture complication is a stimulating yet complicated variation. In my project I've tried to clarify what happens when an IL is mixed with a molecular liquid. To do this I've used a quantity of different techniques aided by the computational results. Here I will present my results on some systems consisting of ionic liquids and molecular liquids binary mixtures. The compounds were chosen to cover a wide range of different properties, such as polarity, hydrophilicity/hydrophobicity, structural considerations and others. While a consistent part of my work involves Ethylammonium Nitrate, other protic ionic liquids were included to achieve a general point of view.

VII. References

- 1 K. R. Seddon, *J. Chem. Technol. Biotechnol.*, 1997, **50**, 351–356.
- 2 J. S. Wilkes, *Green Chem.*, 2002, **4**, 73–80.
- 3 R. D. Rogers and K. R. Seddon, *Science*, 2003, **302**, 792–3.
- 4 H. Ohno, *Bull. Chem. Soc. Jpn.*, 2006, **79**, 1665–1680.
- 5 N. V. Plechkova and K. R. Seddon, *Chem. Soc. Rev.*, 2008, **37**, 123–50.
- 6 H. Weingärtner, *Angew. Chem. Int. Ed. Engl.*, 2008, **47**, 654–70.
- 7 C. A. Angell, *From Slags to Molten Salts to Ionic Liquids: a 50 year joyride*, 2010, vol. 33.
- 8 E. W. Castner and J. F. Wishart, *J. Chem. Phys.*, 2010, **132**, 120901.
- 9 J. Dupont, *Acc. Chem. Res.*, 2011, **44**, 1223–31.
- 10 T. Greaves and C. J. Drummond, *Chem. Rev.*, 2015, **115**, 11379–11448.
- 11 K. Dong, S. Zhang and J. Wang, *Chem. Commun.*, 2016, **52**, 6744–6764.
- 12 C. Yue, D. Fang, L. Liu and T.-F. Yi, *J. Mol. Liq.*, 2011, **163**, 99–121.

- 13 C. Friedel and J. M. Crafts, *Comptes Rendus*, 1877.
- 14 S. Gabriel and J. Weiner, *Berichte der Dtsch. Chem. Gesellschaft*, 1888, **21**, 2669–2679.
- 15 T. L. Greaves, A. Weerawardena, C. Fong, I. Krodziewska and C. J. Drummond, *J. Phys. Chem. B*, 2006, **110**, 22479–22487.
- 16 P. Walden, *Bull. Acad. Imper. Sci St. Petersburg*, 1914, **8**, 405–422.
- 17 C. Greanacher, *Pat. number 1943176*, 1934.
- 18 F. H. Hurley and T. P. Wier, *J. Electrochem. Soc.*, 1951, **98**, 207.
- 19 J. S. Wilkes, *Ion. Liq.*, 2002, **818**, 214–229.
- 20 E. M. Levin, J. F. Kinney, R. D. Wells and J. T. Benedict, *J. Res. Natl. Bur. Stand. Phys. Chem.*, 1974, **78A**, 505–507.
- 21 R. J. Gale, B. Gilbert and R. A. Osteryoung, *Acta Chem. Scand. Inorg. Chem. J. Chem. Soc. Dalt. Trans. J. Chem. SOC. J. Chem. SOC*, 1972, **11**, 367–349.
- 22 M. Freemantle and T. Welton, *An Introduction to Ionic Liquids*, 2009.
- 23 J. S. Wilkes and M. J. Zaworotko, *J. Chem. Soc. Chem. Commun.*, 1992, **98**, 965.
- 24 C. A. Angell, N. Byrne and J.-P. Belieres, *Acc. Chem. Res.*, 2007, **40**, 1228–36.
- 25 J. E. Bara, T. K. Carlisle, C. J. Gabriel, D. Camper, A. Finotello, D. L. Gin and R. D. Noble, *Ind. Eng. Chem. Res.*, 2009, **48**, 2739–2751.
- 26 G. G. Eshetu, M. Armand, H. Ohno, B. Scrosati and S. Passerini, *Energy Environ. Sci.*, 2016, **9**, 49–61.
- 27 <http://ilthermo.boulder.nist.gov/>, .
- 28 B. Kudłak, K. Owczarek and J. Namieśnik, *Environ. Sci. Pollut. Res.*, 2015, **22**, 11975–11992.
- 29 D. J. Couling, R. J. Bernot, K. M. Docherty, J. K. Dixon and E. J. Maginn, *Green Chem.*, 2006, **8**, 82–90.

- 30 W. Gouveia, T. F. Jorge, S. Martins, M. Meireles, M. Carolino, C. Cruz, T. V. Almeida and M. E. M. Araújo, *Chemosphere*, 2014, **104**, 51–56.
- 31 <https://www.sigmaaldrich.com>, *ChemFiles*, 5, 1–24.
- 32 A. E. Visser, R. P. Swatloski, W. M. Reichert, R. Mayton, S. Sheff, A. Wierzbicki, J. H. Davis and R. D. Rogers, *Environ. Sci. Technol.*, 2002, **36**, 2523–2529.
- 33 M. Armand, F. Endres, D. R. MacFarlane, H. Ohno and B. Scrosati, *Nat. Mater.*, 2009, **8**, 621–629.
- 34 T. Torimoto, T. Tsuda, K. Okazaki and S. Kuwabata, *Adv. Mater.*, 2010, **22**, 1196–221.
- 35 J. L. Shamshina, M. Smiglak, D. M. Drab, T. G. Parker, H. W. H. Dykes, R. Di Salvo, A. J. Reich and R. D. Rogers, *Chem. Commun. (Camb.)*, 2010, **46**, 8965–8967.
- 36 C.-T. Wu, K. N. Marsh, A. V. Deev and J. A. Boxall, *J. Chem. Eng. Data*, 2003, **48**, 486–491.
- 37 S. Dai, Y. H. Ju and C. E. Barnes, *J. Chem. Soc. Dalt. Trans.*, 1999, **2**, 1201–1202.
- 38 H. Wang, Q. Lu, C. Ye, W. Liu and Z. Cui, *Wear*, 2004, **256**, 44–48.
- 39 B. Garcia, S. Lavallée, G. Perron, C. Michot and M. Armand, *Electrochim. Acta*, 2004, **49**, 4583–4588.
- 40 T. Welton, *Coord. Chem. Rev.*, 2004, **248**, 2459–2477.

Chapter I: Techniques



*“JUST BECAUSE SOMETHING IS A METAPHOR
DOESN'T MEAN IT CAN'T BE REAL”*

(Bill Door, aka Death - “Reaper Man” - Sir Terry Pratchett)

I. X-ray Diffraction

I.I. Principles

Information on the molecular structure and supramolecular arrangement of a sample can be obtained by measuring the intensity modulation spectrum of an X-ray beam (i.e. electromagnetic wave whose wavelength is comparable to the bond distance between atoms). If only the elastic component of the X-ray/matter interaction is considered (i.e. no kinetic energy loss), for an isotropic sample the diffracted intensity exclusively depends on the variation of the moment modulus of the incident radiation. This variation is indicated by the scalar Q (or q), the scattering variable. The result of the diffraction is therefore a graph of the diffuse intensity as a function of the parameter Q .

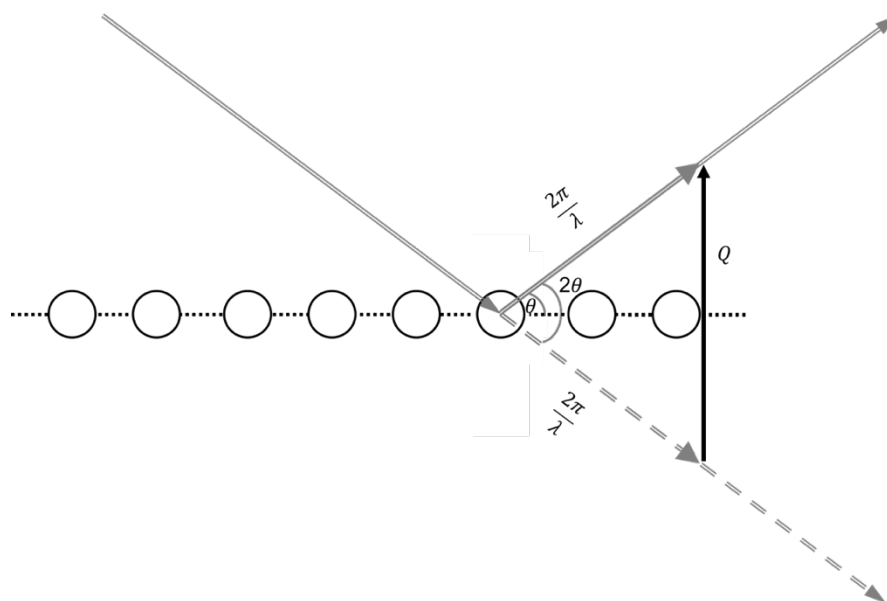


Figure I.1: Schematic representation of the wave vector change during the scattering phenomenon.

$$Q = 2k\sin(\theta) \quad [1.1]$$

being k the modulus of both the wave vectors of the diffracted and non-diffracted radiation. Substituting k with $\frac{2\pi}{\lambda}$, we obtain

$$Q = \frac{4\pi \sin(\theta)}{\lambda} \quad [1.2]$$

Furthermore, since the energy is proportional to k (through its wavelength dependence), we can write the following equation:

$$Q(E, \theta) = \alpha E \sin(\theta) \quad [1.3]$$

with $\alpha \approx 1.014 \text{ \AA}^{-1} \text{ KeV}^{-1}$. To extract information from Equation [1.3] and the diffracted intensity profile, two different methods can be used: i) use a monochromatic beam of X-rays (fixed Energy), such as a fluorescence line, and perform an angular scanning (Angular Dispersive X-ray Diffraction, ADXD), or ii) use the continuous X-ray spectrum, i.e. the Bremsstrahlung radiation, while maintaining the θ angle fixed (Energy Dispersive X-ray Diffraction, EDXD).

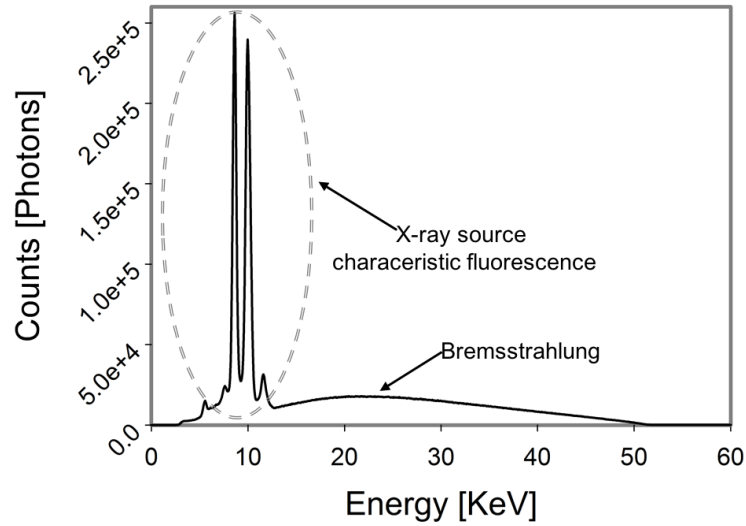


Figure 1.2: Experimental X-ray spectrum of a Tungsten tube

Typical spectrum of an X-ray tube: The characteristic emission lines and Bremsstrahlung are shown. In my work I've used the second procedure, thus variable energy and fixed angle were taken into account. The main features of this technique are listed below.

- Wide region of reciprocal space is accessible, because different energy values of a continuous spectrum (Bremsstrahlung) are used. Basically, it is possible to obtain the desired q range choosing the appropriate set of scattering angles (θ).
- Reduced acquisition time because all the spectrum is collected simultaneously. Using more than one detector, time is further diminished.
- Experimental procedure simplified: any movement of the equipment does not affect the alignment and therefore does not induce a systematic error. The measurement is carried out under static conditions. Even cells having complex geometries can be installed.
- Reduction of the absorption effects.

The X-ray diffraction pattern is the elastically scattered waves superposition of the electrons surrounding the nuclei. To describe the overall effect of the interference, the phase shift of the scattered radiation must be assessed. This can be done by calculating the optical path length of each scattered beam. Since Bremsstrahlung radiation is polarized, the scattered radiation from a single electron at the origin of the axes will have an amplitude much larger than its oscillation when at a distance r , that is:

$$A_0(\Phi) = a(\Phi) \frac{e^{ikr}}{r} \quad [1.4]$$

where

$$a(\Phi) = a_0^i r_0 \sin(\Phi) \text{ with } a_0^i = a_0^{\parallel} \text{ or } a_0^{\perp}$$

The angle Φ is related to angle 2θ by

$$\begin{cases} \Phi^{\parallel} = \frac{\pi}{2} - 2\theta \\ \Phi^{\perp} = \frac{\pi}{2} \end{cases} \Rightarrow \begin{cases} a(\Phi^{\parallel}) = a^{\parallel}(\theta) = a_0^{\parallel} r_0 \cos(2\theta) \\ a(\Phi^{\perp}) = a^{\perp}(\theta) = a_0^{\perp} r_0 \end{cases}$$

Considering two electrons, Equation [1.4] is amended by adding a term that represents the phase shift:

$$A_0(\Phi) = a(\Phi) \frac{e^{ikr}}{r} e^{iQr} \quad [1.5]$$

Extending the treatment to the i^{th} atom Z electrons, and considering that they are distributed according to the square of the wave function, we get:

$$A_0(\Phi) = \sum_{i=1}^N A_i(\theta) = a(\theta) \frac{e^{ikr}}{r} \sum_{i=1}^N x_i f_i(Q) e^{iQr} \quad [1.6]$$

Where x_i is the numerical concentration of the i^{th} atom and $f_i(Q)$ is the scattering factor:

$$f_i(Q) = \sum_{\alpha=1}^N \int |\Phi_{\alpha}|^2 e^{iQ\Delta r_i} d\Delta r \quad [1.7]$$

At this point, since the diffracted intensity is proportional to the summation of the scattering intensities of the two components (i.e. \perp and \parallel):

$$I(\theta) \propto |A(\theta)|^2 = |A(\theta)^{\perp}|^2 + |A(\theta)^{\parallel}|^2 \quad [1.8]$$

Considering the polarization factor and simplifying, we obtain the Debye formula in electron units:

$$S(Q) = \sum_{i=1}^N x_i f_i^2(Q) + I(Q) \quad [1.9]$$

The first member of the EQUATION is simply the sum of the squared atomic scattering factors. The second, called “total (static) structure function” or “reduced intensity”, contains information on the molecular structure of the sample, by the means of interference contributions from different atoms. The function $I(Q)$ is related to the pair correlation functions according to the formula:

$$I(Q) = \sum_{i \neq j} x_i x_j f_i f_j H_{ij}(Q) \quad [1.10]$$

where we have introduced the partial structure functions H_{ij} defined in terms of pair correlation functions by the Fourier integral:

$$H_{ij}(Q) = 4\pi\rho_0 \int_0^{r_{\max}} r^2 (g_{ij}(r) - 1) \frac{\sin(Qr)}{Qr} dr \quad [1.11]$$

here ρ_0 is the bulk numeric density of the system. By inverting this Fourier transform, we get:

$$g_{ij}(r) = 1 + \frac{1}{2\rho_0\pi^2} \int_0^{+\infty} Q H_{ij}(Q) \sin(Qr) dQ \quad [1.12]$$

this quantity, denoted by $g_{ij}(r)$, represents the probability of finding a given atom i in a shell dr placed at a distance r from an atom j chosen as reference.

I.II. In home Instrument

The measurements were made using two different instruments. The first model was the diffractometer shown in figure 1.3 (left). It is a non-commercial diffractometer built in Department of Chemistry, “La Sapienza” University of Rome (Italian Patent #01126484 - 23 June 1993). Four different θ angles are collected for each sample, namely 1° , 3° , 8° and 24° . This procedure enables to cover a q range between 0.2 - 20 \AA^{-1} . The second instrument (figure 1.3 on the right) was thought to further diminish the acquisition time while expanding the accessible q range. A horizontal setting consisting of three independent detectors enables to perform measures in $\sim 3 \text{ h}$ while the former instrument takes over a day. The angles at which two detectors are fixed are 30° and 10° , while the third detector covers alternatively 3° and 1° . The corresponding q range is, therefore, 0.2 - 25 \AA^{-1} .

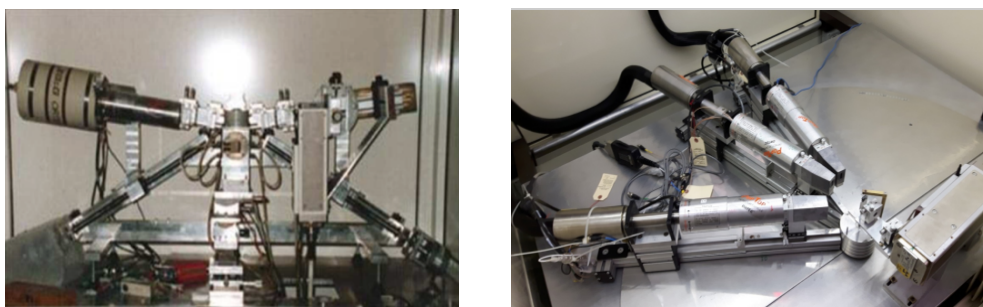


Figure 1.3: First generation EDXD instrument (left); second generation EDXD instrument (right)

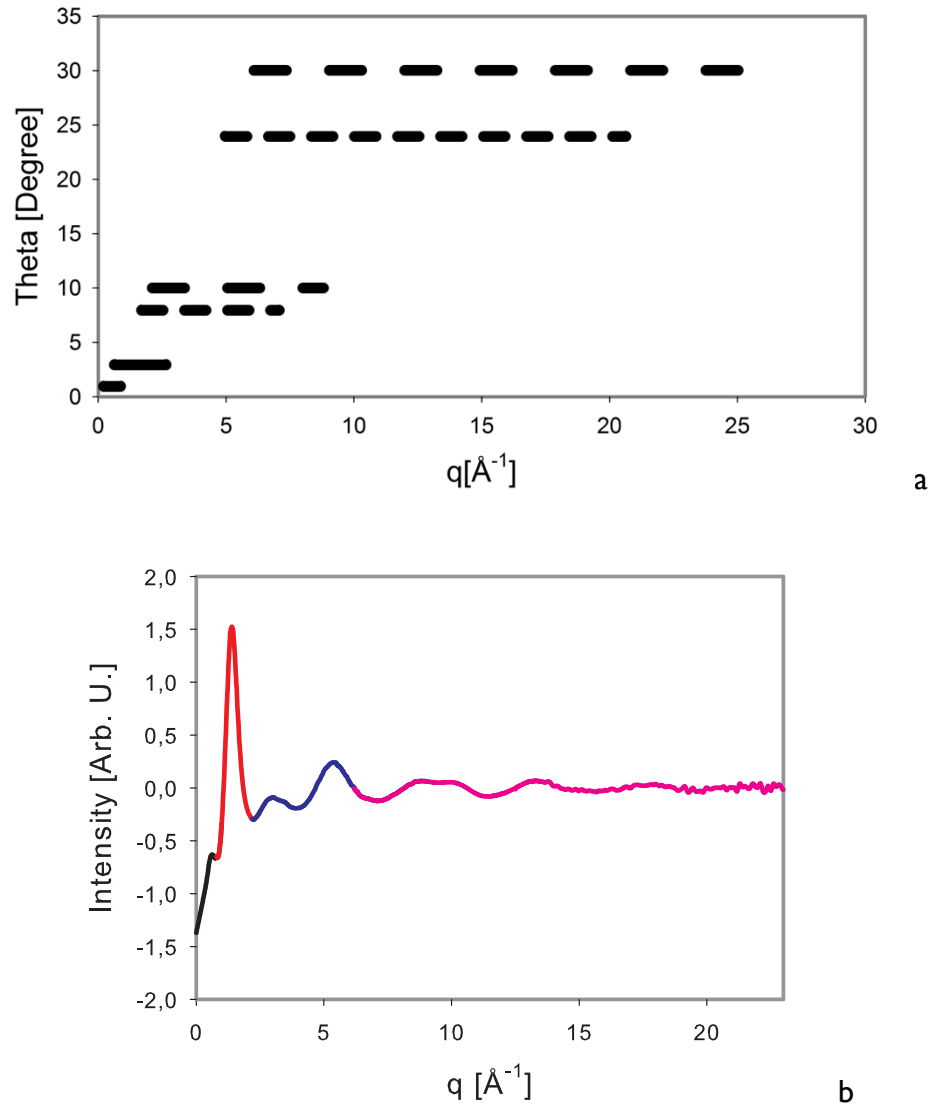


Figure 1.4: (a) q range collected as a function of the angle. Long dashed lines refers to the second generation instrument, short dashed lines to the first generation instrument, solid lines to both. (b) Example of a scattering pattern of a system containing ionic liquids. Different colour refers to different collecting angles. 1° (black); 3° (red); 10° (blue); 30° (pink).

To increase the resolution of the curve at high Q values (see, for instance reference 1), and to limit the truncation error in the calculation of the Fourier transform from the reciprocal space (Q) to real space (r), both experimental and theoretical structure functions were multiplied by Q and a modification function that depends on Q :

$$M(Q) = \frac{f_{atom}^2(Q)}{f_{atom}^2(0)} e^{-0.01Q^2} \quad [1.13]$$

The chosen atom was nitrogen. This function is used to enhance the peaks located at high q values, with the result of obtaining a better Fourier transformation of the $QI(Q)M(Q)$ into a radial distribution function $D(r)$, according to the relation.

$$D(r) = 4\pi r^2 \rho_0^2 + \frac{2\pi}{r} \int_0^{+\infty} QI(Q) M(Q) \sin(Qr) dQ \quad [1.14]$$

by subtracting the uniform distribution, we obtain the radial distribution function which contains only structural information, $Diff(r)$:

$$Diff(r) = \frac{2\pi}{r} \int_0^{+\infty} QI(Q) M(Q) \sin(Qr) dQ \quad [1.15]$$

The structure function $I(Q)$ and the radial distribution function $Diff(r)$ are the Fourier transform of each other and allow to switch from the reciprocal space, Q , to real one, r . Figure I.5 is an example of $I(Q)$ and in its Fourier transform in $Diff(r)$ form: intense peaks at low q , have corresponding peaks at large r values in the $Diff(r)$.

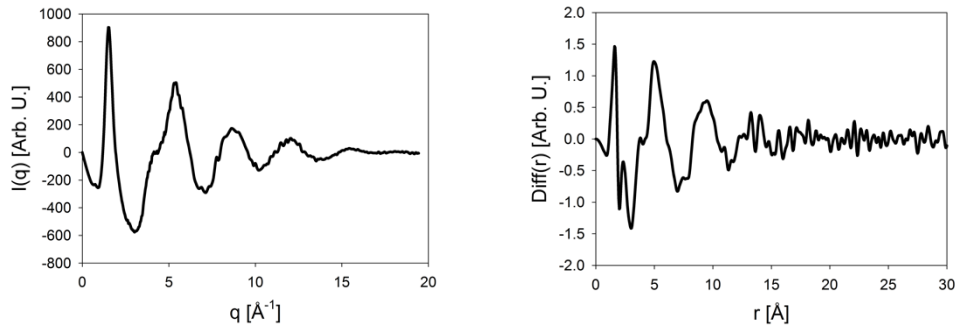


Figure I.5: Structure factor $I(q)$ (left); radial function $Diff(r)$ (right)

In addition, a small interval of Q close to zero, corresponds to a wide range of r in the $Diff(r)$. This is because, at a first approximation, the distance is related to Q by the Bragg Law

$$r = \frac{2\pi}{Q} \quad [1.16]$$

I.III. Synchrotron Radiation

A Synchrotron accelerates charged particles, such as electrons into an orbit at almost the speed of light. When electrons are deflected through magnetic fields

they create extremely bright light, million times brighter than sunlight. A synchrotron uses powerful magnets and radio frequency waves to accelerate charged particles. The powerful magnet and radio frequency waves accelerate negatively charged electron along a stainless steel tube, where they reach high speed. As the magnets are turned on and off, electrons get pulled along the ring of tubes. Since the fast-moving electrons emit a continuous spectrum of light, with various wavelengths and strength, scientists can pick whatever wavelength they need for their experiments e.g. visible light, ultraviolet light or X-rays (soft or hard x-rays). Electrons are accelerated and when they have enough energy to produce light, an injection system transfers them from the booster ring to the storage ring. The process of transferring electrons from booster to storage ring occurs approximately once per second up to 600 cycles (about 10 minutes) as required to reach an average circulating current of e.g. ~200 mA (ESRF-Grenoble). Once in the storage ring, the electrons will circulate four to twelve hours producing photons every time the 6800kg dipole magnets change the direction of the flow of electrons. While the ring looks circular, it is really a series of straight sections. After each turn there is a photon port to allow the light to travel down the beamlines to the research stations. The magnets and steerage ring are shown in the picture below. Each beamline has an optics cabin, the experimental cabin, and the control cabin. The optics cabin has optical instruments used to "tailor" the type of radiation to have the characteristics for the experiment. The experimental cabin contains the support mechanism, and the environment for the sample study. Instruments called detectors record the information produced from the sample. the control cabin allows the researchers to control the experiments and collect the data. In my work I have used the ID02 beamline (ESRF-Grenoble), that has a combined Small and Wide Angle X-ray Scattering (SWAXS) setting. It has an energy range of 8-20 KeV and a detector distance tunable from 0.6 to 30 m, thus covering a q region between 10^{-4} - 6 \AA^{-1} .

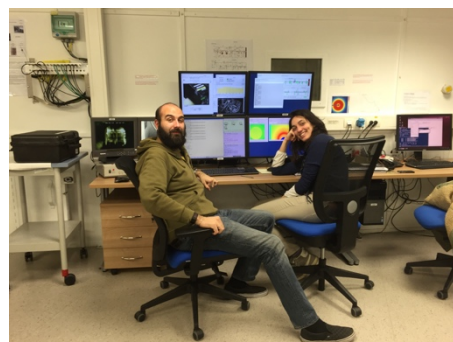
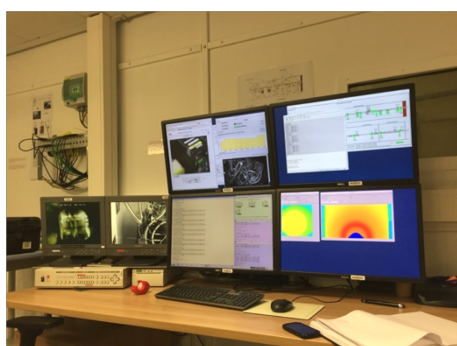
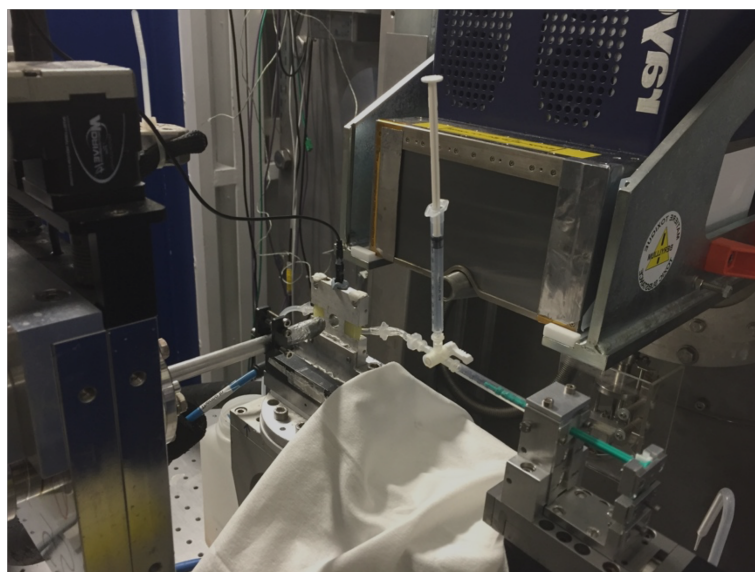


Figure 1.6: Pictures of the beamline ID02 at ESRF – Grenoble, France

II. Molecular Dynamics simulations

II.1. Definition

The interpretation of the experimental data from diffraction experiments, whether they are arising from X-Rays or Neutrons, of non-crystalline systems is often supported by the proposal of a theoretical model that is the result of computational simulation. The classical Molecular Dynamics (MD) is considered one of the most powerful tools in the construction of such molecular models because it can get a variety of information on the studied system, such as structure, mobility, diffusion and self-diffusion coefficients. The MD allows to simulate systems up to several tens of thousands of atoms thanks to an approach that avoids to take into account quantum effects and assuming that the particles are a kind of "balls" whose properties are modelled through a potential, called

Force Field (FF), which contains, in its basic expression, the Lennard -Jones and the charge of each different atom type (i.e. methyl carbon, amide nitrogen, inorganic carbon...). These data are, in turn, derived from *ab initio* calculations of different level of accuracy and are then modulated to fit experimental. There are several FF generated this way (GAFF, OPLS, GROMOS and so on), each of them is more suitable for a particular simulation: it may be more or less of general purposing depending on how many atom types are listed in; it may be more or less versatile depending on the possibility or not to modify their parameters by the user; it may be more or less complex depending on the introduction of advanced and specific parameters such as polarizability. Classical molecular dynamics approaches the potential energy surface with a sum of analytical terms empirically determined. The most common functional form is:

$$\begin{aligned}
 V(r) = & \sum_{bonds} k_b(d - d_0)^2 + \sum_{angles} k_\theta(\theta - \theta_0)^2 + \\
 & + \sum_{dihedrals} k_\phi[1 + \cos(n\phi + \delta)] + \\
 & + \sum_{non\ bonded\ pairs} \left\{ \epsilon_{ij} \left[\left(\frac{\sigma_{ij}}{r_{ij}} \right)^{12} - \left(\frac{\sigma_{ij}}{r_{ij}} \right)^6 \right] + \frac{q_i q_j}{4\pi\epsilon_0 r_{ij}} \right\}
 \end{aligned}$$

The first three terms of this FF describe the strength and geometry of the covalent bonds, where k_b , k_θ and k_ϕ are the respective force constants of the springs attributed to the stretching/bending motions and to the dihedral angles, while the third line describes the Van der Waals and the Coulomb terms, where ϵ_{ij} is the depth of the potential well, and σ_{ij} is proportional to the distance at which the potential reaches its minimum². Implicit in this description is the idea that the system does not change the potential energy surface during the dynamics. There are several different FFs for proteins and nucleic acids, differing either for the kind or analytical form used, or for the parameterization procedure. Of course, a drawback of this kind of approach is the transferability: these FFs are typically parameterized to generate fine results for simulations at room temperature and do not give accurate results at different ones. In spite of these problems, the FF based approaches are the most used to simulate large system because of its integration velocity. In classical molecular dynamics the

temporal evolution is computed by numerical solutions of the classical equations of motion with the forces generated by a FF:

$$M_I \dot{v}_I(t) = -\frac{\partial V}{\partial r_I} \quad [1.17]$$

In a molecular dynamics simulation, as the simulated system is limited in space, you may have edge effects. To minimize them, the atoms of the simulated system are placed in a box, which is replicated in all directions forming an “infinite” periodic system. This schedule set can lead to errors, especially when you consider properties affected by long-range correlation (Fig. (2.9)).

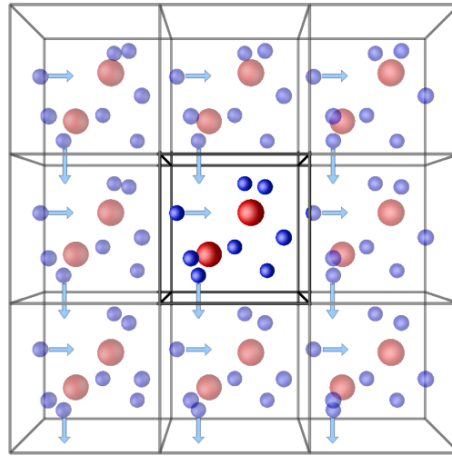


Figure 1.7: Periodic boundary conditions

Within the microcanonical ensemble, *i.e.* for simulations at constant total energy, the equations are solved with algorithms based on the Taylor expansion of the forces and velocities: at each time t , positions, velocities and forces are evaluated, and those at time $t + \Delta t$ are generated as a function of them. For instance, in the velocity Verlet algorithm, one has:

$$r(t + \Delta t) = r(t) + \Delta t v(t) + \frac{\Delta t^2 a(t)}{2} \quad [1.18]$$

$$a(t + \Delta t) = \frac{f(t + \Delta t)}{m} \quad [1.19]$$

$$v(t + \Delta t) = v(t) + \frac{1}{2} \Delta t [a(t) + a(t + \Delta t)] \quad [1.20]$$

However, generally a simulation at constant energy is not the most efficient way to explore the phase space of the system. The choice of the timestep Δt is crucial: it has to be as small as possible for the integration to be accurate, but the largest

possible for the integration to be fast. A good compromise is one tenth of the inverse of the largest typical frequency of the system. The most reliable conditions are constant temperature and pressure. One way to keep the temperature constant is scaling velocities at each timestep:

$$r(t + \Delta t) \leftarrow r(t) + \Delta t v \left(t - \frac{\Delta t}{2} \right) \quad [1.21]$$

$$v(t + \Delta t) \leftarrow (2\eta - 1)v \left(t - \frac{\Delta t}{2} \right) + \eta \Delta t \frac{f}{m} \quad [1.22]$$

$$\eta = \sqrt{\frac{T_{ext}}{T}} \quad [1.23]$$

Alternatively, one can introduce additional fictitious degrees of freedom to describe the coupling with the thermal bath (and/or with the barostate) to accurately simulate the canonical ensemble:

$$H' = \sum_i \frac{|\vec{p}_i|^2}{2m_i} + \Phi(\vec{q}) + \frac{Q}{2} \zeta^2 + gkT \cdot \ln(S) \quad [1.24]$$

here ζ is the velocity (time derivative) associated to the fictitious degree of freedom S , Φ the total potential energy and p , q the canonical variables. The fictitious mass Q and coupling constant g must be chosen to realistically regulate the energy flow velocity between thermal bath and system. This formulation (Nose and Nose-Hoover coupling) ensures that the equilibrium distribution is the Canonical ensemble one³. Molecular dynamics simulations can obtain excellent results in the case of even complex systems made up from electrically neutral molecules as in the case of pure molecular liquids (water, organic liquids), mixtures thereof, macromolecules (polymers, proteins) and also macromolecules in solution with molecular liquids, providing valuable support to the interpretation of different experimental data and offering the chance to observe some system characteristics such as the diffusion mechanism, the microscopic molecular arrangement and all those properties are not experimentally accessible. A major problem, to date, seems to be the simulation of systems in which electrically charged fragments are present as, for example, ionic liquids.

II.II. Critical Issues

In my PhD, I've used mostly the GAFF force field implemented in AMBER (versions 11, 12 and 14). As mentioned above, almost every FF is thought to work on neutral molecules. When net charges are into account, one must modify the FF to make the things working. I have performed several simulations on pure ethylammonium nitrate using always the same Lennard-Jones (GAFF native parameters) but changing each time the atomic charges by calculating or taking them from various sources in the literature. Those potential are reported in the following table.

Fragment	Atom	Atkin⁴	Umebayashi⁵	Varela⁶	B3LYP 6-311++G**	B3LYP aug-cc- pVTZ
Anion	N ⁻	0.845	0.905	0.794	0.291605	1.056896
	O	-0.615	-0.635	-0.598	-0.430535	-0.685632
Cation	C _t	-0.411	-0.05	-0.180	-0.284043	-0.313821
	H _c	0.147	0.06	0.060	0.101615	0.133985
	C _l	0.263	0.04	0.190	0.372982	0.106204
	H _x	0.069	0.13	0.060	0.039449	0.110419
	N ⁺	-0.529	-0.36	-0.300	-0.728247	-0.494366
	H _n	0.366	0.31	0.330	0.418521	0.359730

The simulation box had always an edge of 50Å containing 830 ion pairs, the size of the box was calculated on the basis of the experimental density and the molecular weight of the species according to the formula:

$$Edge = \sqrt[3]{\frac{n \cdot 10MW}{\rho \cdot N_A}} \quad [1.25]$$

where n is the number of molecules, MW is the molecular weight, ρ is the mass density and N_A is the Avogadro constant. The procedure followed for the simulations was:

- Generation of the initial random molecular distribution through the routine PACKMOL.

- 10^7 energy minimization cycles.
- Heating by a short NVT (10 ps) at low temperature (50 K).
- Heating the system at 300 K with an NPT (10 ns)
- NVT equilibration (10 ns)
- NVT productive phase (2 ns).

This ensures to obtain a well equilibrated and representative of the real system simulation box. From the trajectories thus obtained were calculated the X-ray scattering pattern. Below we report the comparison charts between the experimental data and the various simulations.

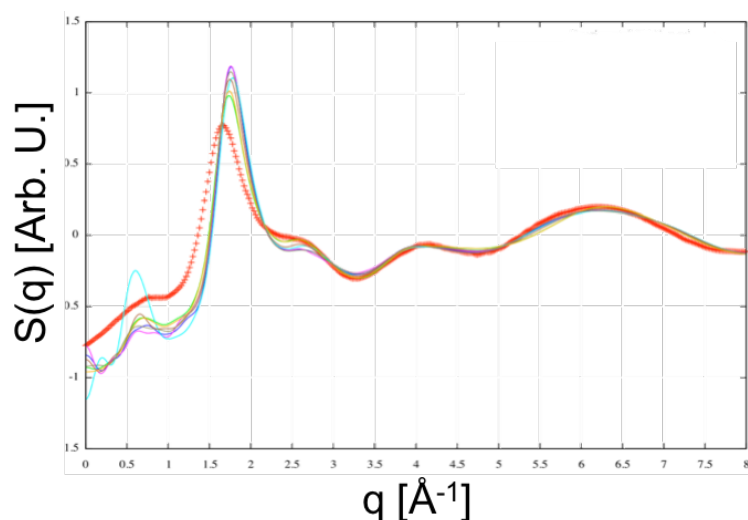


Figure 1.8: Comparison between experimental (red) and computed WAXS patterns for EAN. Atomic charges from: RESP 6-311++G** (green); Atkin (blue); Umebayashi (pink); Varela (cyan); average between RESP and Atkin (brown); Atkin for cation and RESP for anion (orange); RESP for cation and Atkin for anion (grey)

From graphics it is evident that regardless to the potential used the position of the main peak is always shifted towards larger values of q to $\sim 1.85 \text{ \AA}^{-1}$ and is overestimated in intensity. These facts are due to an additional artificial order induced from the calculation. This trick does not affect the curve at higher q values, from 3 \AA^{-1} on, and the overlap with the experimental is more than satisfactory.

II.III. Effect of Dielectric Constant

It is a well-known fact that simulations on protic ionic liquids find advantage from rescale the atomic charges by a factor between 0.8-0.7. This because the columbic forces coupled with hydrogen bond effects both lead to highly

overestimated interactions. I've found that the almost equivalent procedure of setting a multiplicative dielectric constant inside the box has a valuable effect on the overall density of the system.

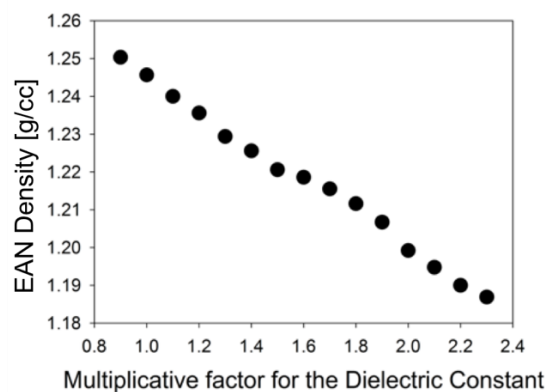


Figure 1.9: Ethylammonium nitrate density as a function of the dielectric constant parameter used in the simulation

EAN experimental density is 1.2106 g/ml at 25 °C, so a value of 1.8 was found to be the best choice. Simulating three different protic ionic liquids using this dielectric constant, namely ethyl, propyl and butyl ammonium nitrate (EAN, PAN and BAN, respectively), a really good agreement was found for the structure factors.

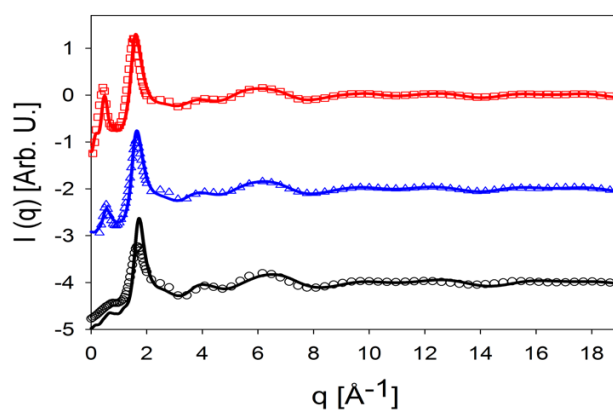


Figure 1.10: Scattering patterns for EAN (black), PAN (blue) and BAN (red). Comparison between experimental (symbols) and computed (solid lines).

III. NMR DOSY

III.1. Principles

The diffusion NMR technique is often referred to as Self-Diffusion (SD)-NMR or Diffusion Ordered Spectroscopy (DOSY)⁷. This is achieved by combining radio-frequency pulses as used in routine NMR spectroscopy with magnetic field gradients that encode spatial information. In the simplest form of the pulsed gradient diffusion experiment called the pulsed field gradient echo (PGSE), the magnetization is excited with a 90° radiofrequency pulse then dispersed using a magnetic field gradient pulse. After a period of $\Delta/2$ a 180° radiofrequency pulse inverts the dispersed magnetization such that after a period of Δ the magnetization is the negative of what it was following the gradient pulse. At this point, a second gradient pulse is applied to refocus the signal as schematically reported in figure 1.11.

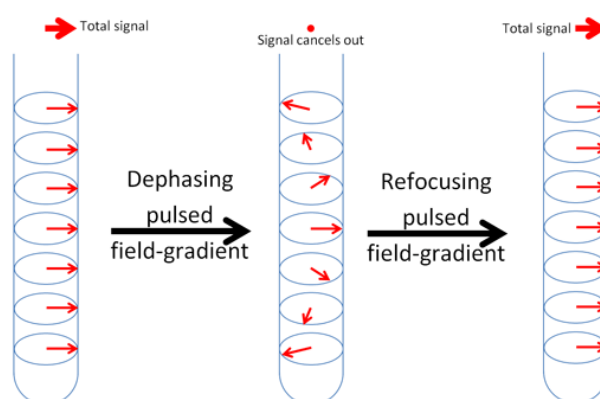


Figure 1.11: Effect of a magnetic field gradient pulse.

Refocusing is only achieved for those nuclei that have not moved significantly up or down the tube. Diffusion causes some of the nuclei to move away from where their signals can be refocused thereby reducing the intensity of the resulting signal.

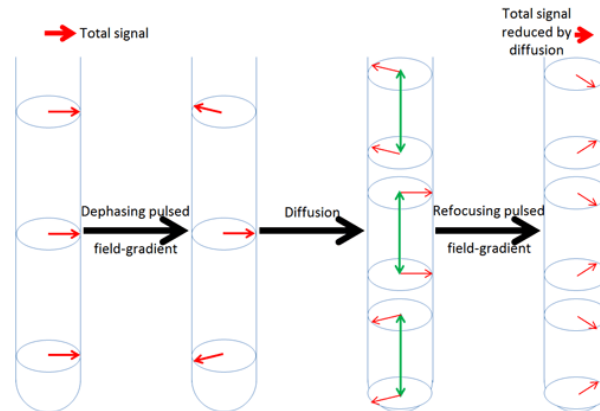


Figure 1.12: Effect of diffusion combined with magnetic field gradient pulses.

The more intense and the longer the magnetic field gradient pulse, the more spatially selective it is and the weaker the resulting signal. The intensity and duration of the magnetic field gradient pulse determine the distance that a nucleus can diffuse and still yield a signal.

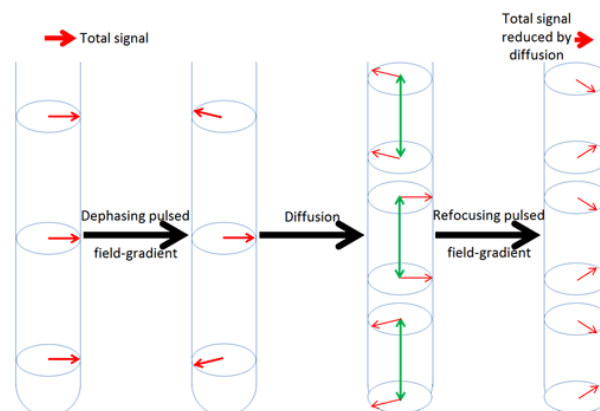


Figure 1.13: The effect of magnetic field gradient strength on signal strength is like focusing on the molecules that have not diffused out of range. The stronger the gradient the smaller the range and the weaker the gradient the larger the range.

The pulse sequence is repeated, a number of times incrementing the gradient strength and keeping the delays constant.

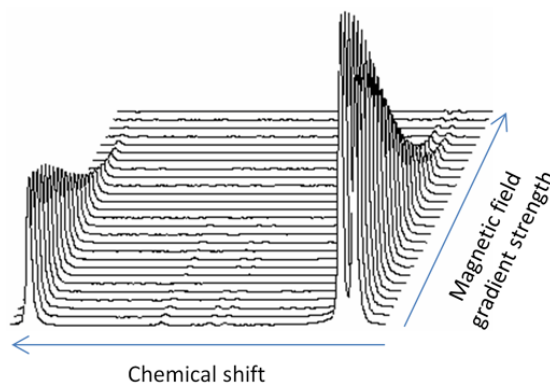


Figure 1.14: Diffusion spectrum. The peak on the left decays faster with increasing gradient strength and has a higher diffusion constant than the peaks on the right.

The peaks areas may fitted the results with the function

$$Y = A + B \cdot e^{-C \cdot x} \quad [1.26]$$

Where A and B are adjustable parameters and C returns directly the diffusion coefficient. Selecting peaks arising from different molecules, allows to determine the diffusion coefficient for each of them. To achieve this goal it may be useful to collect the DOSY spectra for different atoms (e.g. ^1H , ^{13}C , ^{19}F ...) chosen upon convenience.

IV. Redlich-Kister fitting

It is useful to fit some experimental or derived data using an analytical function. In this way one can estimate the value of the given quantity for missing points. For excess quantities (in this manuscript excess molar volume and excess viscosity) the Redlich-Kister polynomial equation is often used⁸⁻¹⁰.

$$\xi^{ex} = \chi_1 * (1 - \chi_1) * \sum_i A_i * (1 - 2\chi_{EAN})^i \quad [1.27]$$

where ξ^{ex} is the generic excess quantity, χ_i is the component I molar fraction and A_i are adjustable parameters. The number i is chosen to minimize σ :

$$\sigma = \sqrt{\frac{1}{N - i} * \sum_{c=1}^N (\xi_c^{exp} - \xi_c^{fit})^2} \quad [1.28]$$

where N is the number of experimental points.

V. References

- 1 R. Caminiti, G. Licheri, G. Piccaluga, G. Pinna and M. Magini, *Rev. In. Chem.*, 1979, **1**.
- 2 H. M. Senn and W. Thiel, in *Atomistic Approaches in Modern Biology: from Quantum Chem. to Molecular Simulations*, 2007, **268**, 173–290.
- 3 B. Frenkel, Daan; Smith, *Understanding Molecular Simulations*, Academic Press Ed, 1996.
- 4 R. Hayes, S. Imberti, G. G. Warr and R. Atkin, *Angew. Chem. Int. Ed. Engl.*, 2012, **51**, 7468–71.
- 5 S. Ishiguro, Y. Umebayashi, R. Kanzaki and K. Fujii, *Pure Appl. Chem.*, 2010, **82**, 1927–1941.
- 6 L. J. Gallego and L. M. Varela, *J. Phys. Chem. B*, 2014, **118**, 761–770.
- 7 C. S. Johnson Jr., *Prog. Nucl. Magn. Reson. Spectrosc.*, 1999, **34**, 203–256.
- 8 O. Redlich and A. T. Kister, *Ind. Eng. Chem.*, 1948, **40**, 345–348.
- 9 J. E. Desnoyers and G. Perron, *J. Solution Chem.*, 1997, **26**, 749–755.
- 10 T. Ono, R. Amezawa, A. Igarashi, M. Ota, Y. Sato and H. Inomata, *Fluid Phase Equilib.*, 2015, **407**, 198–208.

Chapter II: Ionic Liquids Structure



*“It was all very well going on about pure logic
and how the universe was ruled by logic
and the harmony of numbers,
but the plain fact of the matter was that the Disc”
(the flat world, editor’s note)
“was manifestly traversing space on the back of a giant turtle
and the gods had a habit of going round to atheists’ houses
and smashing their windows.”
(“The Colour of Magic” – Sir Terry Pratchett)*

I. Nanoscale segregation

Yet macroscopically homogenous, ionic liquids possess a characteristic nano-structure arising from their intrinsically amphiphilic nature¹⁻⁷. One can easily label two different regions in the molecular structure: a polar (hydrophilic) part consisting of the charged portions, and an apolar (hydrophobic) one made up by the alkyl tails.

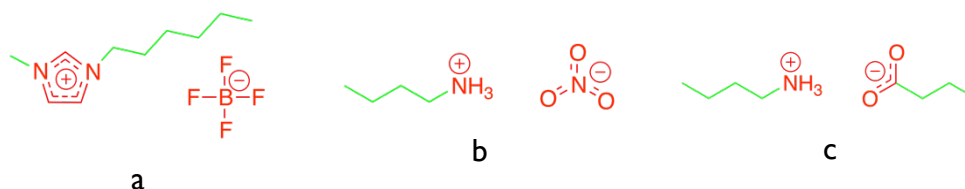


Figure 2.1: (a) 1-hexyl-3-methylimidazolium tetrafluoroborate; (b) butylammonium nitrate; (c) butylammonium butanoate; (d) a vial containing ethylammonium nitrate, the magnifying glass shows the sponge-like structure. Polar domain (red); apolar domain (green)

This organization is often called “sponge like” due to its resemblance to a bath-sponge. Obviously this is a dynamic structure and these domains are continuously formed and destroyed. Nevertheless, they retain a nano-heterogeneous, bipercolating arrangement. The fingerprint of such a structure is a characteristic “Low q Peak” (LqP) in the SAXS pattern, indicating a distance correlation of the order of tens of Ångstrom. The first observation of this phenomenon was in 2007, when Triolo *et al.* reported the LqP for a series of Imidazolium-based ionic liquids¹. To date, this effect has not been reported in aprotic ILs with alkyl tails shorter than four carbon atoms long, while for protic ionic liquids a chain consisting of an ethyl fragment is sufficient to make this feature appear^{4,8-11}. So hydrogen bonding effects tend to induce some strong kosmotropic effects, not surprising considering the structure of water. Polar substituents in the alkyl chain(s) (e.g. ethers, hydroxyl, amino) have a destructive effect on such an organization¹².



Figure 2.2: (a) 1-((ethoxymethoxy)methyl)-3-methylimidazolium tetrafluoroborate; (b) butanolammonium nitrate

The introduction of polar groups prevents the phase-segregation, thus LqP vanishes. It has been demonstrated that the repeating distance between two anions is the main responsible for the LqP. This distance is modulated by the alkyl tail(s) length, as schematically shown^{13,14}.

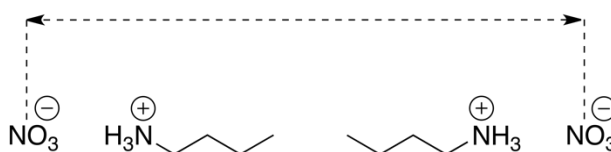


Figure 2.3: Schematic representation of the distance responsible for the LqP in protic ionic liquids

In table I some LqP positions are reported, it is evident how the q value depends directly by the alkyl chain length.

	EAN [Å ⁻¹]	PAN [Å ⁻¹]	BAN [Å ⁻¹]	C4mim BF ₄ [Å ⁻¹]	C6mim BF ₄ [Å ⁻¹]	C8mim BF ₄ [Å ⁻¹]
LqP position	0.67	0.54	0.49	0.42	0.35	0.28

Table 2.1: Low q peak positions for some ionic liquids

II. Ionic Liquids used

During my PhD fellowship, I studied some different Ionic Liquids, with the aim of finding some common behaviours and also to highlight specific differences. Most of my work was on Ethylammonium Nitrate (EAN)¹⁵, taken as a prototype of protic ionic liquids. I have also studied its two upper homologues, namely Propyl and Butyl ammonium nitrate (PAN² and BAN¹⁶, respectively).

II.1. Ethylammonium Nitrate

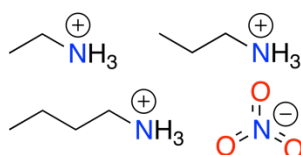


Figure 2.4: Ethylammonium, propylammonium and butylammonium cations, nitrate anion

EAN is probably the most studied protic ionic liquid. It is the smallest room temperature IL with a reported LqP. EAN shows the characteristic nano-segregated organization of most ILs, moreover an extended 3D hydrogen bonded network is observed¹⁷. Several computational studies describing its structure have been published, but the limitations exposed in the Chapter I, lead to unsatisfying results. By date, the best results obtained with classical molecular dynamics are the ones proposed by myself *et al.*¹⁸.

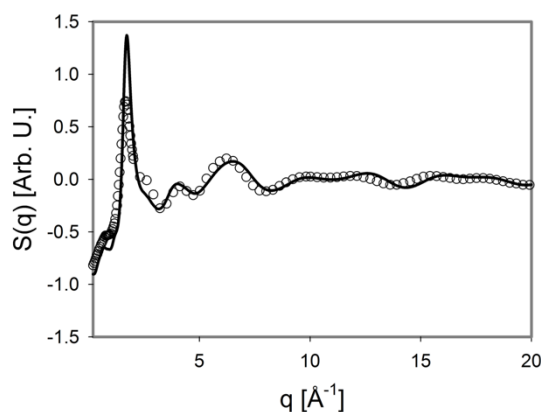


Figure 2.5: WAXS pattern for ethylammonium nitrate. Experimental (symbols); computed (solid line)

From the model we were able to extract some useful informations on the structure and the dynamics of the system. The first analysis performed was the study of Pair Distribution Functions (PDFs) and of Coordination Numbers (CNs) which are related by

$$CN(r)_{ij} = 4\pi \int_0^{+\infty} r^2 \cdot g(r)_{ij} \cdot \rho \, dr \quad [2.1]$$

where i and j are two atoms, $g(r)$ is the pair distribution function between the same atoms and ρ is the density. The results are shown in figures 2.6 and 2.7.

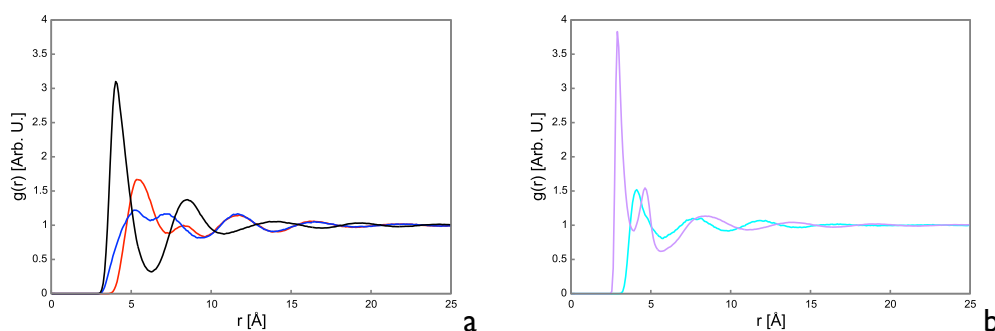


Figure 2.6: Pair distribution functions of some interactions in EAN. (a) cation-anion (black); anion-anion (blue); cation-cation (red); (b) $\text{NH}_3\text{-NO}_3$ (N-O distance) (purple); $\text{CH}_3\text{-CH}_3$ (C-C distance) (cyan)

From panel a of figure 2.6 it is clear the cation-anion alternation: like-charged ions correlation shows maxima whereas cation-anion shows minima and viceversa. Panel b of figure 2.6 considers the two main interactions in EAN, namely the hydrogen bond $\text{-NH}_3^+ \cdots \text{O}_3^-$ and the aliphatic interaction between the terminal methyl groups.

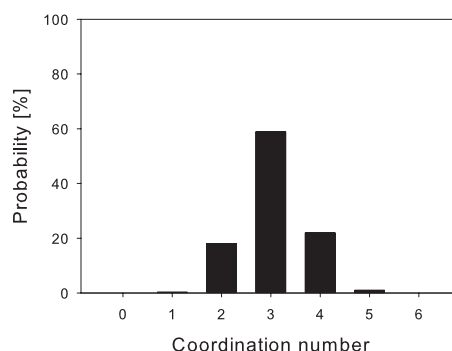


Figure 2.7: Cation-anion interaction coordination number for EAN

From figure 2.7 we can say that on average a single cation is directly hydrogen bonded to 3.0 anions on average. A deeper characterization of the hydrogen bonds may be achieved combining the $N_{\text{cation-O}_{\text{anion}}}$ PDF with the Angular Distribution Function (ADF) observing the angle defined as in figure 2.8.

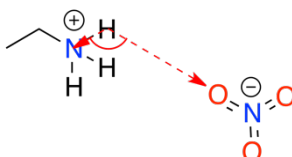


Figure 2.8: Schematic representation of the angle of the hydrogen bond in EAN

A short and linear correlation suggests that hydrogen bond correlation is established. In figure 2.9 the isolevel surface is shown

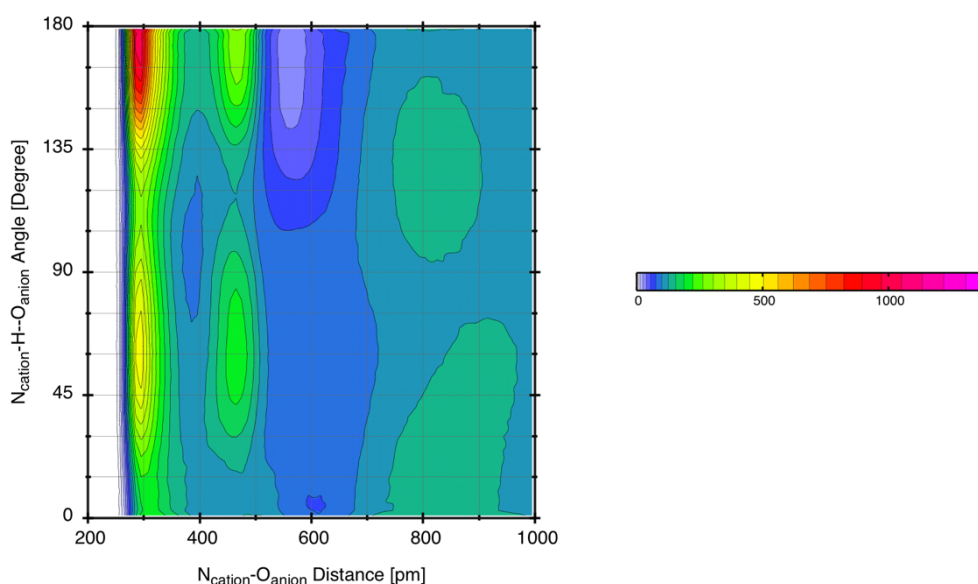


Figure 2.9: Combined radial-angular distribution function for the hydrogen bond in EAN

It appears clear that the anion and the cation are interacting via hydrogen bonds, because a strong correlation is observed at short distances (2.8-3.1 Å) and angles that tend to linearity (>135°). Using a really short timestep during the simulation (i.e. 0.5 fs) it is possible to observe fast processes like atomic vibrations or intermolecular interactions lifetime. It is interesting to compute the latter for the hydrogen bond interactions because it is possible to retrieve the interaction energy by¹⁹

$$\Delta G_T^\ddagger = RT \cdot \ln \left(\frac{\tau \cdot k_B T}{h} \right) \quad [2.2]$$

where R is the gas constant, T the temperature in Kelvin, τ is the characteristic time of a certain process, k_B is the Boltzmann constant and h is the Plank constant. The values for τ are obtained by fitting the autocorrelation function $C(t)$ with

$$C(t) = a \cdot e^{\frac{-t}{\tau_1}} + (1 - a) \cdot e^{\frac{-t}{\tau_2}} \quad [2.3]$$

where t is the time, a is a constant that determines the weight of the specific process, τ_1 and τ_2 are the characteristic times for the process 1 or 2 respectively. The process 1, which is faster, is the breaking of the hydrogen bond geometry, while the slower process 2 is the migration of the fragments outside the solvent cage. For EAN the results are shown in figure 2.10 and table 2.3.

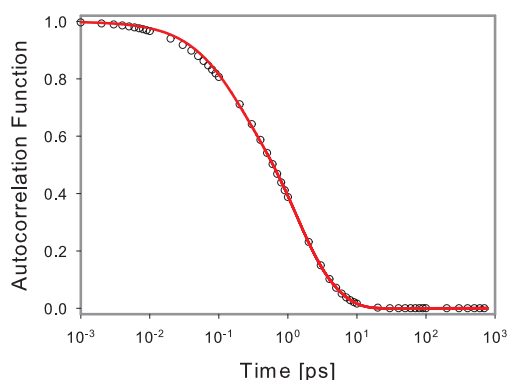


Figure 2.10: Hydrogen bond lifetime in EAN

a	0.4719
τ_1 [ps]	0.3165
τ_2 [ps]	2.5012
ΔG_1 [kJ/mol]	1.7008
ΔG_2 [kJ/mol]	6.8571
ΔG_{tot} [kJ/mol]	8.5579

Table 2.3: Fitting parameters and derived free energies of the hydrogen bond in EAN

The a parameter is a qualitative probe of the strength of the hydrogen bond itself: if a has a value greater than 0.5, then the interaction lifetime is dominated by the breaking up of the geometry (i.e. distance and angular conditions to have a hydrogen bond), otherwise the diffusion outside the solvent cage has a central role. In this case the hydrogen bond is weak because the geometry breaking up is not the kinetic relevant process. In fact, the Gibbs free energy content of an hydrogen bond is generally between 4 and 21 kJ/mol, and the calculated value for EAN is ~ 8 kJ/mol. So rather small. Self-diffusion is an important property, especially in potential electrochemical applications. DOSY NMR experiments

allows to obtain the diffusion coefficient for a certain molecule in a system if it has some suitable NMR signal. EAN ^1H NMR chemical shifts are reported in table 2.4.

$\text{H}_3\text{C}-\overset{\text{H}_2}{\underset{\text{NH}_3^+}{\text{C}}}$	$\text{H}_3\text{C}-\overset{\text{H}_2}{\underset{\text{NH}_3^+}{\text{C}}}$	$\text{H}_3\text{C}-\overset{\text{H}_2}{\underset{\text{NH}_3^+}{\text{C}}}$
1.48 ppm	3.34 ppm	7.76 ppm

Table 2.4: ^1H NMR chemical shifts in EAN

The results for neat EAN are reported in figure 2.11.

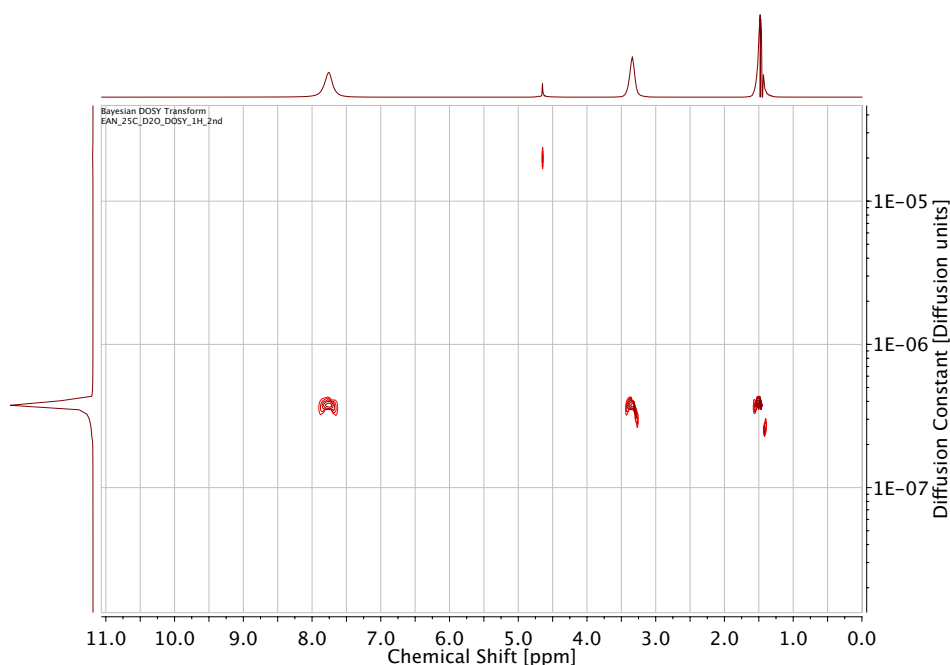


Figure 2.11: ^1H NMR DOSY for EAN

From the Bayesian analyses^{20,21} it results that the diffusion coefficient is $3.80 \cdot 10^{-11} \text{ m}^2 \text{ s}^{-1}$ for the ethylammonium cation, much slower than water for which a value of $2.3 \cdot 10^{-9} \text{ m}^2 \text{ s}^{-1}$ is known. This is due to several factors: i) EAN viscosity is 32.07 mPa*s while water viscosity is 0.89 mPa*s both at 25 °C. ii) the ethylammonium cation has a Van der Waals volume²² of 55.48 Å³ while water volume is 17.35 Å³. iii) EAN molecules interact by both hydrogen bonds and columbic forces while water molecules experience much weaker columbic forces.

II.II. Propyl/Butyl-ammonium Nitrate

To understand the effect of the alkyl tail, I have studied EAN's two *brothers*: Propylammonium Nitrate (PAN) and Butylammonium Nitrate (BAN). For both of them I have performed all the analyses done for EAN, with the exception of DOSY for BAN. Results comparison is shown in the following figures.

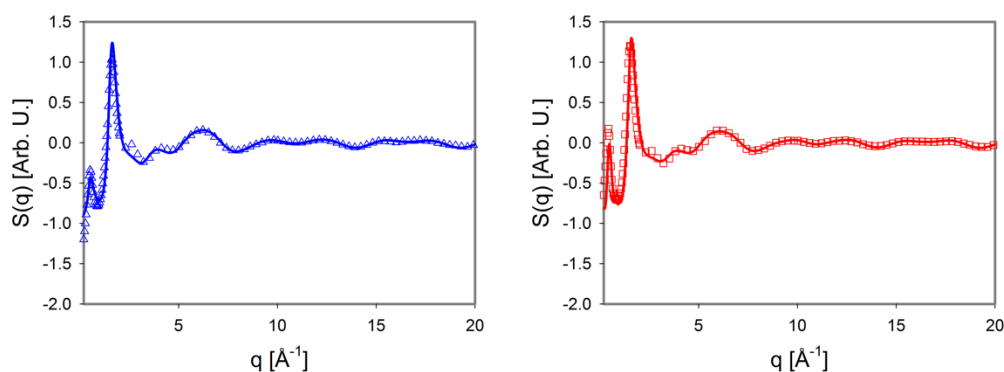


Figure 2.12: WAXS patterns for PAN (blue) and BAN (red). Experimental (symbols); model (solid lines)

The reliability of the simulated structure function for both these two ILs is outstanding. The main reason why here the results are much better than for EAN, is that here the columbic part is less important and, as said in chapter I, the force field can better reproduce the molecules and their interactions. As for EAN, the most interesting pair distribution functions are reported below.

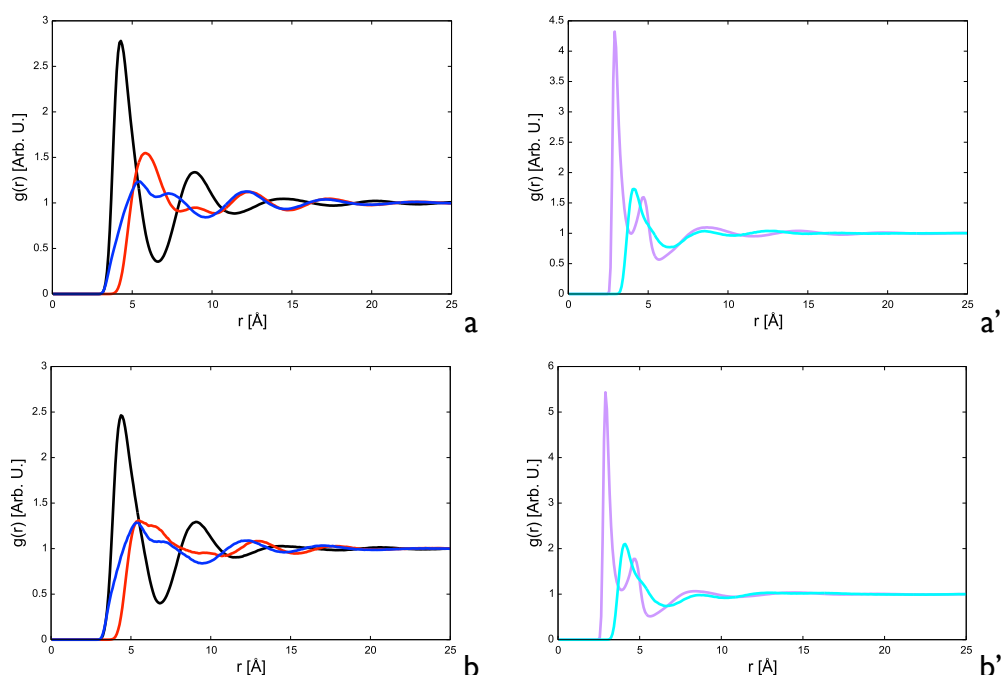


Figure 2.13: Pair distribution functions for PAN (a) and BAN (b). . (plain letters) cation-anion (black); anion-anion (blue); cation-cation (red); (primes) $\text{NH}_3\text{-NO}_3$ (N-O distance) (purple); $\text{CH}_3\text{-CH}_3$ (C-C distance) (cyan)

A comparison between the three hydrogen bond interaction, shows that the strength of the correlation is always the same (considering the length of the bond as a probe). Nevertheless, it is more likely to find a hydrogen bonded ion pair in BAN than in PAN than in EAN, probably for the increasing viscosity and consequent less mobility.

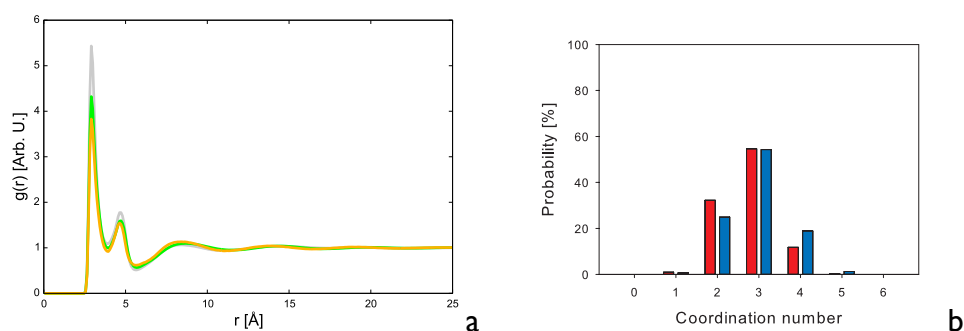


Figure 2.14: (a) Pair distribution functions for the $\text{NH}_3\text{-NO}_3$ interaction in EAN (orange), PAN (green) and BAN (gray); (b) Cation-anion interaction coordination number for PAN (red) and BAN (blue)

At the same time, the second solvation shell is slightly more ordered in EAN, this is because the dispersion forces are minimized in that system. To understand why in BAN there is the highest probability to find an hydrogen bonded ion pair, I have analysed the lifetime of the dimer.

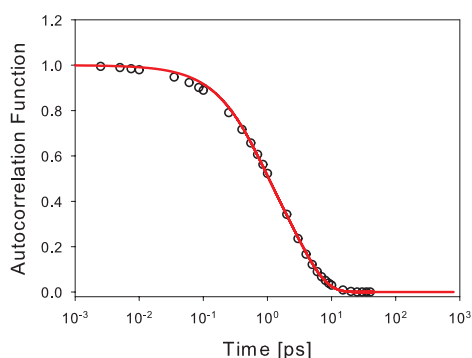


Figure 2.15: Hydrogen bond lifetime in PAN

a	0.3749
τ_1 [ps]	0.5413
τ_2 [ps]	3.1260
ΔG_1 [kJ/mol]	3.0394
ΔG_2 [kJ/mol]	7.4133
ΔG_{tot} [kJ/mol]	10.4527

Table 2.5: Fitting parameters and derived free energies of the hydrogen bond in PAN

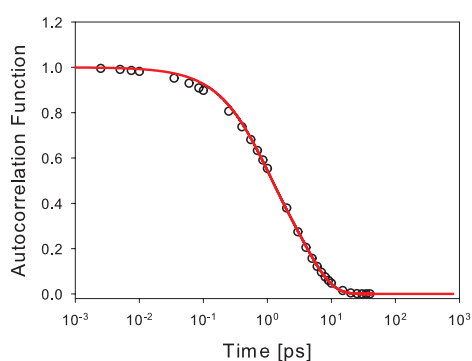


Figure 2.16: Hydrogen bond lifetime in BAN

a	0.4021
τ_1 [ps]	0.6398
τ_2 [ps]	3.8343
ΔG_1 [kJ/mol]	3.4564
ΔG_2 [kJ/mol]	7.9227
ΔG_{tot} [kJ/mol]	11.3791

Table 2.6: Fitting parameters and derived free energies of the hydrogen bond in BAN

The hydrogen bonds in BAN appears to be the strongest, but why? Here we are taking into account the lifetime of the interaction to calculate its energy. It is a valid and correct approach, but the Free Energy obtained that way is the overall energy needed to break the hydrogen bond, thus including a series of contributions and not only the interaction energy itself. The activation energy of the viscosity flow plays a major role here. To obtain this quantity, I have performed a series of viscosity measurements on these three ionic liquids as a function of temperature.

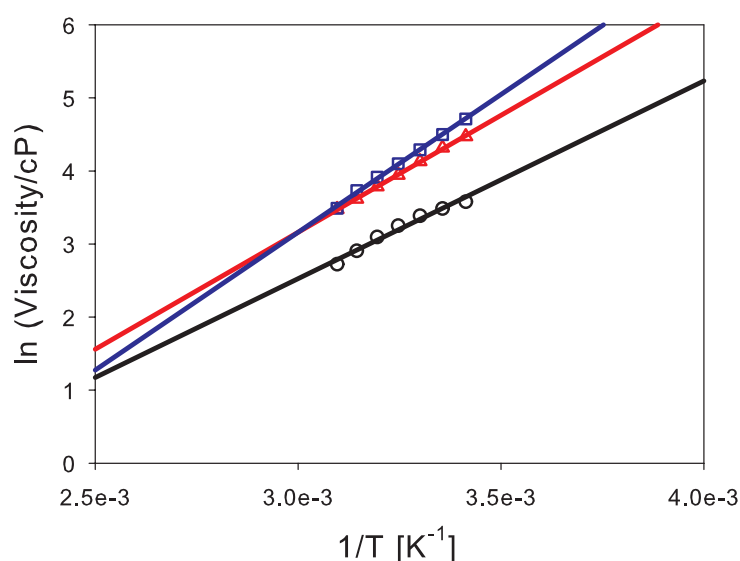


Figure 2.17: Arrhenius plot for viscosity of EAN (black), PAN (red) and BAN (blue)

Temperature [°C]	EAN [cP]	PAN [cP]	BAN [cP]
20	35.81	87.55	111.35
25	32.68	74.83	89.91
30	29.60	62.19	73.03
35	25.80	51.58	60.26
40	22.10	44.06	50.10
45	18.31	37.13	41.65
50	15.22	32.34	32.78

Table 2.7: Viscosities for EAN, PAN and BAN

The data were fitted using the Arrhenius law

$$\eta = \eta_0 \cdot e^{-\frac{E_a}{RT}} \quad [2.4]$$

where η is the viscosity expressed in cP, η_0 is the hypothetical viscosity at infinite temperature, E_a is the activation energy of the viscosity flow, R is the gas constant and T the temperature in Kelvin. Plotting the logarithm of the viscosity against the inverse of the temperature, one may extract the activation energy from the data. Results for EAN, PAN and BAN are reported below.

System	η_0	Activation Energy [kJ/mol]
EAN	-5.5869	22.4889
PAN	-6.4435	26.6201
BAN	-8.1622	28.1581

Table 2.8: Fitting parameters for viscosities of EAN, PAN and BAN

BAN is the most viscous, meaning that the molecules move more slowly compared to the other two PILs. As a consequence, the hydrogen bond interaction lasts longer and the free energy derived from its lifetime is higher than expected. A simple way to take this into account is to normalize the interaction energy by the relative activation energy, obtaining a number that better quantifies the strength of the hydrogen bond.

$$C_{HB} = \frac{\Delta G_{lifetime}}{\Delta H_{Arrhenius}} \quad [2.5]$$

Where $\Delta G_{lifetime}$ is the ΔG_{tot} in tables 2.3, 2.5 and 2.6, and $\Delta H_{Arrhenius}$ is the activation energy obtained by the fit and calculated at 298 K.

	EAN	PAN	BAN
C_{HB}	0.38	0.39	0.40

Table 2.9: C_{HB} parameter for EAN, PAN and BAN

To have a comparison, water has a C_{HB} equal to ~ 1.44 . Finally, we can say that the hydrogen bond itself has almost the same strength in the three ionic liquids examined, as can be expected considering that the interaction is always between NH_3^+ and NO_3^- . As for EAN, the diffusion coefficient was determined for PAN by means of NMR DOSY experiments.

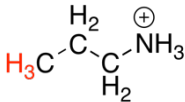
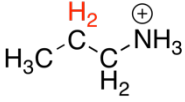
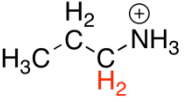
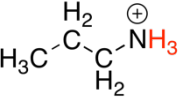
			
1.13 ppm	1.90 ppm	3.22 ppm	7.83 ppm

Table 2.10: ^1H NMR chemical shifts for PAN

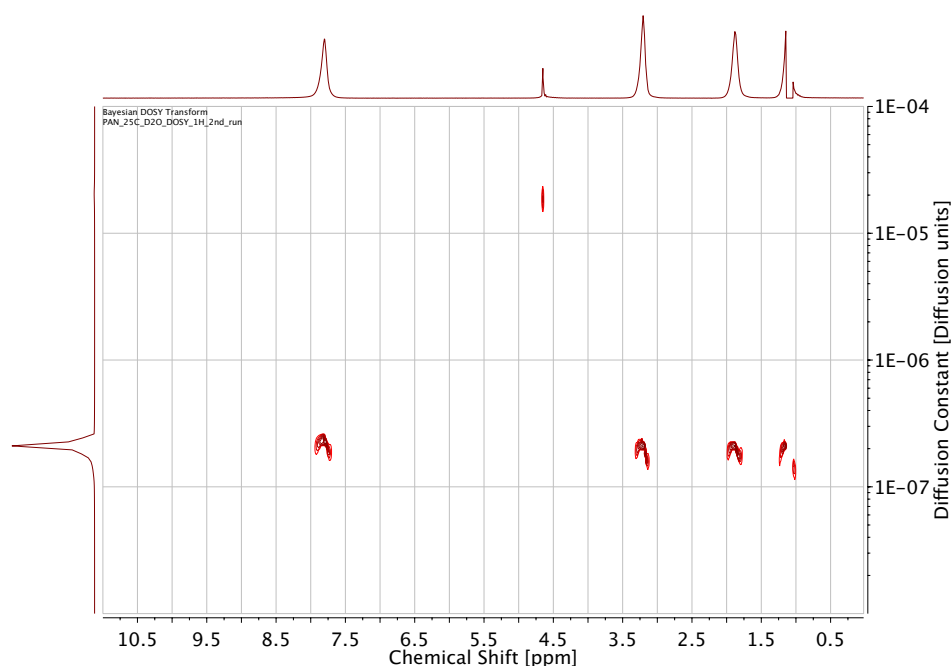


Figure 2.18: ^1H NMR DOSY for PAN

A value smaller than EAN is found for PAN, namely $1.95 \times 10^{-11} \text{ m}^2\text{s}^{-1}$. Again, this is due to highest viscosity of this PIL.

III. Effect of Pressure

Stimuli responsive materials are of great interest in chemistry and engineering. They found a variety of usages due to their versatility and unique properties. Recently it has been established that some ILs can respond to applied pressure modifying their mesoscopical structure. The pioneering work of Yoshimura²³ showed that the characteristic LqP of Imidazolium based ILs with BF_4 anion progressively vanishes when pressure is raised. An explanation was given by Triolo *et al.*²⁴ who states that high pressures induce the folding of the cation alkyl tail, thus reducing the dispersion forces preventing the formation of the polar/apolar domains segregation. They called this model “the Scorpion model” because of the resemblance with the arachnid. This name is quite inadequate for

a linear molecule, though. There is no a “scorpion body”. So we introduced another model for this kind of structure and named it “Asclepius model” due to the resemblance to the coiled snake in the universally known medicine symbol.



Figure 2.19: Scorpion and Asclepius models

III.I. Alkylammonium Nitrates

As said in the Introduction of this dissertation, PILs may show the LqP even if their alkyl chain(s) is(are) really short, as in the case of EAN⁴. Shorter chain(s) means stiffer chain(s), so the pressure effect should be much less pronounced on this set of compounds. To support this theory, I have performed a series of molecular dynamics simulations on EAN, PAN and BAN at four different external pressures: atmospheric, 1 kbar, 5 kbar and 10 kbar. Previous works ensured that the compounds are in the liquid phase when exposed to such compression^{25,26}. The computed structure factors for the three ILs as a function of pressure are shown in figure 2.20

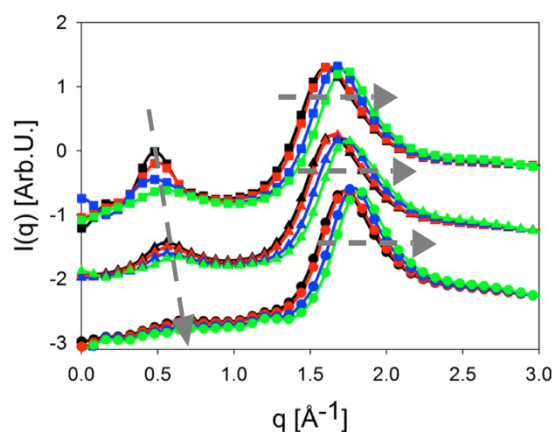


Figure 2.20: Computed SAXS patterns for EAN (circles); PAN (triangles); BAN (squares). 100kPa (black); 100 MPa (red); 500 MPa (blue); 1 GPa (green)

The arrows in figure 2.20 help to individuate the changes due to the pressure increase. Both the features in this q region are shifted to higher values of the exchange momentum, meaning that the corresponding distances obtained by:

$$d = \frac{2\pi}{q} \quad [2.6]$$

become smaller and smaller as the pressure is raised. The most interesting observation is about the peaks intensity. While the main peak remains almost constant, the LqP is strongly affected by the compression, and the effect is more pronounced the longer is the alkyl chain starting from an almost unaffected pattern for EAN, passing through sensitive effects in PAN, to some deep changes in BAN. I have analysed the intramolecular conformation of the cations and their relative population, searching for some significant difference that could confirm or deny the “chain folding” model. Due to the different length of the three cations, I have chosen different variables to follow the structural changes: the $N_{\text{cation}}-C_{\text{terminal}}$ pair distribution for EAN, the $N_{\text{cation}}-C_1-C_2-C_{\text{terminal}}$ dihedral angle distribution for PAN, and the $N_{\text{cation}}-C_2-C_{\text{terminal}}$ angular distribution for BAN.

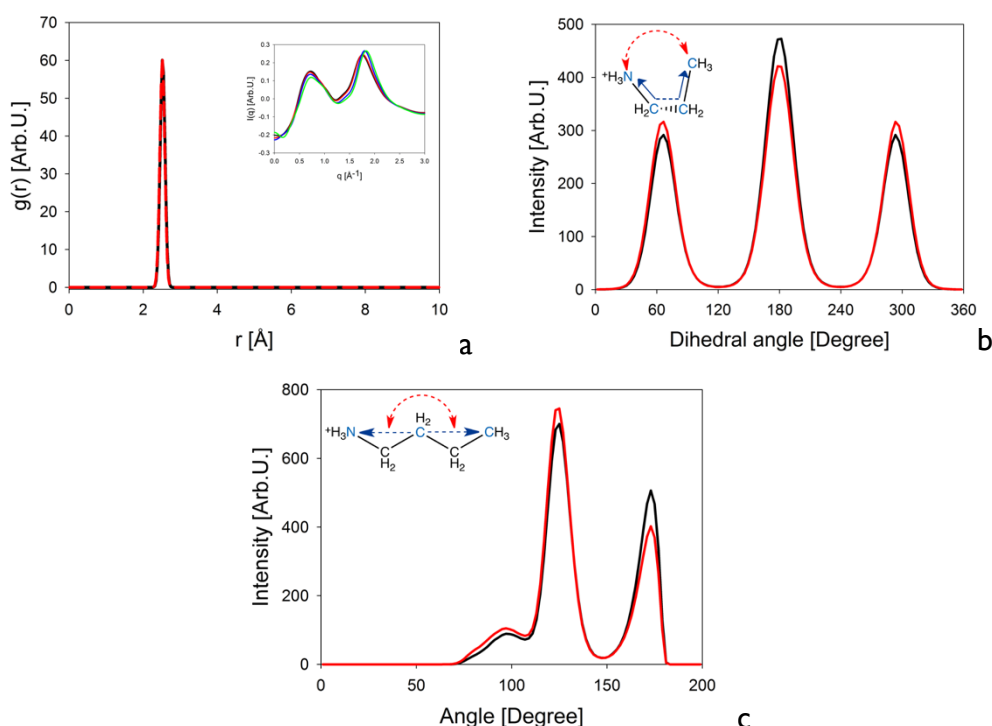


Figure 2.21: (a) Intramolecular pair distribution function for $N-C_{\text{terminal}}$ in EAN, in the inset computed small angle neutron scattering for EAN at 100 kPa (black); 100 MPa (red); 500 MPa (blue); 1 GPa (green). (b) Angular distribution function for PAN. (c) Dihedral distribution function for BAN. The angles taken into account for PAN and BAN are shown in the respective insets. 100 kPa (black); 1 GPa (red)

It is evident how the EAN pair distribution function shows absolutely no differences between the two pressures under consideration. It is consistent with the negligible effect on the SAXS (as well as SANS) pattern. The EAN alkyl tail is just two-carbon long, so it cannot be folded in any way. The PAN dihedral distribution function exhibits a clear enhanced intensity for the two (equivalent) peaks at $\sim 60^\circ$ and $\sim 300^\circ$, while a decreased intensity is found for the peak at 180° . In the table below the conformers associated to the peaks are shown along with their populations at 1 bar and 10 kbar.

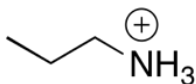
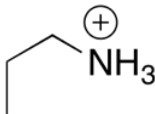
Conformation	Dihedral angle	1 bar population	10 kbar population
	180°	52.1%	43.8%
	$\sim 60^\circ; \sim 300^\circ$	47.9%	56.2%

Table 2.11: Population of PAN conformers

The shrunk conformation is preferred when the pressure is raised to 10 kbar. The same trend is observed when a further methylene group is added to the alkyl chain, i.e. with BAN. The angle distribution function in figure 2.21.c shows three distinct peaks, each one associated to a different cation conformation. The peak at 180° is due to the fully elongated form, the one at $\sim 125^\circ$ to a meso-form, and the one at $\sim 100^\circ$ is associated to the completely shrunk conformer. Even in this case the intensity of the fully elongated feature is decreased at high pressure, while the other two peaks are raised.

Conformation	Angle	1 bar population	10 kbar population
	180°	35.3%	31.1%
	$\sim 125^\circ$	44.5%	34.6%
	$\sim 100^\circ$	20.2%	34.3%

Table 2.12: Population of BAN conformers

At 10 kbar the system is almost an equimolar mixture of the three forms. All these results are consistent with the Scorpion/Asclepius model, thus confirming it and making it of general application. A further confirmation came from my study on n-Alcohols under the same conditions. The next step in the understanding of what happens when PILs are compressed, was the determination of the polar/apolar domains volumes. To achieve this, I have used the TRAVIS²⁷ Voronoi analysis tool. Details on the method can be found elsewhere²⁸. For the purpose of this dissertation, it is sufficient to know that the Voronoi analysis allows to determine the spatial extension of a correlation between certain atoms.

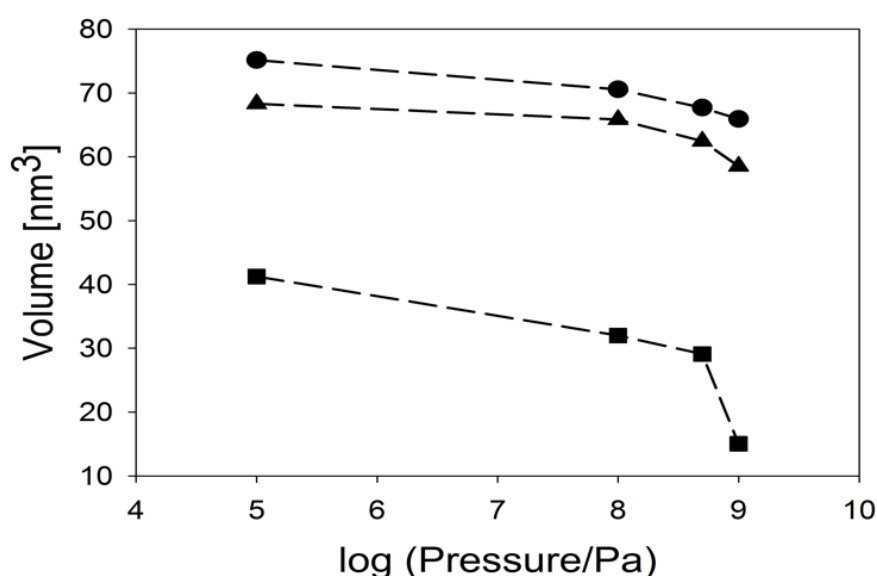


Figure 2.22: Volume of the apolar domain(s) in EAN (circles), PAN (triangles) and BAN (squares) as a function of pressure, computed with Voronoi analysis

From figure 2.22 it is evident how pressure compresses the apolar domain of all the three PILs but, more importantly, the effect is stronger the longer is the alkyl tail. A smaller apolar domain has a consequence to produce a LqP at higher q , as it is in fact observed. Such a compression can be explained only by the Asclepius model. Finally, the calculation of the spatial distribution functions for some atoms elucidated the molecular three-dimensional arrangement, highlighting the deep structural differences between ambient pressure and 10 kbar.

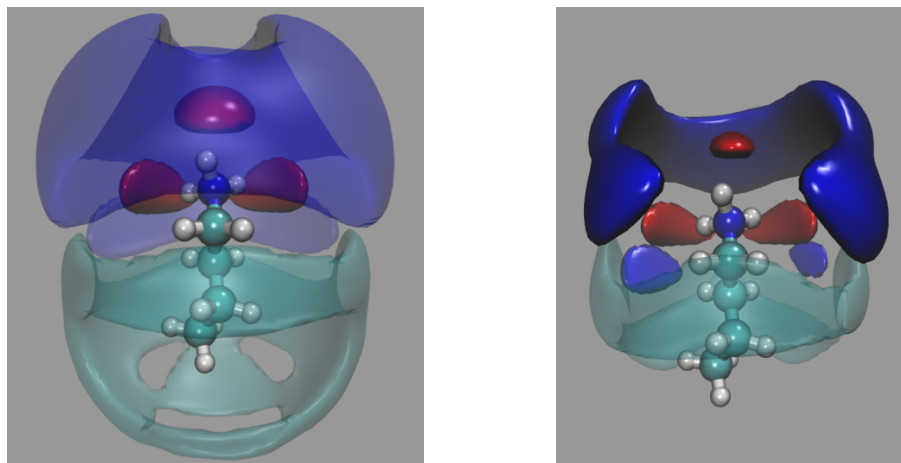


Figure 2.23: Spatial distribution functions for BAN. Room pressure (left); 1 GPa (right). Cation nitrogen (blue); anion oxygen (red); cation terminal methyl group (cyan)

The aliphatic aggregation of the alkyl tails is almost completely obliterated at high pressures, even the bridging correlation cation – anion – cation is strongly diminished in such drastic conditions. All these considerations lead to the conclusion that the pressure has a destructive effect on the PILs structure, inducing a chain folding (more pronounced the longer is the chain) that reduces the dispersive forces needed to establish the polar/apolar domain segregation, thus driving the system through a homogenous state.

IV. Contextualization

The structural organization of simple protic ionic liquid has been widely studied over the last decade¹¹. In particular, ethylammonium nitrate is possibly one of the most studied ILs of all times. Mainly five research groups have investigated the structure of monoalkylammonium nitrate ionic liquids: Rob Atkin *et al.*^{2,4,8,9,29–31} (University of Newcastle, Australia), Calum J. Drummond *et al.*^{3,11,32–35} (RMIT University, Melbourne, Australia), Yasuhiro Umebayashi *et al.*^{36–38} (Niigata University, Japan), Ralf Ludwig (Rostock University, Germany) *et al.*^{17,39–43}, and our group^{14,18,44,45}. As said, PILs show the LqP even when the alkyl tail is just an ethyl group. This is due to the complex and distorted 3D hydrogen bond network in the bulk^{17,38}. Such interaction generates a mesoscopic grade of order (tens of Angstroms) which is responsible of the feature between 0.3 and 0.7 Å⁻¹ found in these compounds. Our group has demonstrated that the main contribution to the LqP is from the anion-anion distance¹⁴, that is modulated by the alkyl chain

length (the longer the chain, the higher and left-shifted is the LqP), see table 2.1. My work aimed at clarifying what are the implications of the *sponge-like* structure in PILs and to understand the role of the hydrogen bond. To do this I have taken advantage of classical Molecular Dynamics simulations, because this technique is the state of the art to study large scale (5-10 nm) systems obtaining both static (structure) and dynamical (hydrogen bond lifetime, diffusivity) results. This procedure has been extensively used in recent years obtaining outstanding results for aprotic ILs⁴⁶⁻⁴⁸, while for PILs the speciation from the equilibrium



Scheme 2.1: Protic ionic liquids equilibrium

makes the things hard. Nevertheless, the results that I have obtained are good enough to make quantitative interpretations starting from my models. In general, I have obtained structural pictures completely in line with the literature, confirming, once more, the nano-heterogeneity of EAN, PAN and BAN. Of course BAN shows the most pronounced domain segregation, and it is also the system that is most affected by compression. Both the observations are linked to its alkyl tail, more hydrophobic (more segregation), and more flexible (more mechanical-responsive). The results for the pressure-induced disorder obtained for these short molecules confirms the model proposed by Triolo²⁴ on the basis of the same effect on ether-substitute-chain aprotic ILs¹². A further confirmation of the Scorpion/ Asclepius model came from my study on the pressure effect on n-Alcohols from propanol to octanol. The results obtained for the diffusivity are the first one of this kind in the literature, so a comparison is not possible. In any case the trend is easily explained in terms of the different viscosity, which is in line with other sources^{16,49}.

V. Summary

In this chapter I have exposed my findings on the ionic liquid family of Alkylammonium Nitrates. In particular, during my PhD I have worked a lot with ethylammonium nitrate (see following chapters) mainly for four reasons:

1. It is cheap, about 150€/l, whereas other ILs can cost up to 1000€/l and over.
2. It is easy to synthesize by the simple titration of nitric acid with ethylamine.
3. A huge amount of literature is available.
4. Yet structurally simple, it is a perfect prototype for protic ionic liquids.

PAN and BAN are the only other two single-chained compounds of this family that are liquid at room temperature. It is interesting to see the effect of the alkyl chain length on a series of properties. Here we have seen that:

- Protic ionic liquids are mesoscopically heterogeneous. This feature is shared with a number of other ILs, the particularity here is the fact that while aprotic ILs should have an alkyl tail longer than four carbon atoms, ethylammonium nitrate shows clearly the LqP in the SAXS pattern. This is mainly due to the extended hydrogen bond network, that facilitates the domain segregation.
- The hydrogen bond in all the three liquids is moderately strong. It appears to be almost linear ($>135^\circ$) albeit slightly too long (2.9-3.1 Å). Taking into account the viscosity effect, the strength of the interaction is almost identical in EAN, PAN and BAN.
- The viscosity rises rapidly with the alkyl tail length. This effect is analogue to the one in n-Alkanes, where from methane to butane they are gaseous, from pentane to heptadecane are liquids with increasing viscosities and from octadecane on they are solids. While n-Alkanes experiences just dispersive forces and Van der Waals interactions, alkylammonium nitrates are subjected to hydrogen bonding and columbic forces, too. So pentylammonium nitrate is a solid.
- The diffusivity (measured just for the cation) follows the trend of the viscosity.
- High pressures destroy the mesoscopic organization of the studied PILs (as well as other ILs). This is because the alkyl tail is forced to fold, reducing the dispersive forces that are fundamentals to achieve the domain segregation.

VI. References

- 1 A. Triolo, O. Russina, H.-J. Bleif and E. Di Cola, *J. Phys. Chem. B*, 2007, **111**, 4641–4.
- 2 R. Hayes, S. Imberti, G. G. Warr and R. Atkin, *Phys. Chem. Chem. Phys.*, 2011, **13**, 13544–51.
- 3 T. L. Greaves, D. F. Kennedy, A. Weerawardena, N. M. K. Tse, N. Kirby and C. J. Drummond, *J. Phys. Chem. B*, 2011, **115**, 2055–66.
- 4 R. Hayes, S. Imberti, G. G. Warr and R. Atkin, *Phys. Chem. Chem. Phys.*, 2011, **13**, 3237–47.
- 5 O. Russina, A. Triolo, L. Gontrani and R. Caminiti, *J. Phys. Chem. Lett.*, 2012, **3**, 27–33.
- 6 O. Russina and A. Triolo, *Faraday Discuss.*, 2012, **154**, 97–109.
- 7 T. Méndez-Morales, J. Carrete, J. R. Rodríguez, Ó. Cabeza, L. J. Gallego, O. Russina and L. M. Varela, *Phys. Chem. Chem. Phys.*, 2015, **17**, 5298–307.
- 8 R. Atkin and G. G. Warr, *J. Phys. Chem. B*, 2008, **112**, 4164–4166.
- 9 R. Atkin and G. G. Warr, *ACS Symp. Ser.*, 2009, **1030**, 317–333.
- 10 E. Bodo, S. Mangialardo, F. Ramondo, F. Ceccacci and P. Postorino, *J. Phys. Chem. B*, 2012, **116**, 13878–88.
- 11 T. Greaves and C. J. Drummond, *Chem. Rev.*, 2015, **115**, 11379–11448.
- 12 K. Shimizu, C. E. S. Bernardes, A. Triolo and J. N. Canongia Lopes, *Phys. Chem. Chem. Phys.*, 2013, **15**, 16256–62.
- 13 H. K. Kashyap, J. J. Hettige, H. V. R. Annapureddy and C. J. Margulis, *Chem. Commun.*, 2012, **48**, 5103–5.
- 14 M. Campetella, L. Gontrani, F. Leonelli, L. Bencivenni and R. Caminiti, *Chemphyschem*, 2015, **16**, 197–203.
- 15 P. Walden, *Bull. Acad. Imper. Sci St. Petersburg.*, 1914, **8**, 405–422.

- 16 Y. Xu, B. Chen, W. Qian and H. Li, *J. Chem. Thermodyn.*, 2013, **58**, 449–459.
- 17 K. Fumino, A. Wulf and R. Ludwig, *Angew. Chem. Int. Ed. Engl.*, 2009, **48**, 3184–6.
- 18 A. Mariani, R. Caminiti, M. Campetella and L. Gontrani, *Phys. Chem. Chem. Phys.*, 2016, **18**, 2297–2302.
- 19 D. Van Der Spoel, P. J. Van Maaren and P. Larsson, *J. Phys. Chem. B*, 2006, **110**, 4393–4398.
- 20 G. L. Bretthorst, *J. Magn. Reson.*, 1990, **88**, 533–551.
- 21 D. Xing, S. J. Gibbs, J. A. Derbyshire, E. J. Fordham, T. A. Carpenter and L. D. Hall, *J. Magn. Reson. Ser. B*, 1995, **106**, 1–9.
- 22 Y. H. Zhao, M. H. Abraham and A. M. Zissimos, *J. Org. Chem.*, 2003, **68**, 7368–7373.
- 23 Y. Yoshimura, M. Shigemi, M. Takaku, M. Yamamura, T. Takekiyo, H. Abe, N. Hamaya, D. Wakabayashi, K. Nishida, N. Funamori, T. Sato and T. Kikegawa, *J. Phys. Chem. B*, 2015, **119**, 8146–8153.
- 24 O. Russina, F. Lo Celso and A. Triolo, *Phys. Chem. Chem. Phys.*, 2015, **17**, 29496–29500.
- 25 E. Bodo, P. Postorino, S. Mangialardo, G. Piacente, F. Ramondo, F. Bosi, P. Ballirano and R. Caminiti, *J. Phys. Chem. B*, 2011, **115**, 13149–61.
- 26 F. Capitani, C. Fasolato, S. Mangialardo, S. Signorelli, L. Gontrani and P. Postorino, *J. Phys. Chem. Solids*, 2015, **84**, 13–16.
- 27 M. Brehm and B. Kirchner, *J. Chem. Inf. Model.*, 2011, **51**, 2007–2023.
- 28 C. Schröder, G. Neumayr and O. Steinhauser, *J. Chem. Phys.*, 2009, **130**, 194503.
- 29 P. Niga, D. Wakeham, A. Nelson, G. G. Warr, M. Rutland and R. Atkin, *Langmuir*, 2010, **26**, 8282–8288.
- 30 R. Hayes, S. Imberti, G. G. Warr and R. Atkin, *Angew. Chemie*, 2013, **125**, 4721–4725.

- 31 R. Hayes, S. Imberti, G. G. Warr and R. Atkin, *J. Phys. Chem. C*, 2014, **118**, 13998–14008.
- 32 T. L. Greaves, A. Weerawardena, I. Krodkiewska and C. J. Drummond, 2008, 896–905.
- 33 D. F. Kennedy and C. J. Drummond, *J. Phys. Chem. B*, 2009, **113**, 5690–3.
- 34 T. L. Greaves, D. F. Kennedy, S. T. Mudie and C. J. Drummond, *J. Phys. Chem. B*, 2010, **114**, 10022–31.
- 35 Y. Shen, D. F. Kennedy, T. L. Greaves, A. Weerawardena, R. J. Mulder, N. Kirby, G. Song and C. J. Drummond, *Phys. Chem. Chem. Phys.*, 2012, **14**, 7981–92.
- 36 Y. Umebayashi, W.-L. Chung, T. Mitsugi, S. Fukuda, M. Takeuchi, K. Fujii, T. Takamuku, R. Kanzaki and S. Ishiguro, *J. Comput. Chem. Japan*, 2008, **7**, 125–134.
- 37 S. Ishiguro, Y. Umebayashi, R. Kanzaki and K. Fujii, *Pure Appl. Chem.*, 2010, **82**, 1927–1941.
- 38 X. Song, H. Hamano, B. Minofar, R. Kanzaki, K. Fujii, Y. Kameda, S. Kohara, M. Watanabe, S. Ishiguro and Y. Umebayashi, *J. Phys. Chem. B*, 2012, **116**, 2801–13.
- 39 K. Fumino, E. Reichert, K. Wittler, R. Hempelmann and R. Ludwig, *Angew. Chemie - Int. Ed.*, 2012, **51**, 6236–6240.
- 40 V. N. Emel'Yanenko, G. Boeck, S. P. Verevkin and R. Ludwig, *Chem. - A Eur. J.*, 2014, **20**, 11640–11645.
- 41 K. Fumino, S. Reimann and R. Ludwig, *Phys. Chem. Chem. Phys.*, 2014, **16**, 21903–29.
- 42 K. Fumino, V. Fossog, P. Stange, K. Wittler, W. Polet, R. Hempelmann and R. Ludwig, *ChemPhysChem*, 2014, **15**, 2604–2609.
- 43 K. Fumino, V. Fossog, P. Stange, D. Paschek, R. Hempelmann and R. Ludwig, *Angew. Chemie Int. Ed.*, 2015, **54**, 2792–2795.
- 44 L. Gontrani, E. Bodo, A. Triolo, F. Leonelli, P. D. Angelo, V. Migliorati and R. Caminiti, *J. Phys. Chem. B*, 2012, **116**, 13024–13032.

- 45 M. Campetella, L. Gontrani, E. Bodo, F. Ceccacci, F. C. Marincola and R. Caminiti, *J. Chem. Phys.*, 2013, **138**, 184506.
- 46 R. M. Lynden-Bell, M. G. Del Pópolo, T. G. a Youngs, J. Kohanoff, C. G. Hanke, J. B. Harper and C. C. Pinilla, *Acc. Chem. Res.*, 2007, **40**, 1138–45.
- 47 T. Köddermann, D. Paschek and R. Ludwig, *Chemphyschem*, 2007, **8**, 2464–70.
- 48 S. Zahn, M. Brehm, M. Brüssel, O. Hollóczki, M. Kohagen, S. Lehmann, F. Malberg, A. S. Pensado, M. Schöppke, H. Weber and B. Kirchner, *J. Mol. Liq.*, 2014, **192**, 71–76.
- 49 J. A. Smith, G. B. Webber, G. G. Warr and R. Atkin, *J. Phys. Chem. B*, 2013, **117**, 13930–13935.

Chapter III: Binary Systems



*'Why don't we just mix up absolutely everything and see what happens?' he said.
And Ridcully responded with the traditional response.
'It's got to be worth a try,' he said.
("Hogfather" – Sir Terry Pratchett)*

I. From Neat Compounds to Mixtures

To study and use an Ionic Liquid, one must presuppose that this compound is as pure as possible. Impurities, water in the first place, were seen as to be avoided because "enemies" of the ILs¹. Initially, it was thought that it was possible to modify the properties of these compounds at will by altering only the constituent ions, thus having a structural-design approach²; in this way, however, it was tricky to achieve a fine control on the chemical-physical properties changes. They could also be dramatically different as a result of point changes of the structure.

	Appearance at Room Temperature	SAXS Low q Peak	1-Octanol miscibility
Ethylammonium Nitrate	Liquid	yes	partial
Butylammonium Nitrate	Liquid	yes	full
Pentylammonium Nitrate	Solid	yes	full
Ethanolammonium Nitrate	Solid	no	no

Table 3.1: Examples of Physical and Chemical changes in structurally similar ionic liquids

The wide variety of anions and cations that may be used, makes it easy to imagine the vastness of "specific tasks"^{3,4} that this class of compounds can fulfil. To do so, the main method is probably to add some specific functional groups in order to satisfy the specific need. Functionalized ILs are known in electrochemical applications⁵⁻⁹, gas absorption^{10,11}, coordination of metals^{12,13}, liquid crystals¹⁴⁻¹⁶ and in the pharmaceutical field^{17,18}. For example, if we need an ionic liquid capable of bonding itself to a gold surface, then we will add a thiol functional group to

the end of the alkyl tail. We need an ionic liquid that is very hydrophobic? Add long and branched alkyl tails. A really hydrophilic one? Change the alkyl tails with ether ones. Some of these ILs generally has higher melting points and/or viscosity due to the increase of the molecular mass and of the stoichiometric volume which inevitably increases the interactions between the various constituent entities. Moreover, to start a new synthesis (not knowing if the resulting compound will fulfil our expectations) for each potential application is time/resources consuming. In order to achieve almost the same properties tunability, a new strategy is to mix the liquid salts with other compounds^{19,20}, be they in turn ILs or molecular liquids such as organic solvents or water depending on the needs. Ideally, the mixing of two miscible liquids leads to a solution whose chemical and physical properties are predictable given the knowledge of the starting components and the final percentage composition. Moreover, a full set of unexpected features may appear upon mixing, making this procedure even more interesting. This field is currently one of the most active in this area of research and one of the most challenging. To date, just a really small fraction of the possible systems has been (partially) studied. An indicative list of the studied systems (considering some EAN and PAN mixtures only) is reported in table 3.2.

Ionic Liquid	Molecular Liquid
EAN	Water ^{21,22}
	Methanol ^{23–25}
	Ethanol ^{26,27}
	I-Propanol ²⁶
	I-Butanol ^{26,27}
	I-Pentanol ²⁸
	I-Octanol ^{27,29,30}
	DMSO ³¹
	Ethylene Glycol ³²
	1,2-Dimethoxy Ethane ³³
	1,4-Diamino Butane ³³
PAN	Water ^{22,34}
	I-Butanol ^{26,27}
	I-Octanol ²⁷
	I-Dodecanol ²⁷

Table 3.2: Examples of studied mixtures of ionic liquids and molecular liquids

II. Similia Similibus Solvuntur

When a molecular compound is mixed with an ionic liquid there are a series of possible events. On the macroscopic scale they may appear as a homogenous or a heterogeneous system.



Figure 3.1: Examples of homogenous and heterogenous mixtures, both micro and macroscopic

On the left side of Figure 3.1 the EAN:Ethanethiol 1:1 system is shown, both the real system and a portion of the simulated one. This sample clearly exhibits a phase separation consisting in molecular liquid floating on the ionic liquid because the latter is the denser one (0.86 g/ml vs. 1.21 g/ml, respectively). On the other side of the figure, the homogenous EAN:Ethanol 1:1 system is shown. Albeit oxygen and sulphur belong both to the VI group of the periodic table, the difference in electronegativity (3.44 and 2.58 respectively) leads to dramatically different interactions between molecules.

	Melting Point [°C]	Boiling Point [°C]	Vapour Pressure [kPa]	Dipole Moment [Debye]	Dielectric Constant
Ethanol	-114	78	5.95	1.69	24.5
Ethanethiol	-148	35	58.16	1.57	6.9

Table 3.3: Properties of ethanol and ethanethiol

Probably, the lack in the ability to form strong hydrogen bonds together with the low dielectric constant prevent EAN and Ethanethiol from mixing. Protic ionic liquids are supposed to mix with substances having alkyl region of similar size as the one of the PIL²⁷, that are able to accept and/or donate hydrogen bonds³⁵, sufficiently polar (in terms of dipole moment)³⁶, and with a moderate-high dielectric constant²². Short and medium chained alcohols are, thus, the perfect partner to study the mixing process and, in fact, they are the most used

compounds^{26,27,37,38}. Other small amphiphilic molecules have been studied as reported in table 3.2, while a relative small amount of data for non-amphiphilic compounds can be found^{22,26,33,39}. On the other hand, at the mesoscopic and microscopic levels we may undergo a variety of situations, from simple complete mixing²² to stoichiometric complexes formation³¹, from clustering⁴⁰ to nano-emulsions²⁸. In the following paragraphs I will cover the results that I've obtained on macro-meso-microscopical homogenous EAN-molecular liquid mixtures, and in the next chapter I will expose findings on macroscopical homogenous yet meso-microscopically heterogeneous systems

III. Results

III.1. EAN+DMSO

DMSO is a common molecular liquid with wide applications as a solvent in a variety of fields^{41,42}. Its interesting behaviour when mixed with water⁴³⁻⁴⁵, is the main cause for choosing it as a probe for the mixing properties of EAN. In fact, as said, EAN and water have a number of similarities, and to clarify why they share so many properties, a study on this system could help. DMSO:water systems show an interesting phase diagram, in which a deep eutectic point at ~2:1 composition. Here

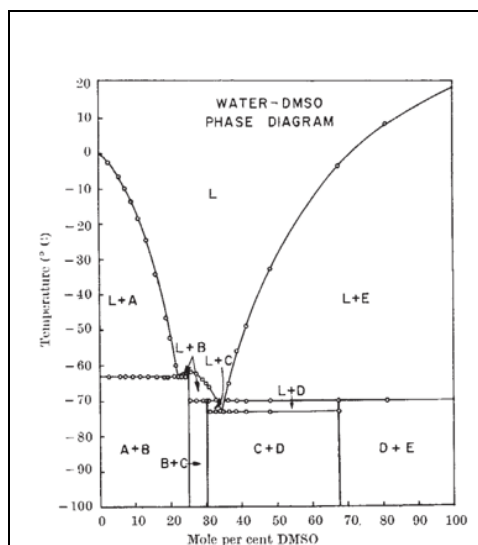


Figure 3.2: Water:DMSO phase diagram from reference 44

the melting point of the mixture is -75 °C, whereas the ones for the two components are 19 °C and 0 °C respectively⁴⁶⁻⁴⁸. This phenomenon is mostly due to the interaction of the large dipole moment (3.96 D) with the hydrogen bond network of water, stressing and deforming it at the point to avoid the crystallization^{45,47-49}. In order to understand if DMSO behaves in the same way with EAN, I have performed some analysis. The small angle X-ray scattering patterns collected show a clear, neat dependency of the LqP from EAN concentration.

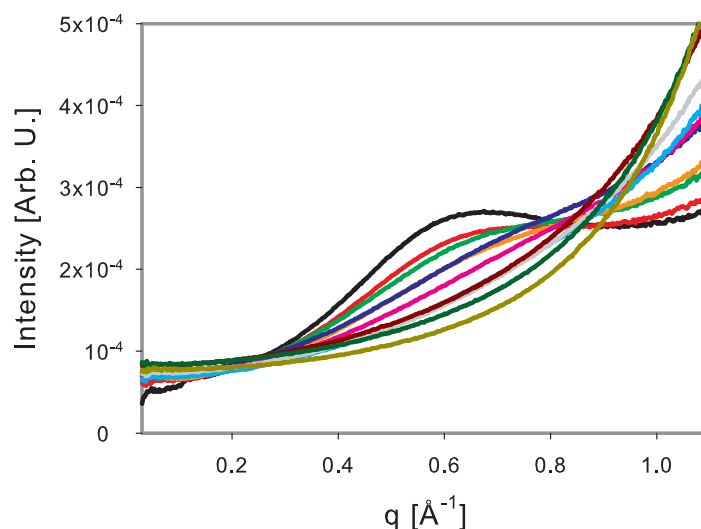


Figure 3.3: SAXS patterns for EAN+DMSO systems. EAN (black); DMSO (gold); ED9 (red); ED8 (green); ED7 (blue); ED6 (orange); ED5 (pink); ED4 (cyan); ED3 (gray); ED2 (brown); ED1 (dark green)

It appears clear from figure 3.3 that as DMSO is added to EAN, the characteristic LqP is gradually right-shifted and lowered in intensity. This means that the native sponge-like structure of the ionic liquid is completely wiped away when EAN is the minority compound. Measuring the density of the prepared compounds one may calculate the excess molar volume for the mixtures by:

$$V^{Ex} = \frac{\chi_1 \cdot MW_1 + \chi_2 \cdot MW_2}{\rho_{sys}} - \sum \frac{\chi_i \cdot MW_i}{\rho_i} \quad [3.1]$$

For EAN-DMSO systems the measured densities and the calculated excess molar volumes are reported in table 3.4.

System	χ_{EAN}	Density [g/ml]	Excess molar volume [ml/mol]
EAN	1.0	1.2102	0.0000
ED9	0.9	1.2031	-0.1625
ED8	0.8	1.1962	-0.3670
ED7	0.7	1.1882	-0.5147
ED6	0.6	1.1798	-0.6647
ED5	0.5	1.1711	-0.8187
ED4	0.4	1.1617	-0.9566
ED3	0.3	1.1506	-1.0124
ED2	0.2	1.1364	-0.9063

EDI	0.1	1.1192	-0.6466
ED05	0.05	1.1091	-0.4335
DMSO	0.0	1.0953	0.0000

Table 3.4: Name, composition, density and excess molar volumes for EAN+DMSO systems

Plotting the excess molar volume as a function of the ionic liquid molar fraction, one can obtain an insightful graph that can help answer some questions

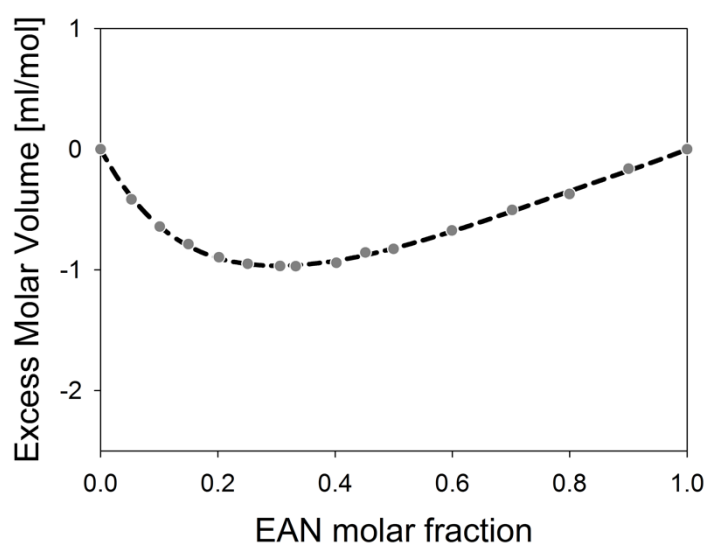


Figure 3.4: Excess molar volume for EAN+DMSO systems at 25 °C

The obtained results are always negative, meaning that the overall interaction between EAN and DMSO is favourable (this is witnessed also by the fact that the systems became hot when mixed during the samples preparation). Figure 3.4 shows a clear minimum at 2:1 composition (DMSO:EAN), so the same composition for the deep eutectic mentioned above for the DMSO:water system⁴⁴. To get an insight into these observations, I've performed a series of DFT and molecular dynamics simulations. The reliability of MD simulations was checked comparing computed and experimental WAXS patterns and densities.

System	Exp. Density [g/ml]	Calc. Density [g/ml]
EAN	1.2106	1.2143
ED9	1.2031	1.2056
ED8	1.1962	1.1986
ED7	1.1882	1.1889
ED6	1.1798	1.1802
ED5	1.1711	1.1715
ED4	1.1617	1.1615
ED3	1.1506	1.1500
ED2	1.1364	1.1363
ED1	1.1192	1.1190
DMSO	1.0953	1.0952

Table 3.5: Comparison between experimental and computed mass densities for EAN+DMSO systems

MD simulations shows clearly a progressive disruption of the sponge-like structure upon DMSO content increasing. This may be checked by simple visual inspection of the simulation boxes.

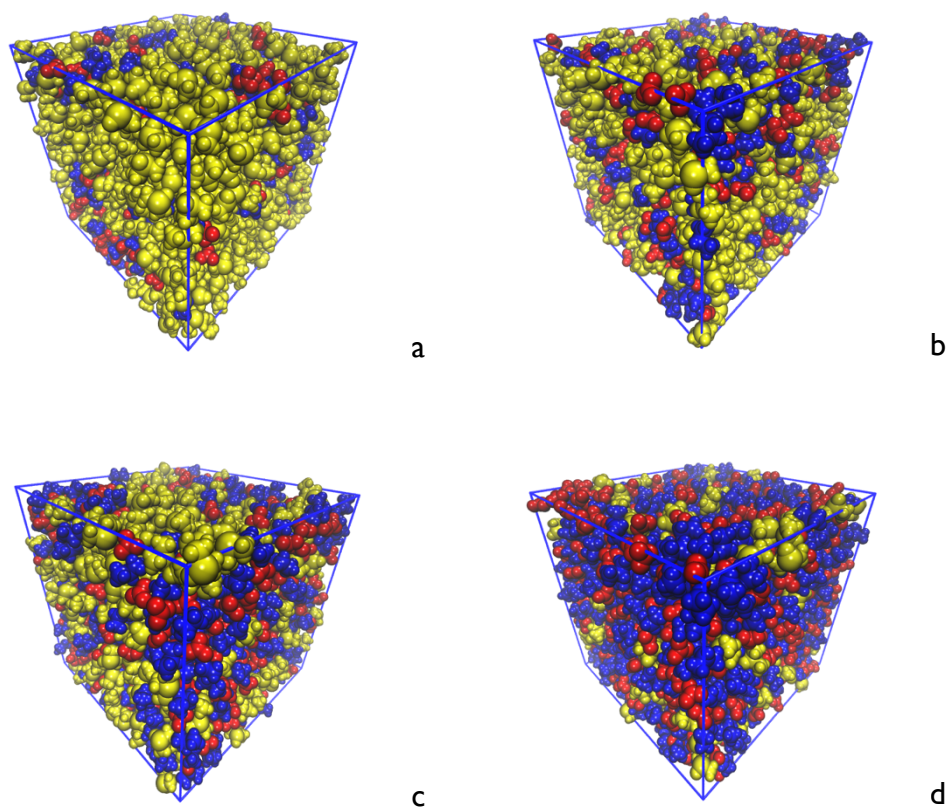
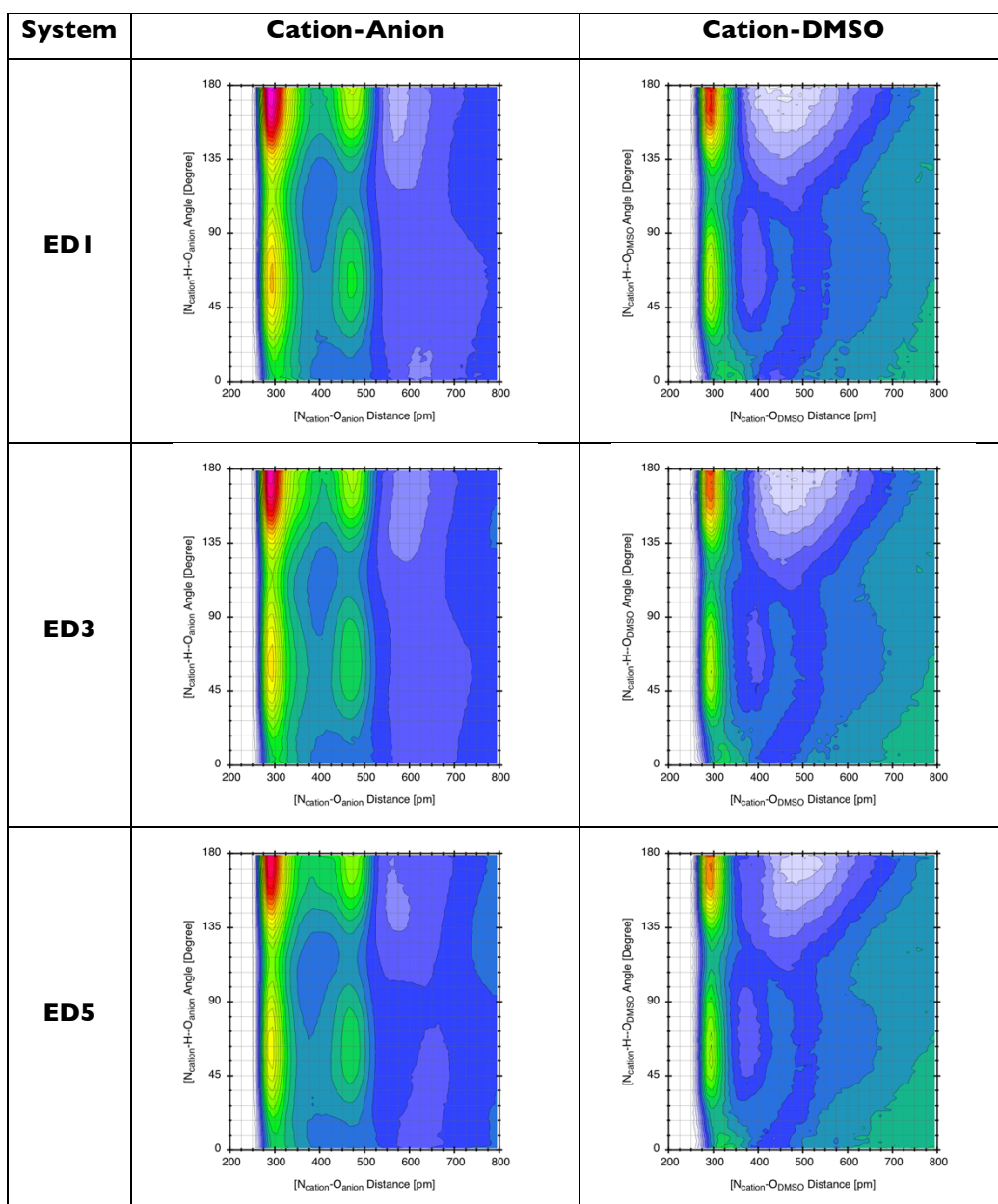


Figure 3.5: Snapshots of the simulation boxes for EAN+DMSO systems. (a) ED2; (b) ED3; (c) ED5; (d) ED8. Cation (blue); anion (red); DMSO (yellow)

A series of further analyses was performed in order to obtain a complete picture of the overall molecular arrangement. Similarly to neat ionic liquids in Chapter II, the analysis of the hydrogen bond by means of geometry plays a central role. In this system there are two different possible interactions of this kind, namely cation-anion and cation-DMSO. Results are shown in the following figures



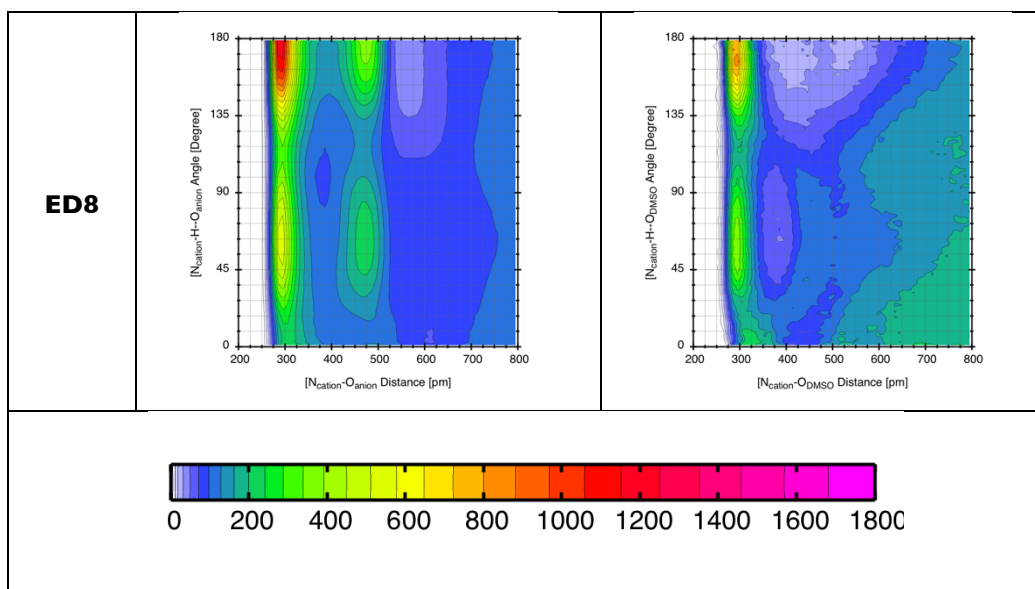
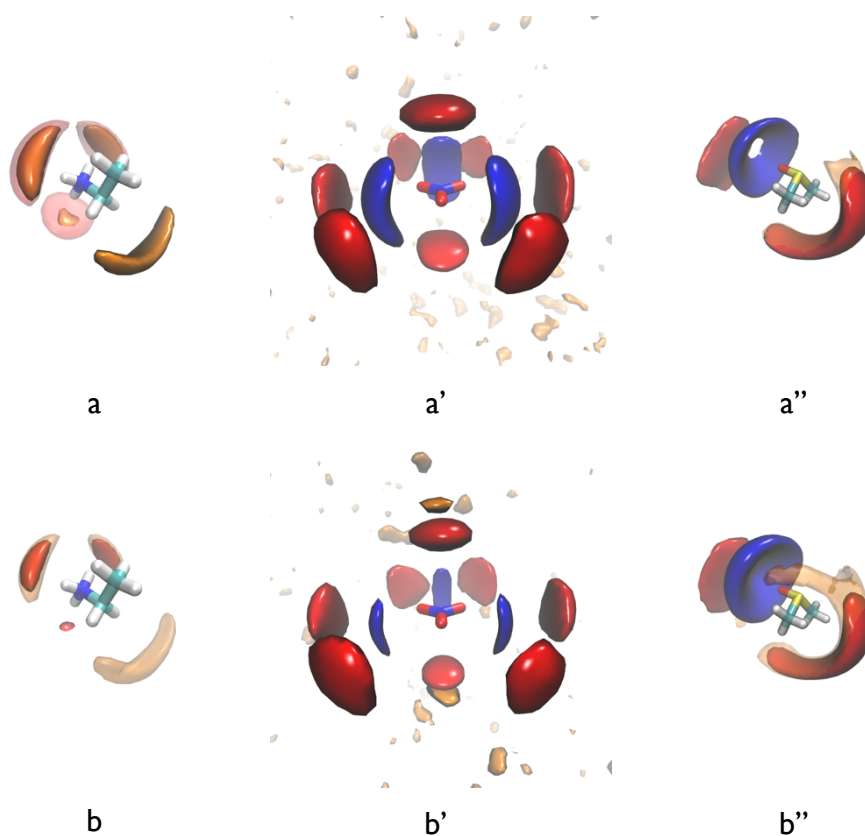


Figure 3.6: Combined radial-angular distribution functions for EAN+DMSO systems

From the above maps, we can say that the strength of the two hydrogen bonds is pretty similar, in fact we can always observe an almost linear (angle $>135^\circ$) correlation together with a N-O distance between 2.9 and 3 Å. Finally, a three dimensional view of the system was achieved through some spatial distribution functions.



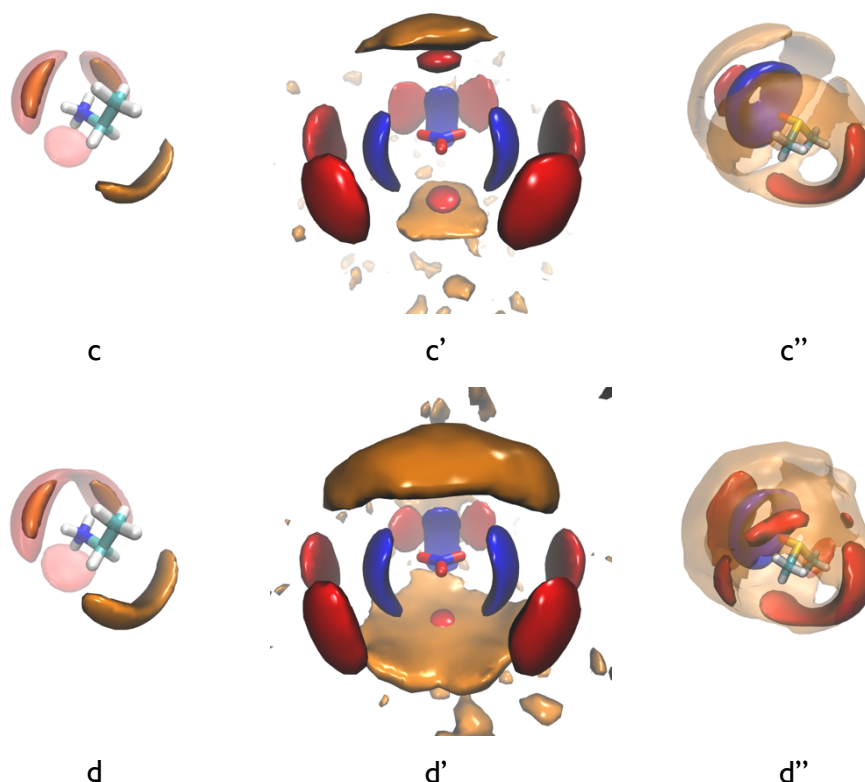


Figure 3.7: Spatial distribution functions for EAN+DMSO systems. (a) ED2; (b) ED3; (c) ED5; (d) ED8. Plain letters refers to cation environment; primes to anion environment; double prime to DMSO environment. DMSO oxygen (orange); cation nitrogen (blue); anion oxygen (red)

From figure 3.7 we are able to say that the cation is strongly solvated by anions and DMSO. It should be pointed out how the anions occupy always three regions, corresponding to the hydrogens of the ammonium group, while DMSO appears to prefer just two of them, and slightly interacts with the third hydrogen only when in large excess. Notably anions are always the closest species to the cation except in the 2:3 composition, suggesting once more the formation of stable stoichiometric complexes of approximate formula $[\text{cation} \cdot \text{DMSO}_2]^+ [\text{anion}]^-$. In the second column there are two interesting features. The first one is that DMSO shows absolutely no correlations with the anion when in large excess and prefers to occupy axial positions when EAN is added to the mixture. This is probably due to the fact that in these positions, the partial positive charge of the nitrogen atom of the nitrate is less shielded by the oxygens. The second is that the correlation between anion and cation is always almost identical with the exception of the 2:1 composition, where it is strongly depleted, in line with the association stated above. In the last column, the situation around the DMSO is

shown. The only remarkable feature is that the DMSO-cation correlation is clearly stronger in the ED3 system. I have performed a DFT calculation of the stoichiometric complex, obtaining its equilibrium geometry, which is reported in figure 3.8.

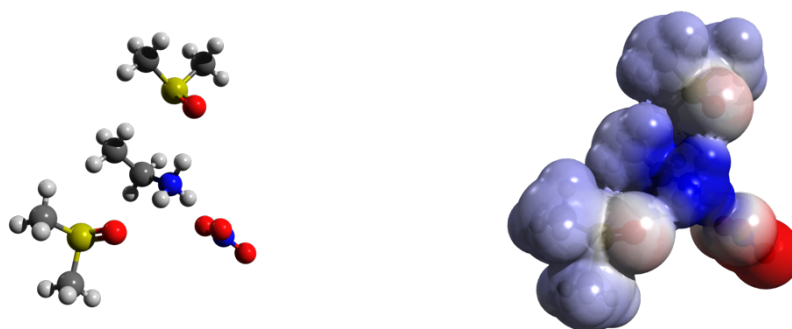


Figure 3.8: $[EA(DMSO)_2]^+[NO_3]^-$ complex. The right side of the figure reports the electrostatic surfaces

III.II. EAN+Ethylene Glycol

Ethylene glycol (1-2,ethanediol), usually called glycol, is the simplest (non geminal) diol. It was first prepared by Wurtz in 1859 who treated 1,2-dibromoethane with silver acetate obtaining ethylene glycol acetate, which was then hydrolysed to ethylene glycol. Ethylene glycol was first used industrially in place of glycerol during World War I as an intermediate for explosives (ethylene glycol dinitrate), but has since developed into a major industrial product. The worldwide capacity for the production of ethylene glycol via the hydrolysis of ethylene oxide is estimated to be 7×10^6 tons/year. Ethylene glycol is used mainly as antifreeze in automobile radiators and as a raw material for the manufacture of polyester fibres. From a structural point of view, it is interesting to point out that having two hydroxyl groups, it may establish an intramolecular hydrogen bond. In neat ethylene glycol, the *closed* form (see Figure π right) is the main one. This system is part of a project in which I wanted to check the effect of various substitutions on simple organic molecules. In the same set there are: ethanol, 2-amino-1-ethanol, 2-methoxy-1-ethanol and 1,2-dimethoxyethane. Also in this system, a nice, monotonic trend in the SAXS patterns is observed. The LqP is gradually right-

shifted and its intensity lowered as the glycol is added to the system. But the shift is larger than in the case of DMSO, while the intensity falls off more slowly.

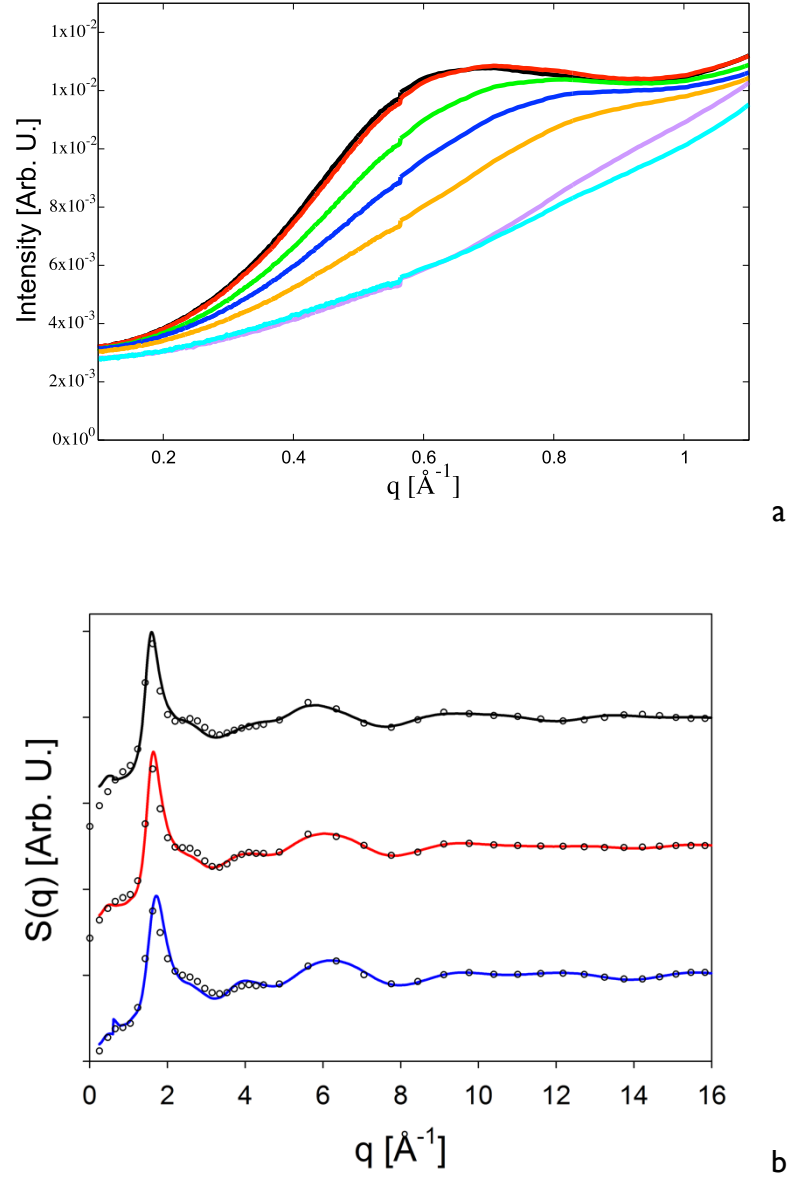


Figure 3.9: (a) SAXS patterns for EAN+ethylene glycol systems. EAN (black); ethylene glycol (cyan); EG1 (purple); EG3 (orange); EG5 (blue); EG7 (green); EG9 (red); (b) WAXS pattern and experimental (symbols) comparison with models (solid lines) for EG2 (black); EG5 (red); EG8 (blue)

These considerations mean that the effect of glycol is always that of destroying the sponge-like structure of EAN, but in a different way compared to DMSO. The computation of the excess molar volume yields to significantly different results than before.

System	χ_{EAN}	Density [g/ml]	Excess molar volume [ml/mol]
EAN	1	1.2106	0
EG9	0.9	1.2049	-0.0861
EG7	0.7	1.1920	-0.2006
EG5	0.5	1.1764	-0.2923
EG3	0.3	1.1557	-0.2829
EG1	0.1	1.1285	-0.1804
GLY	0	1.1104	0

Table 3.6: Name, composition, density and excess molar volumes for EAN+ethylene glycol systems

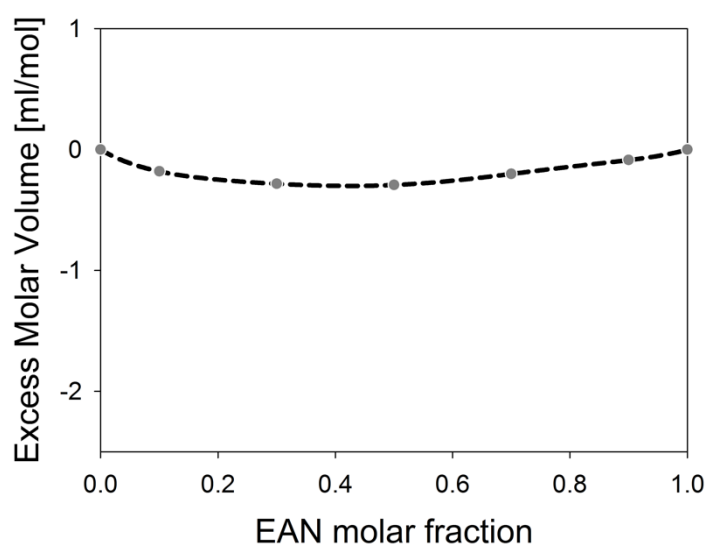


Figure 3.10: Excess molar volume for EAN+ethylene glycol systems

Two main difference from DMSO-containing systems are immediately evident. The minimum position is shifted to an almost equimolar composition, and the absolute value of the excess is much smaller. Both of these observations suggest that this system deviates less from ideality. The thermodynamic definition of ideal solution is that the mixture must have no excess molar volume and zero enthalpy of mixing. To check this last property, I have visited Prof. Alberto Schiraldi and Prof. Dimitrios Fessas at the DeFENS department of the University of Milan. There I was able to measure the enthalpy of mixing for this system, and the results are reported below.

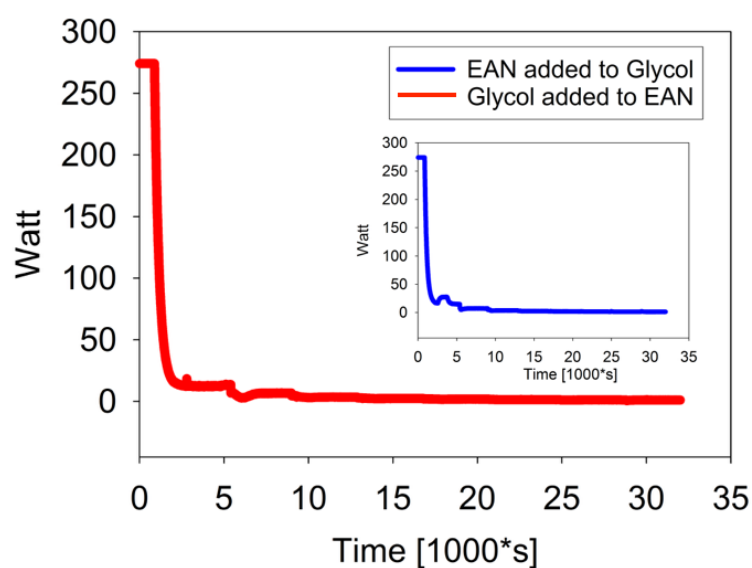


Figure 3.11: Heat exchanged upon EAN and ethylene glycol mixing

It appears clear that there is absolutely no heat exchange when glycol is added to EAN or viceversa (injection of 15 μl every 5000 s), so this system is indeed almost ideal. I have made a series of molecular dynamics simulations to check the molecular interactions in this system.

System	Exp. Density [g/ml]	Calc. Density [g/ml]
EAN	1.2106	1.2143
EG9	1.2049	1.2076
EG7	1.1920	1.1953
EG5	1.1764	1.1767
EG3	1.1557	1.1558
EG1	1.1285	1.1283
GLY	1.1104	1.1106

Table 3.7: Comparison between experimental and computed mass densities for EAN+ethylene glycol systems

The snapshots of the simulations boxes show no major differences from the previous case, an increasing lack of mesoscopic correlation is observed when glycol content increases.

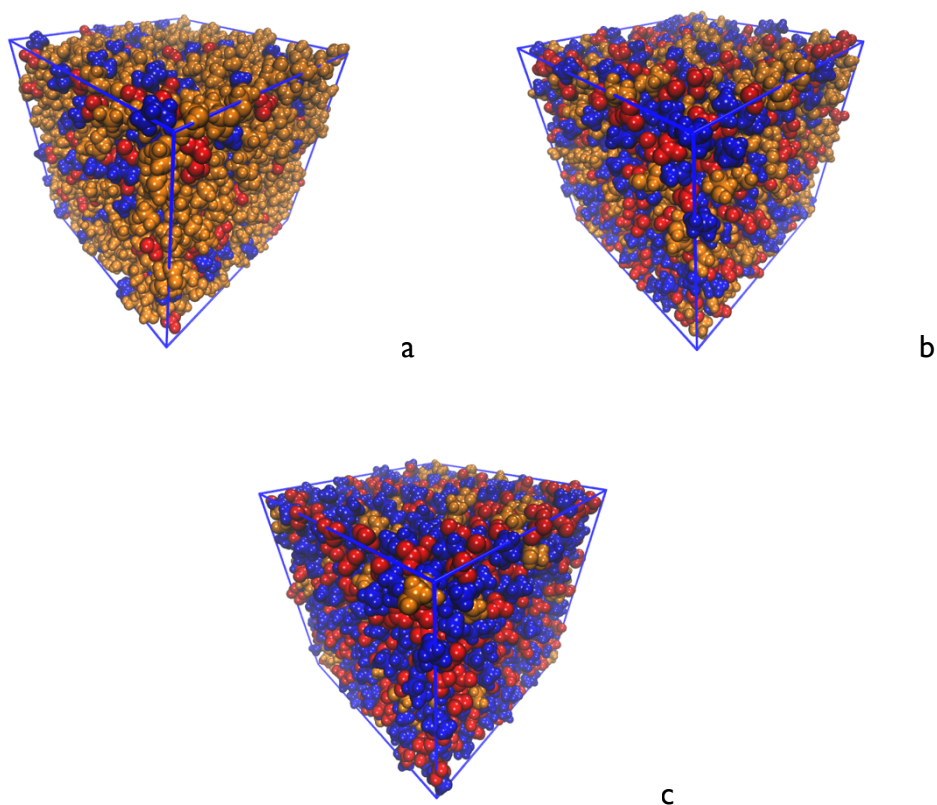
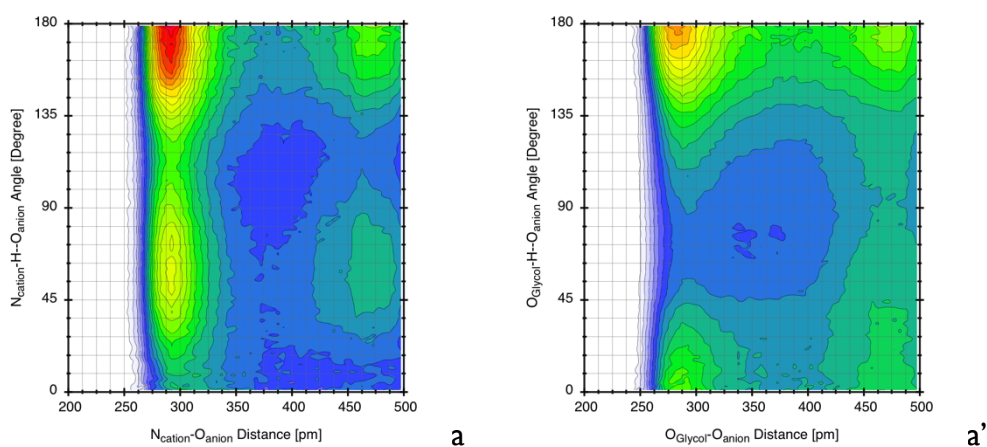
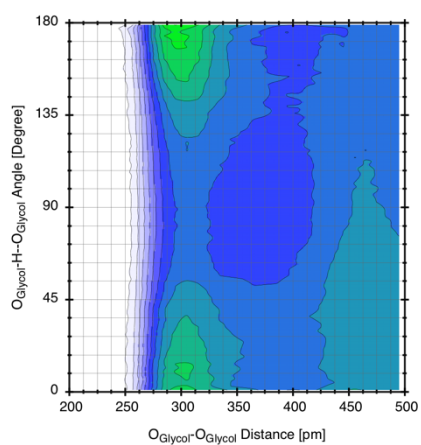


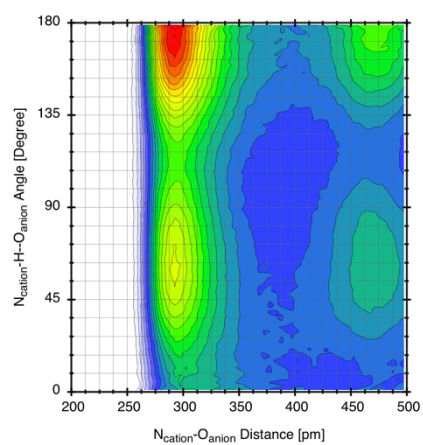
Figure 3.12: Snapshots of the simulation boxes for EAN+ethylene glycol systems. (a) EG2; (b) EG5; (c) EG8. Cation (blue); anion (red); ethylene glycol (orange)

In this case, the hydrogen bond network is more complex because glycol may act as both donor and acceptor, so the possible interactions are: cation-anion, cation-glycol, anion-glycol, glycol-glycol

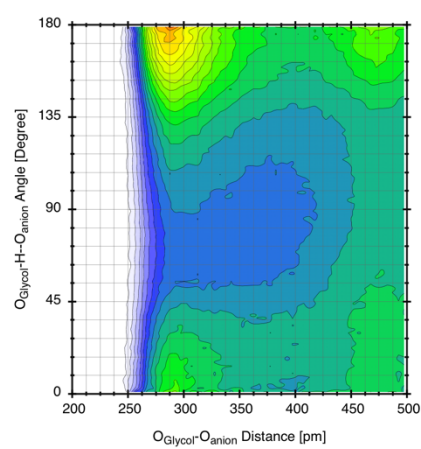




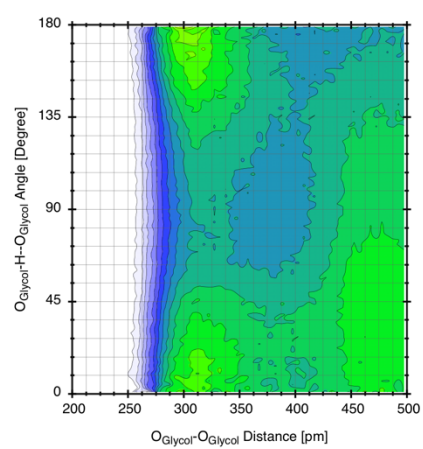
a''



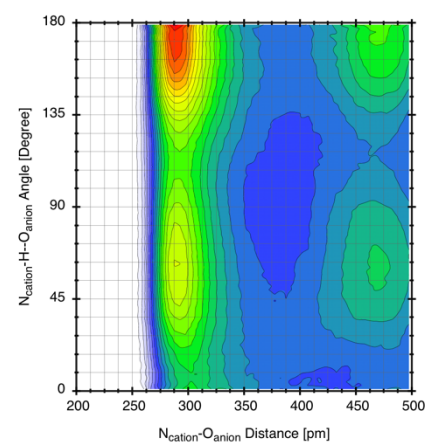
b



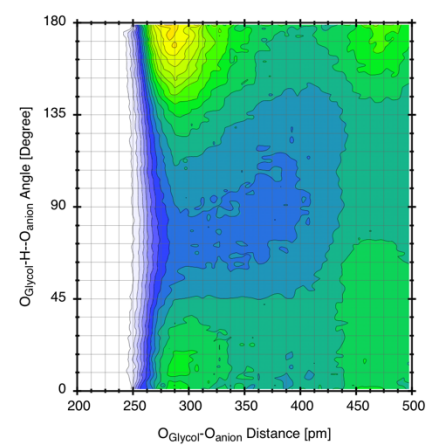
b'



b''



c



c'

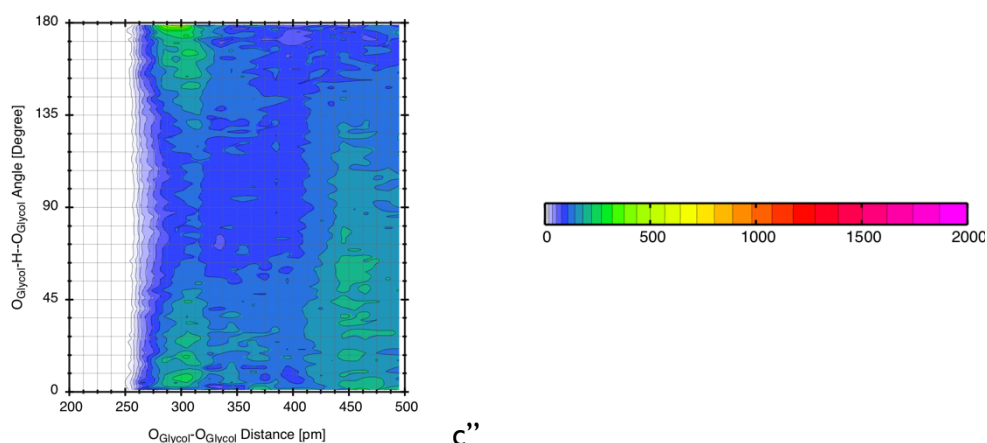


Figure 3.13: Combined radial-angular distribution functions for EAN+ethylene glycol systems. (a) EG2; (b) EG5; (c) EG8. Plain letters refers to $\text{NH}_3\text{-NO}_3$ interaction; primes to OH-NO_3 interaction; double primes to OH-OH (intermolecular) interaction.

Here we can see that the hydrogen bond strength goes in the way glycol-anion > cation-anion > glycol-cation, thus glycol is able to overcome the columbic interaction and binds nitrates preferentially. For this system there is a peculiar observation. Ethylene glycol may establish an intramolecular hydrogen bond, and ~75% of the molecules are in the closed form in the neat liquid.

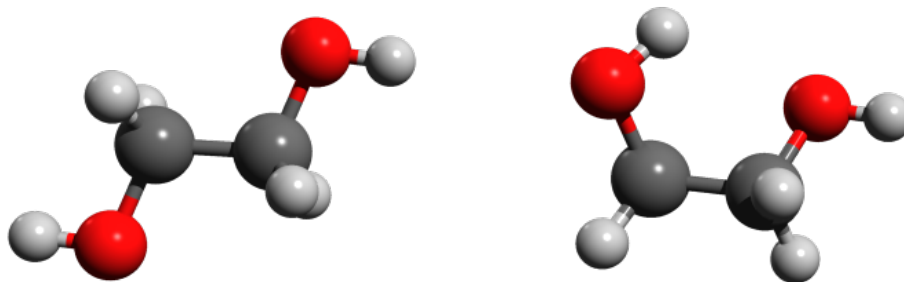


Figure π: Conformations of ethylene glycol. Opened (left); closed (right)

From the analysis of the pair distribution function of this correlation, I was able to observe that ethylammonium nitrate further favours the closed form.

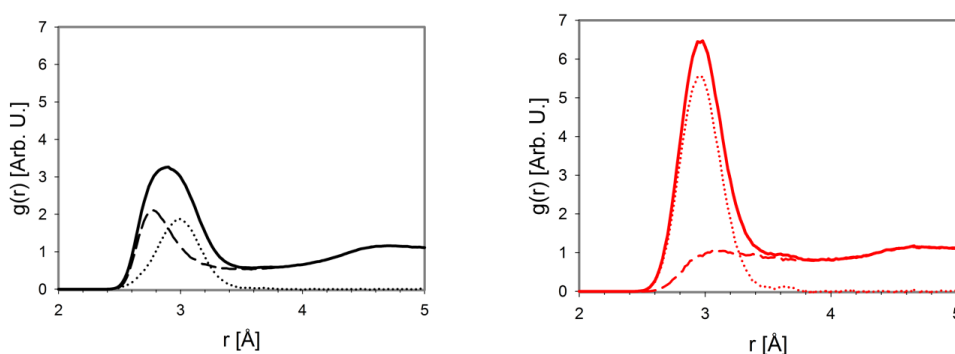


Figure 3.15: Radial distribution functions of the OH-OH interaction (O-O distance). Neat ethylene glycol (left); EG5 (right). Intramolecular interaction (dotted line); intermolecular interaction (dashed line); total interaction (solid line)

In figures 3.15 the overall correlation between the oxygens of glycol is splitted into its intra-molecular and inter-molecular contributions. First of all, the position of the overall peak is shifted in EG from 2.88 Å to 2.96 Å in EGE5, indicating a weakening of the interaction, while its intensity is nearly doubled meaning that this correlation is more persistent. These are apparently two contrasting observations, but the deconvolution of this PDF into its contributions shows a clear picture. The intra-molecular correlation remains stable in its position at 3 Å, and the intensity rises, meaning that there are more glycol molecules in the closed form. On the other hand, the inter-molecular peak is almost completely absent in the EGE5 system, meaning that glycol molecules preferentially do not bond with each other. The CNs for those correlations behave similarly. The intra-molecular hydrogen bond CN is always exactly 1.00, as it is expected, while the CN for the inter-molecular correlation drops from 1.15 in EG to 0.33 in EGE5.

System	Anion-Cation	Anion-Anion	Glycol-Glycol		Glycol-Cation	Glycol-Anion
			intra	inter		
EAN	2.98	7.12	--	--	--	--
EGE5	2.30	4.96	1.00	0.33	0.61	1.98
EG	--	--	1.00	1.15	--	--

Table 3.8: Average coordination numbers for some interactions in EAN+ethylene glycol systems

The spatial distribution functions for EG2, EG5 and EG8 are shown below.

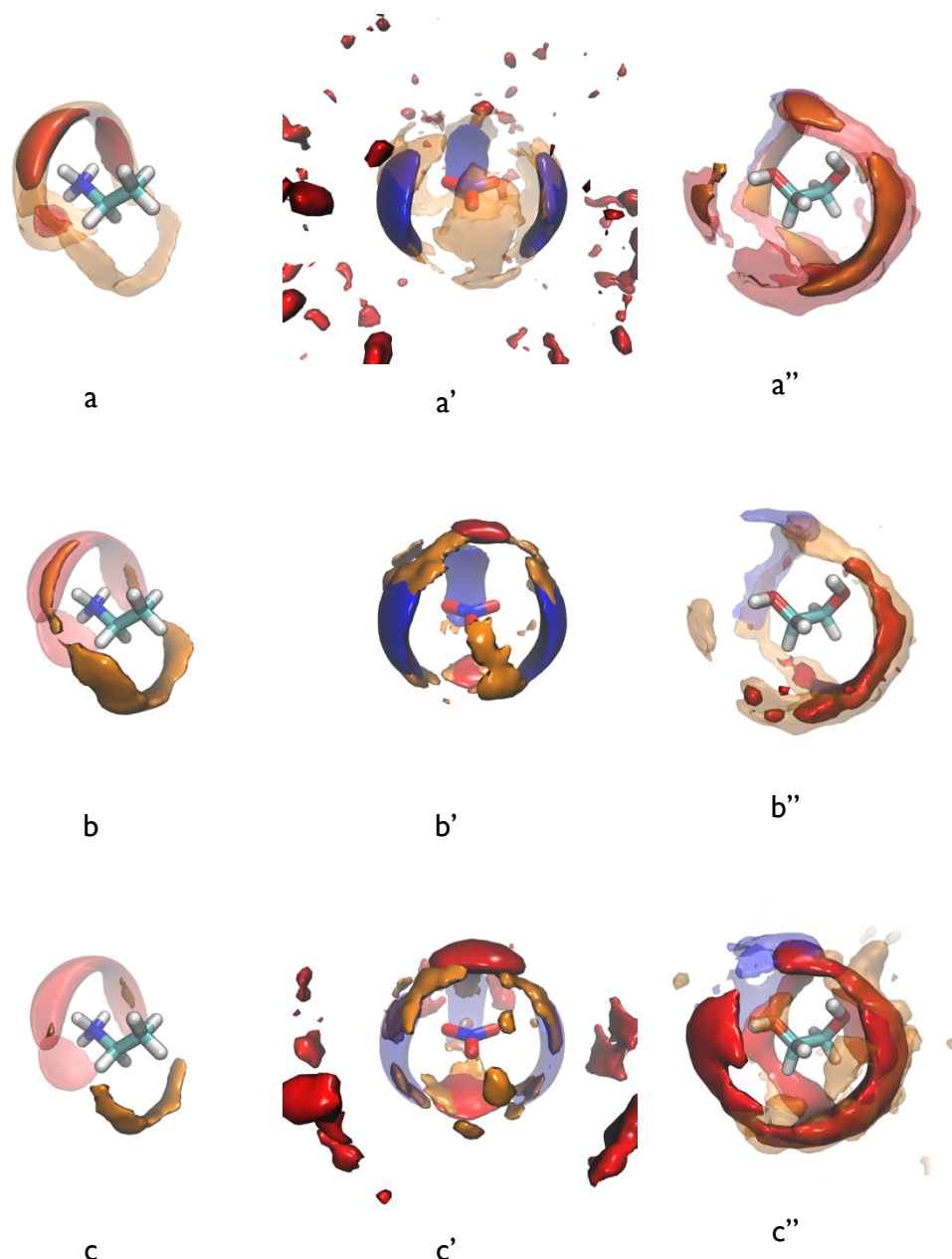


Figure 3.16: Spatial distribution functions for EAN+ethylene glycol systems. (a) EG2; (b) EG5; (c) EG8. Plain letters refer to cation environment; primes to anion environment; double primes to ethylene glycol environment. Cation nitrogen (blue); Anion oxygen (red)

Here the situation is much more chaotic than in the previous system. When EAN is the minority component (first row) there is absolutely no anion-anion correlation, leading to the disappearance of the LqP. On the other hand, the nitrate anions solvate the glycol molecules quantitatively. Adding ionic liquid to the mixture, the bipyramidal coordination of the anion reappears. Another interesting observation is that the glycol does not *like* to interact with the anion and binds it only when the ionic liquid is the minority compound.

III.III. EAN+2-Amino-1-Ethanol

Because 2-amino-1-ethanol (EOA) combines the properties of amines and alcohols, EOA exhibits the unique capability of undergoing reactions common to both groups. As an amine it is mildly alkaline and reacts with acids to form salts or soaps. As an alcohol it is hygroscopic and can be esterified. It is widely used as an additive to detergents, in the textile industry and in the treatment of wood. For our purposes, EOA is a perfect probe to check how EAN interacts with both NH_2 and OH simultaneously without the complication of a ternary system.

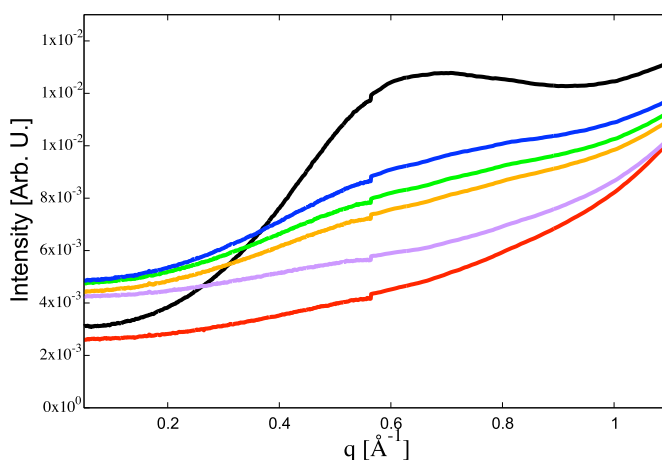


Figure 3.17: SAXS patterns for EAN+2-amino-1-ethanol systems. EAN (black); 2-amino-1-ethanol (red); ENO1 (purple); ENO3 (orange); ENO5 (green); ENO7 (blue). See Table 3.9 for systems name

It appears clear how the LqP is strongly affected by the presence of the EOA. The effect is similar to the one of DMSO. Yet the most interesting feature is the raised intensity in the extreme low q region (below 0.2 \AA^{-1}). Simple liquids should not show any scattering there but something odd is observable. Albeit in this case there is not any distinguishable feature (*i.e.* there is no evidence of a peak), this is the precursor to a phenomenon that will be discussed in the next chapter.

System	χ_{EAN}	Density [g/ml]	Excess molar volume [ml/mol]
EOA	0	1.012	0
ENO1	0.1	1.04988	-0.6031
ENO3	0.3	1.09962	-0.6936
ENO5	0.5	1.13689	-0.4718
ENO7	0.7	1.16967	-0.3257
EAN	1	1.2106	0

Table 3.9: Name, composition, density and excess molar volumes for EAN+ 2-amino-1-ethanol systems

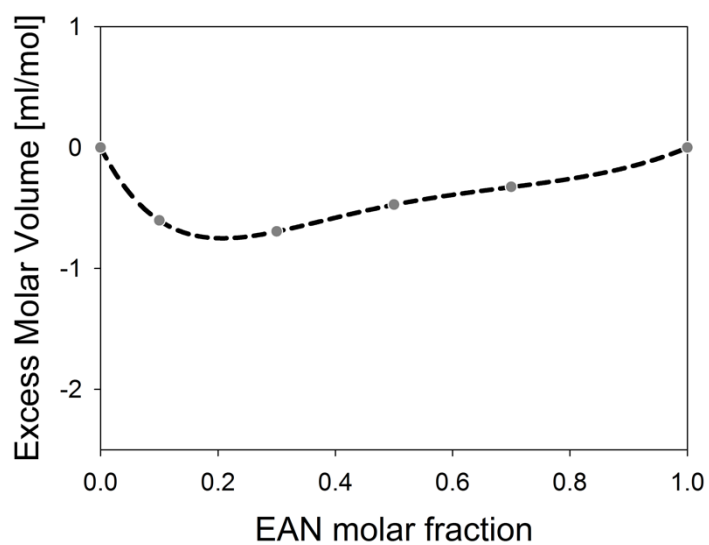
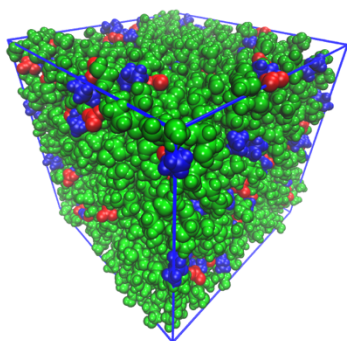


Figure 3.18: Excess molar volume for EAN+2-amino-1-ethanol systems at 25 °C

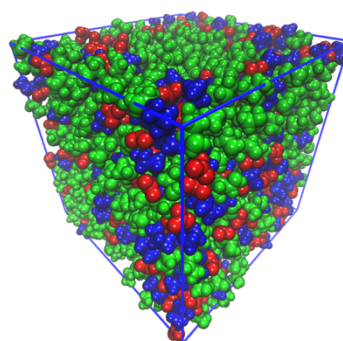
Also here the minimum is located around EAN molar fraction 0.3. The molecular dynamics simulations show a good agreement with the experiments.

System	Exp. Density [g/ml]	Calc. Density [g/ml]
ENO1	1.04988	1.0501
ENO3	1.09962	1.1024
ENO5	1.13689	1.1354
ENO7	1.16967	1.1688

Table 3.10: Comparison between experimental and calculated mass densities for EAN+2-amino-1-ethanol systems



a



b

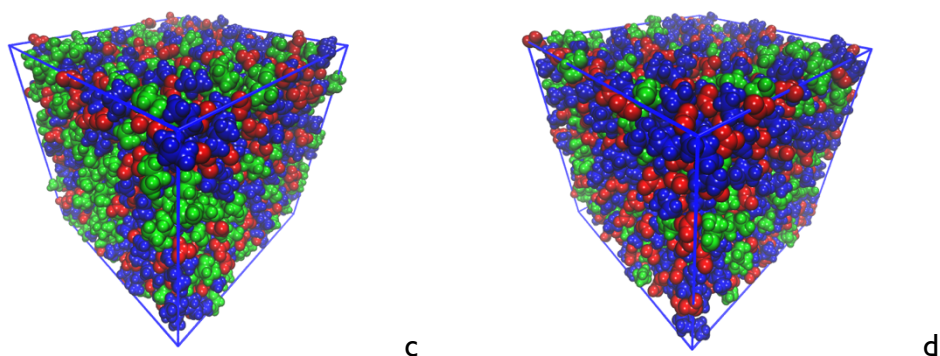
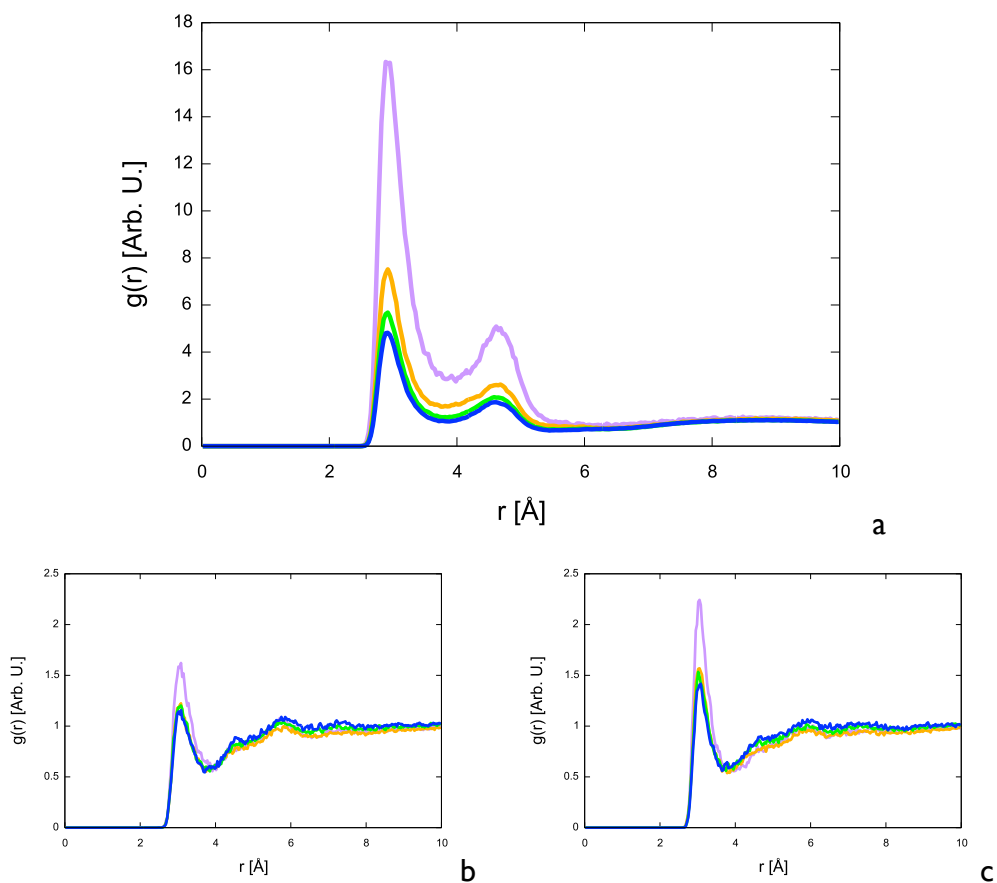


Figure 3.19: Snapshots of the simulation boxes for EAN+2-amino-1-ethanol systems. (a) ENO1; (b) ENO3; (c) ENO5; (d) ENO7. Cation (blue); anion (red); 2-amino-1-ethanol (green)

The simulation boxes show an almost homogeneous mixing of the components, even if some EAN nano-segregation is observed when EAN is the minority compound. The hydrogen bond analysis has a central role in this case because our aim is to elucidate if EAN prefers to interact with the amino or the hydroxyl group. For the sake of clarity, here I will show only the pair distribution functions.



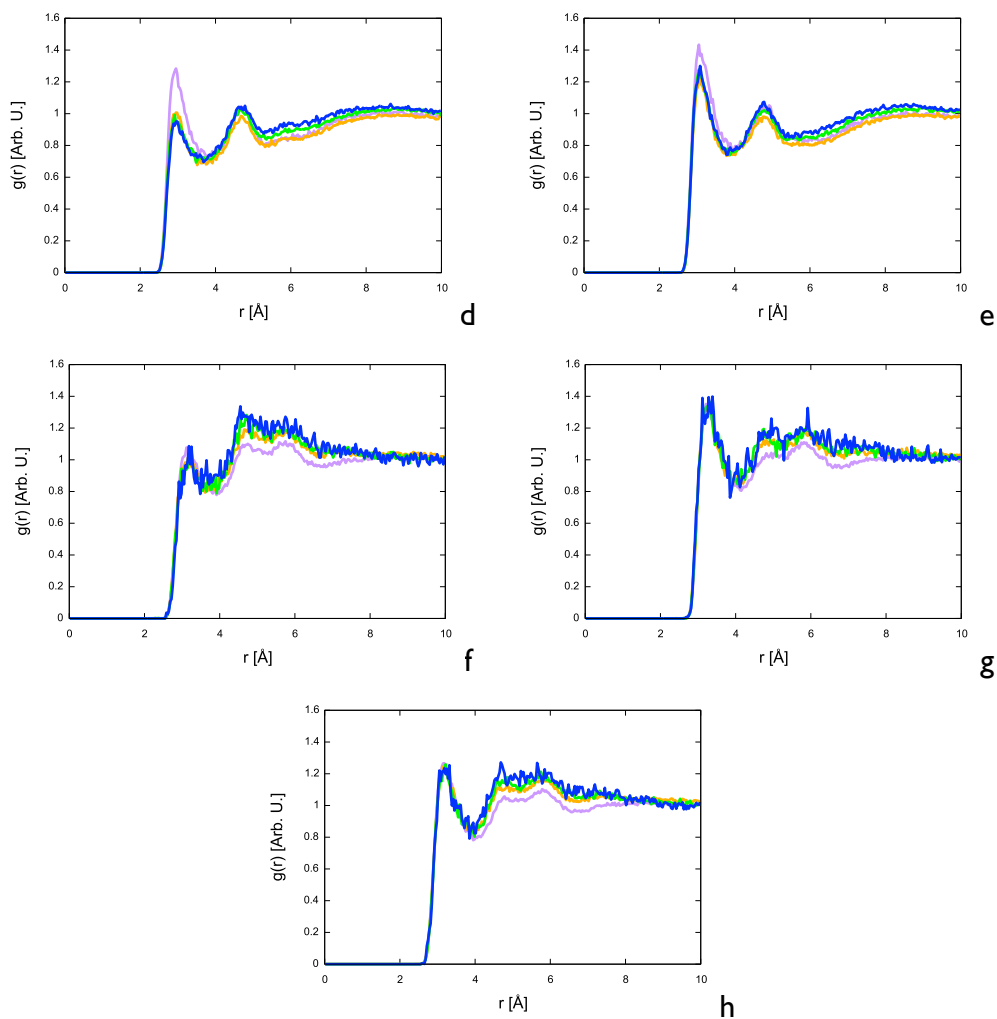


Figure 3.20: Pair distribution functions for all the possible hydrogen bonding interactions in EAN+2-amino-1-ethanol systems. Donor-acceptor: (a) $\text{NH}_3\text{-NO}_3$; (b) $\text{NO}_3\text{-OH}$; (c) $\text{NH}_3\text{-NH}_2$; (d); OH-NO_3 ; (e) $\text{NH}_2\text{-NO}_3$; (f) OH-OH ; (g) $\text{NH}_2\text{-NH}_2$; (h) $\text{NH}_2\text{-OH}$. ENO1 (blue); ENO3 (green); ENO5 (orange); ENO7 (purple)

The complexity of the system requires a more detailed inspection, so the spatial distribution functions were computed.

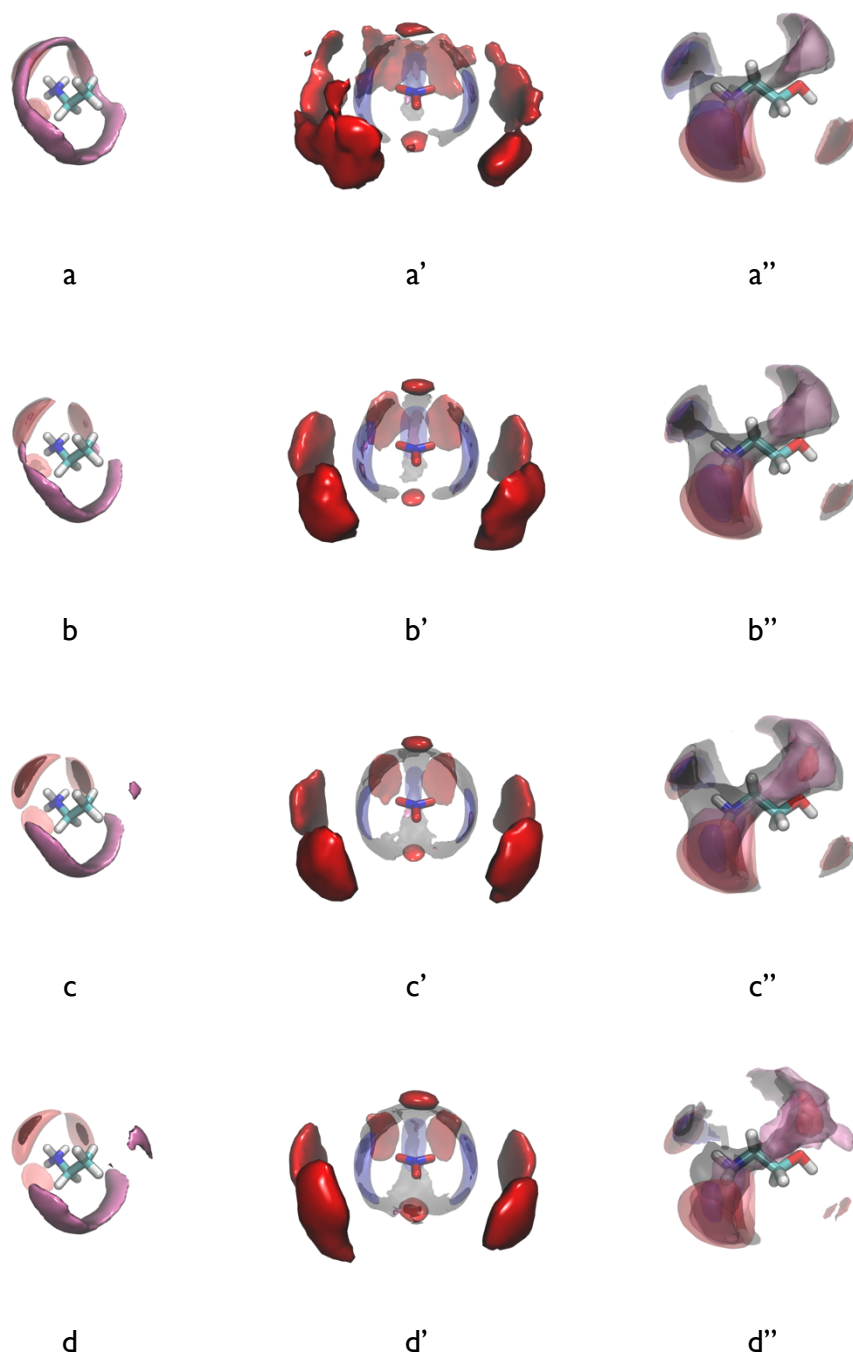


Figure 3.21: Spatial distribution functions for EAN+2-amino-1-ethanol systems. (a) ENO1; (b) ENO3; (c) ENO5; (d) ENO7. Plain letters refer to cation environment; primes to anion environment; double primes to 2-amino-1-ethanol environment. Cation nitrogen (blue); anion oxygen (red); 2-amino-1-ethanol nitrogen (black); 2-amino-1-ethanol oxygen (purple)

While it is difficult to see the single contributions in the overall pictures reported above, an analysis on the single *voxel clouds* returns some interesting results. First we see that both the cation and the anion surprisingly prefer to interact with the aminic-end of EOA. To further understand this finding, I have extracted the

coordination numbers for the first solvation shell of every possible hydrogen bond, imposing two geometric conditions: distance between heavy atoms less than 3 Å and angle of the interaction between 135° and 180°. Results are shown below.

Interaction		ENO1	ENO3	ENO5	ENO7
Acceptor	Donor				
-NH ₂	-NH ₃	1.1113	0.6502	0.4326	0.2315
-OH	-NH ₃	0.9255	0.5594	0.3733	0.2023
NO ₃	-NH ₂	2.1489	1.4049	0.9666	0.5453
NO ₃	-OH	0.1561	0.7946	0.4945	0.2591
NO ₃	-NH ₃	1.7876	2.4258	2.8253	3.1011
-OH	-NH ₂	0.6504	0.4835	0.3263	0.1857
-NH ₂	-OH	0.1380	0.1372	0.0825	0.0451
-OH	-OH	0.2100	0.1402	0.0856	0.4517
-NH ₂	-NH ₂	0.5950	0.4426	0.2973	0.1686

Table 3.11: Average coordination numbers for all the intermolecular hydrogen bonds for EAN+2-amino-1-ethanol systems.

For the intramolecular hydrogen bonds I have taken into account not the heavy atoms, but the hydrogens, so while maintaining the same angular condition, the distance was chosen to be less than 2.5 Å.

Interaction		ENO1	ENO3	ENO5	ENO7
Acceptor	Donor				
-OH	-NH ₂	0.9254	0.7342	0.2135	0.0387
-NH ₂	-OH	0.5478	0.9637	1.2567	1.8630

Table 3.12: Average coordination numbers for all the intramolecular hydrogen bonds for EAN+2-amino-1-ethanol systems.

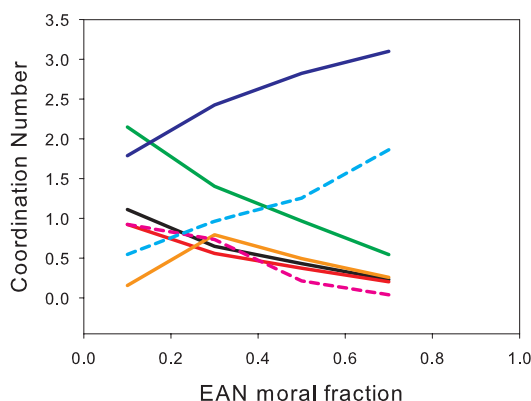


Figure 3.22: Average coordination numbers for all the hydrogen bonds for EAN+2-amino-1-ethanol systems. Donor-acceptor: NH₃-NO₃ (blue); NH₃-OH (red); NH₃-NH₂ (black); OH-NO₃ (orange); NH₂-NO₃ (green); OH-NH₂ (pink); NH₂-OH (cyan). Intermolecular (solid lines); intramolecular (dashed lines)

The picture is quite complex and a quantitative interpretation is beyond the possibilities of a classical molecular dynamics simulation, because here electronic effects play a major role. Nevertheless, we can say that both cation and anion prefer to interact with NH_2 rather than OH . Similarly to ethylene glycol, ethanolamine can establish intramolecular hydrogen bonds, but here we have two possibilities.

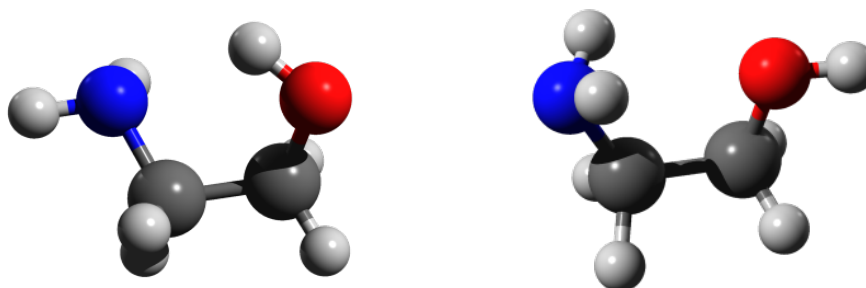


Figure 3.23: Conformations of 2-amino-1-ethanol. Closed on aminic group (left); closed on hydroxyl group (right)

The conformation in figure 3.23 left may explain why the OH group is limited as hydrogen bond donor in intermolecular interactions, while the one in figure 3.23 right rationalize why NH_2 is a stronger acceptor for other molecules. As said above, a classical model is not fully adequate to finely describe observations. Further investigations are needed to elucidate the nature of this system and DFT calculations together with RAMAN and infrared spectroscopies will be used in future studies.

III.IV. *EAN+2-Methoxy-1-Ethanol*

2-methoxy-1-ethanol (MEO), also known as methyl-glycol, is an ethylene glycol ether that has been known since the 1920s, but its use significantly increased in the 1970s. Cellosolve was a solvent product containing glycol ethers and registered in the 1920s by Carbide and Carbon Chemicals Corp. Glycol ethers are derived from either ethylene oxide (E-series) or propylene oxide (p-series) combined with an alcohol. MEO is an E-series glycol ether derived from methanol and ethylene oxide. MEO is a highly flammable, colourless liquid that readily dissolves in water. Its chemical properties allow it to be used mainly in surface coatings. It is widely used in paints, lacquers, stains, nail polishes, surface coatings, and food-contact plastics. It is also used in printing, inks, leather

processing, photography and photolithography processes such as in the semiconductor industry, and textile finishing. For our purposes it is interesting to see what is the effect of the hydrogen bond in the EAN+ethylene glycol mixtures series: di-hydroxyl; methoxy-hydroxyl; di-methoxy.

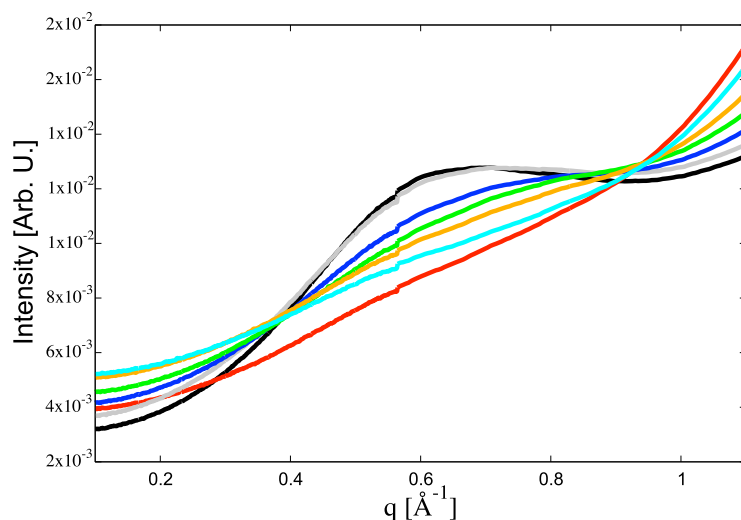


Figure 3.24: SAXS patterns for EAN+2-methoxy-1-ethanol systems. EAN (black); 2-methoxy-1-ethanol (red); EMEOI (cyan); EMEO3 (orange); EMEO5 (green); EMEO7 (blue); EMEO9 (grey)

Also here, it may be noticed an odd intensity increasing in the extreme low q region, especially for the low-EAN-containing mixtures. Again, this is the precursor of an effect discussed in the next chapter.

System	χ_{EAN}	Density [g/ml]	Excess molar volume [ml/mol]
MEO	0	0.96029	0
EMEO1	0.1	1.00474	-1.3355
EMEO3	0.3	1.06062	-1.4894
EMEO5	0.5	1.10997	-1.3461
EMEO7	0.7	1.15301	-0.9232
EMEO9	0.9	1.19224	-0.3969
EAN	1	1.2106	0

Table 3.13: Name, composition, density and excess molar volumes for EAN+2-methoxy-1-ethanol systems

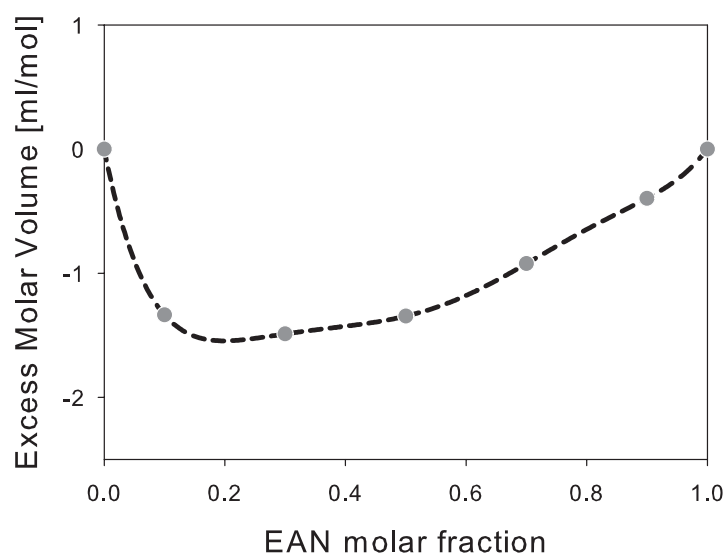


Figure 3.25: Excess molar volume for EAN+2-methoxy-1-ethanol systems

This is the system for which the minimum in the excess molar volume is located leftmost, at about 0.2 EAN molar fraction, suggesting that about four MEO molecules are needed to fully coordinates EAN.

System	Exp. Density [g/ml]	Calc. Density [g/ml]
EMEO1	1.00474	1.0052
EMEO3	1.06062	1.0644
EMEO5	1.10997	1.1231
EMEO7	1.15301	1.1611
EMEO9	1.19224	1.2063

Table π: Comparison between experimental and calculated mass densities for EAN+2-methoxy-1-ethanol systems

Also here the simulations show an excellent agreement with the experiments.

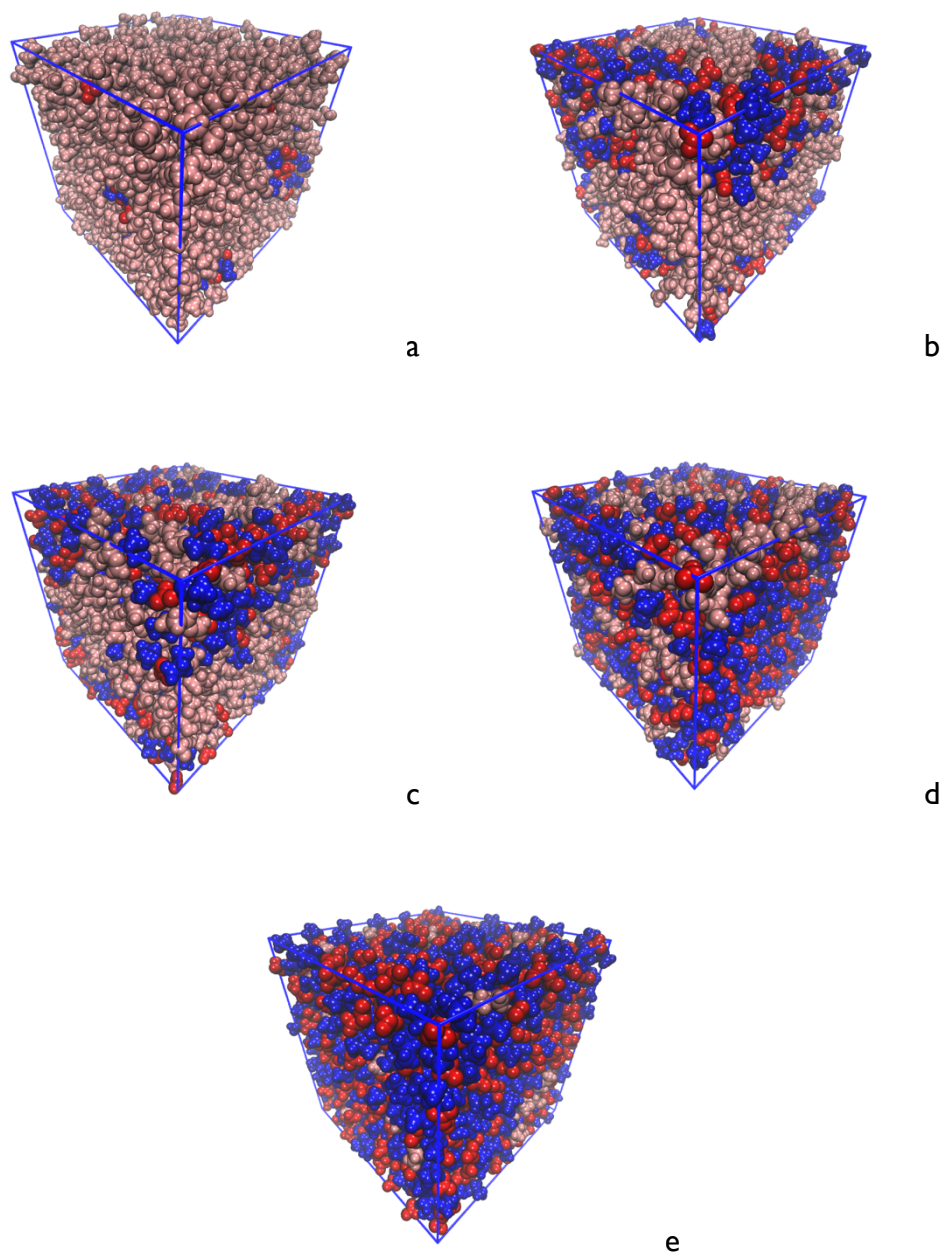


Figure 3.26: Snapshots of the simulation boxes for EAN+2-methoxy-1-ethanol systems. (a) EME01; (b) EME03; (c) EME05; (d) EME07; (e) EME09. Cation (blue); anion (red) 2-methoxy-1-ethanol (pink)

Boxes visual inspection shows always a rather homogeneous system, albeit in the EAN-poor region the IL appears to slightly prefer to bind itself. The hydrogen bond analysis for the inter molecular interactions returns non surprising results.

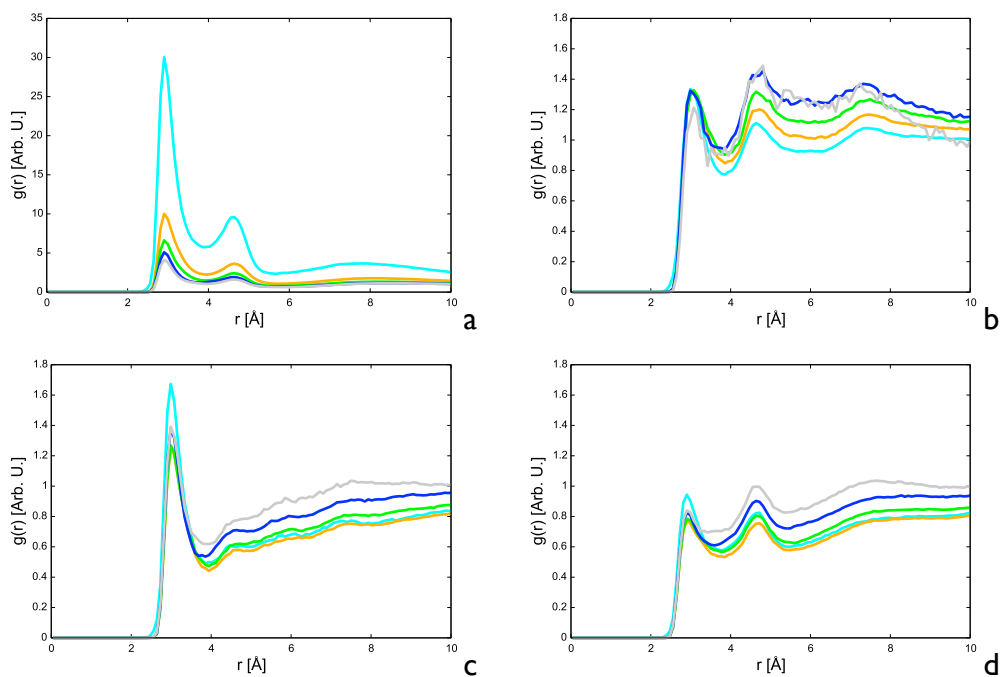


Figure 3.27: Pair distribution functions for some interactions in EAN+2-methoxy-1-ethanol systems. (a) $\text{NH}_3\text{-NO}_3$; (b) OH-OH ; (c) $\text{NH}_3\text{-OH}$; (d) OH-NO_3 . EME01 (cyan); EME03 (orange); EME05 (green); EME07 (blue); EME09 (grey)

Also here it is important to consider the opened and closed conformations of the co-solvent



Figure 3.28: Conformations of 2-methoxy-1-ethanol. Opened (left); closed (right)

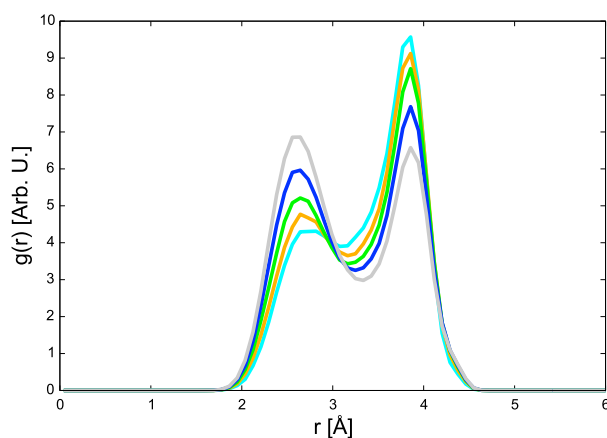
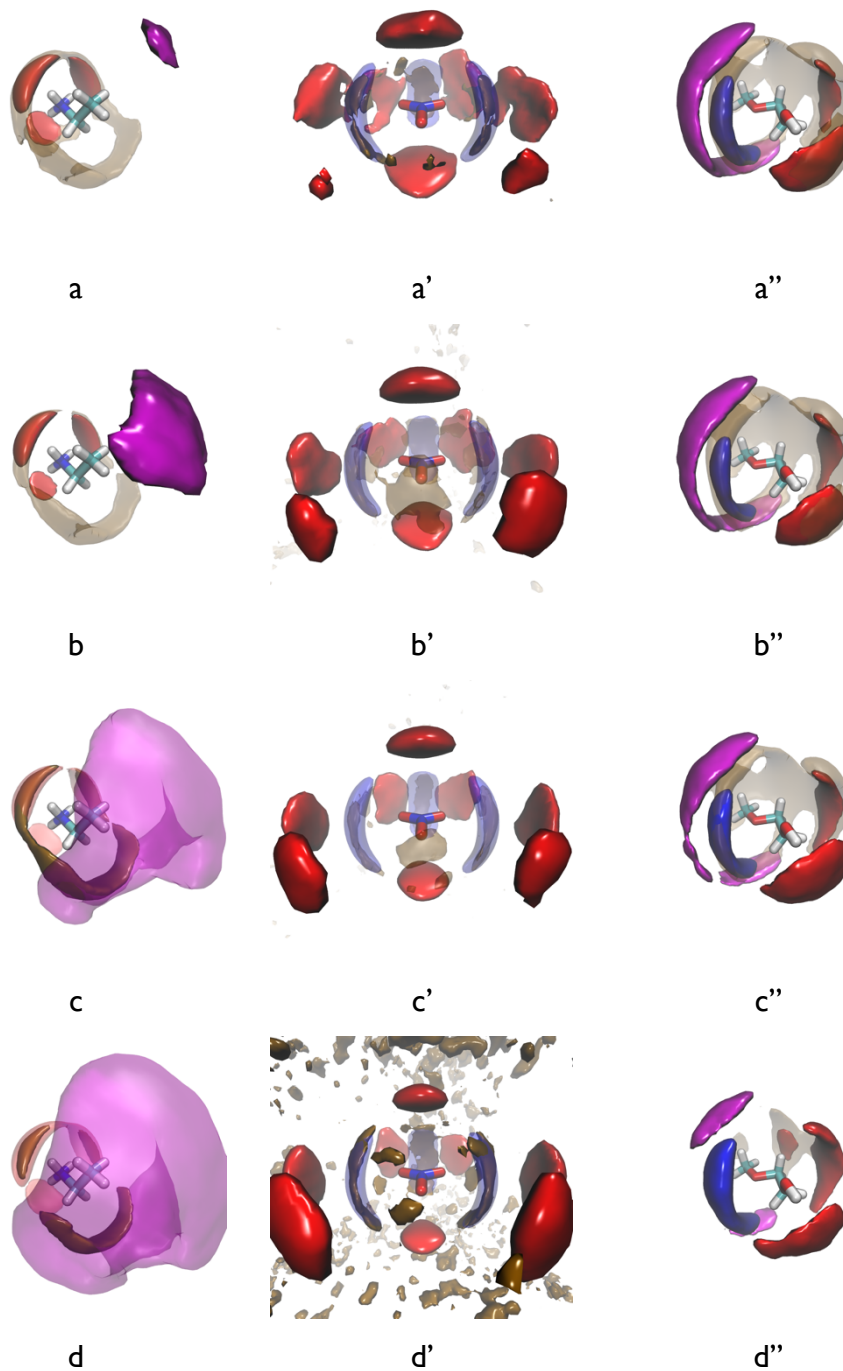


Figure 3.29: Intramolecular pair distribution functions of the O-O interaction for EAN+2-methoxy-1-ethanol systems. EME01 (cyan); EME03 (orange); EME05 (green); EME07 (blue); EME09 (grey)

From figure 3.29 it is evident how the closed form (first peak) is favoured at low EAN concentrations, while the opened conformation (second peak) is enhanced when the IL is the majority compound. This suggests that MEO undergoes a structural transition mediated by the influence of EAN. The spatial distribution functions allowed me to rationalize the observation.



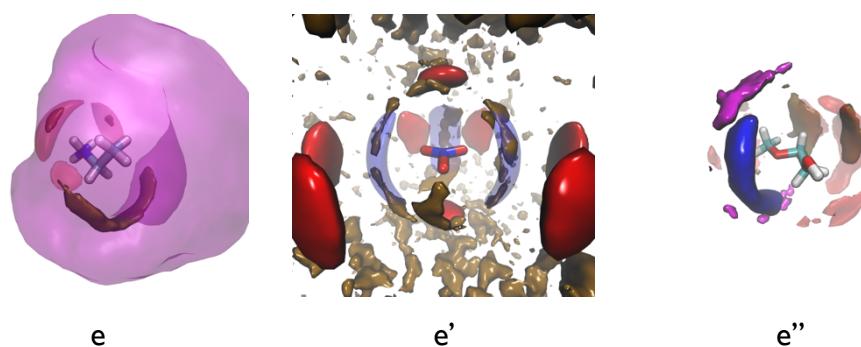


Figure 3.30: Spatial distribution functions for for EAN+2-methoxy-1-ethanol systems. . (a) EMEO1; (b) EMEO3; (c) EMEO5; (d) EMEO7; (e) EMEO9. Cation nitrogen (blue); anion oxygen (red); 2-methoxy-1-ethanol oxygen (gold); 2-methoxy-1-ethanol methyl group (violet)

Going from EMEO1 to EMEO9 the interaction between MEO and EAN radically changes. In the low-IL regime (i.e. when is in its opened configuration) MEO is able to establish hydrogen bonds with the cation, the anion and other methylglycol molecules. Gradually adding EAN to the mixture, MEO changes conformation to the closed form. This affects strongly the interactions where it acts like an hydrogen bond donor (i.e. with the nitrate anions and other methylglycol molecules), almost destroying these correlations, while its acceptor capacity are much less affected, maintaining the interaction with the cation. On the other hand, the aliphatic solvation of the ethylammonium continuously increase with the IL concentration and while the MEO environment is generally depleted of its analogues, the cation neighbourhood is enriched in methylglycol.

IV. Contextualization

As said in section I, recently the study of mixtures based on ionic liquids is in the spotlight^{18,20,21,23,26,37,40,50–64}. This is because the addition of a molecular co-solvent often results in lowering the viscosity^{65,66} and thus enhancing the conductivity⁶⁷. Other advantage is the possibility to tune the physical and chemical properties of an IL by mixing with another compound instead of tackling the synthesis of a brand new compound with the same characteristics. While for aprotic ionic liquids a wide range of the three dimensional space (anion, cation and co-solvent) has already been explored, PILs have received less attention, probably for the complications due to their speciation. Nevertheless, this class of compounds has really unique characteristics⁶⁸ and the knowledge of how they interact with other

molecules is of primary importance to find new potential applications. An enormous amount of papers on this topic is found in the literature, but for the purpose of this dissertation I will review only those concerning either ethylammonium nitrate or the molecular co-solvents that I have presented in this chapter. EAN+DMSO system was first studied by Mancini *et al.*⁶⁹ in 2004 by means of spectrometric measurements of the Reichardt parameters. They found that this system shows some interesting features in its hydrogen bonding properties, such as high polarizability, moderate hydrogen bond basicity and high hydrogen bond acidity. They explained their findings in terms of strong association between the cation and DMSO, exactly as proposed ten years later using more advanced and complete techniques³⁶. DMSO was also used and studied in mixture with other PILs such as N-methyl-imidazolium tetrafluoroborate ($C_1\text{Im BF}_4$) and triethylammonium triflate (TEATf). In the first case, Rai *et al.*⁷⁰ reported how the mixing of DMSO to the IL is endothermic because the broken hydrogen bonds were stronger respect the new ones. By contrast, for the ED system the situation is the reverse. Although I have no experimental data, I have noticed that when the samples were prepared the mixtures became hot, indicating an exothermic process associated to the formation of a strongly bonded complexes. The divergence with the results from Rai *et al.*⁷⁰ arises from the PIL nature, in fact while EAN has three available hydrogen bond donors, $C_1\text{IM BF}_4$ has only one, so breaking it means to break also the ion pair. On the other hand, replacing one or two nitrate anions by DMSO molecules, preserves the contact between the charges species. This interpretation is also supported by Fumino *et al.*⁷¹ who have shown how TEATf is strongly solvated by DMSO, and how it is able to separate the ionic pair thanks to its high polarity. Both Rai⁷⁰ and Fumino⁷¹ have shown how other co-solvents such as acetonitrile and methanol behave differently due to their lower polarity. Ethylene glycol was mixed with $C_1\text{IM BF}_4$ and the enthalpy of mixing was measured observing an exothermic behaviour, in contrast to our observation where no thermal exchange was observed. The explanation for the different results resides once again in the nature of the PIL. It appears evident from the calorimetry and from the excess molar volume that EAN+ethylene glycol mixtures are almost ideal because the dimensions and hydrogen bonding properties of the diol are pretty similar to the ones found in pure EAN. On the

other hand, $C_{12}lm\ BF_4$ is very different both structurally and for its hydrogen bond properties, as said before. To date no works on IL mixed with ethanolamine or methyl-glycol have been published. EAN has been studied in mixture with a series of compounds. Hayes *et al.*²² reported how water induces some solvophobic effect forcing the sponge-like structure of EAN to change into a near cylindrical self-assembled structure. This is because the polar domain is enlarged by accommodating the water molecules rising the interfacial curvature around the nonpolar regions. Nevertheless, the local structure of both EAN and water is nearly unperturbed until very diluted mixtures, indicating that these molecules do not interact strongly as one may expect. Greaves *et al.*⁷² also studied EAN+water mixtures reporting similar results, moreover they found that the LqP position undergo a particular evolution as water is added to EAN. They suggested that at EAN molar fraction $\sim 0.2-0.3$ there is a transition from EAN-EAN dominating correlations to EAN-water. Albeit water is a special case, these results are in line with our findings. We have noticed how the structural arrangement of EAN is really persistent upon co-solvent addition and sensible changes happen only when EAN is the minority compound. The only exception is for ethanolamine where the LqP vanishes even for small additions. This is probably due to the extreme similarity between the cation and the co-solvent and to the fact that ethanolamine does not have a polar/apolar duality. These two properties may allow ethanolamine to destroy the sponge-like structure replacing the cation without being able to build a segregated apolar domain like in ethanolanmonium nitrate. EAN-alcohols mixtures^{26,27} are of high interest for a variety of reasons and have been studied in detail by a number of groups, but such systems will be discussed in the next chapter.

V. Summary

In this chapter I have exposed my findings on some EAN+molecular liquid binary mixtures. The main findings were:

- DMSO is able to replace the anion almost quantitatively from the first solvation shell of the cation, forming a stable stoichiometric complex of approximated formula $[EA(DMSO)_2]^+[NO_3]^-$.

- EAN+ethylene glycol mixtures act almost like ideal mixtures, due to the similarity of hydrogen bond network of the two neat compounds and the mixed systems.
- Ethanolamine destroys the sponge-like structure of EAN by replacing the cation.
- In EAN+methyl-glycol systems the open-closed equilibrium of MEO is highly perturbed by the IL. As a consequence, the interactions undergo a transition following the conformation of methyl-glycol.

VI. References

- 1 Y. Kohno and H. Ohno, *Chem. Commun. (Camb.)*, 2012, **48**, 7119–30.
- 2 H. Ohno, *Bull. Chem. Soc. Jpn.*, 2006, **79**, 1665–1680.
- 3 R. D. Rogers and K. R. Seddon, *Science*, 2003, **302**, 792–3.
- 4 C. Yue, D. Fang, L. Liu and T.-F. Yi, *J. Mol. Liq.*, 2011, **163**, 99–121.
- 5 B. M. Quinn, Z. Ding, R. Moulton and A. J. Bard, *Langmuir*, 2002, **18**, 1734–1742.
- 6 M. Galiński, A. Lewandowski and I. Stepniak, *Electrochim. Acta*, 2006, **51**, 5567–5580.
- 7 A. Lewandowski and A. Świdarska-Mocek, *J. Power Sources*, 2009, **194**, 601–609.
- 8 V. Borgel, E. Markevich, D. Aurbach, G. Semrau and M. Schmidt, *J. Power Sources*, 2009, **189**, 331–336.
- 9 M. Piana, J. Wandt, S. Meini, I. Buchberger, N. Tsiouvaras and H. a. Gasteiger, *J. Electrochem. Soc.*, 2014, **161**, 1992–2001.
- 10 J. E. Bara, T. K. Carlisle, C. J. Gabriel, D. Camper, A. Finotello, D. L. Gin and R. D. Noble, *Ind. Eng. Chem. Res.*, 2009, **48**, 2739–2751.
- 11 Z.-Z. Yang, Y.-N. Zhao and L.-N. He, *RSC Adv.*, 2011, **1**, 545.
- 12 A. P. Abbott and K. J. McKenzie, *Phys. Chem. Chem. Phys.*, 2006, **8**, 4265–4279.
- 13 S. Ishiguro, Y. Umebayashi, R. Kanzaki and K. Fujii, *Pure Appl. Chem.*, 2010, **82**,

1927–1941.

- 14 R. Atkin, S. M. C. Bobillier and G. G. Warr, *J. Phys. Chem. B*, 2010, **114**, 1350–60.
- 15 T. L. Greaves, D. F. Kennedy, S. T. Mudie and C. J. Drummond, *J. Phys. Chem. B*, 2010, **114**, 10022–31.
- 16 T. L. Greaves and C. J. Drummond, *Chem. Soc. Rev.*, 2013, **42**, 1096–120.
- 17 R. Sheldon, *Chem. Commun.*, 2001, 2399–2407.
- 18 H. Mizuuchi, V. Jaitely, S. Murdan and a T. Florence, *Eur. J. Pharm. Sci.*, 2008, **33**, 326–31.
- 19 K. N. Marsh, J. A. Boxall and R. Lichtenthaler, *Fluid Phase Equilib.*, 2004, **219**, 93–98.
- 20 A. A. H. Pádua, M. F. Costa Gomes and J. N. A. Canongia Lopes, *Acc. Chem. Res.*, 2007, **40**, 1087–96.
- 21 R. Kanzaki, K. Uchida, X. Song, Y. Umebayashi and S. Ishiguro, *Anal. Sci.*, 2008, **24**, 1347–9.
- 22 R. Hayes, S. Imberti, G. G. Warr and R. Atkin, *Angew. Chem. Int. Ed. Engl.*, 2012, **51**, 7468–71.
- 23 O. Russina, A. Sferrazza, R. Caminiti and A. Triolo, *J. Phys. Chem. Lett.*, 2014, **5**, 1738–1742.
- 24 O. Russina, A. Mariani, R. Caminiti and A. Triolo, *J. Solution Chem.*, 2015, **44**, 699–685.
- 25 A. Mariani, O. Russina, R. Caminiti and A. Triolo, *J. Mol. Liq.*, 2015, **212**, 947–956.
- 26 T. L. Greaves, D. F. Kennedy, N. Kirby and C. J. Drummond, *Phys. Chem. Chem. Phys.*, 2011, **13**, 13501–9.
- 27 H. J. Jiang, P. A. FitzGerald, A. Dolan, R. Atkin and G. G. Warr, *J. Phys. Chem. B*, 2014, **118**, 9983–90.
- 28 A. Triolo, W. H. Schroer and O. Russina, *J. Phys. Chem. B*, 2016, **9**, 2638–2643.

- 29 A. Oleinikova and M. Bonetti, *J. Chem. Phys.*, 1996, **104**, 3111.
- 30 A. Oleinikova and M. Bonetti, *J. Solution Chem.*, 2002, **31**, 397–413.
- 31 O. Russina, M. Macchiagodena, B. Kirchner, A. Mariani, B. Aoun, M. Russina, R. Caminiti and A. Triolo, *J. Non. Cryst. Solids*, 2015, **407**, 333–338.
- 32 A. Mariani, M. Campetella, C. Fasolato, M. Daniele, F. Capitani, L. Bencivenni, P. Postorino, S. Lupi, R. Caminiti and L. Gontrani, *J. Mol. Liq.*, 2016.
- 33 A. Mariani, R. Dattani, R. Caminiti and L. Gontrani, *J. Phys. Chem. B*, 2016.
- 34 S. Porcedda, B. Marongiu, M. Schirru, D. Falconieri and A. Piras, *J. Therm. Anal. Calorim.*, 2010, **103**, 29–33.
- 35 R. Zarrougui and M. Dhahbi, *J. Solution Chem.*, 2010, **39**, 1531–1548.
- 36 O. Russina, M. Macchiagodena, B. Kirchner, A. Mariani, B. Aoun, M. Russina, R. Caminiti and A. Triolo, *J. Non. Cryst. Solids*, 2015, **407**, 333–338.
- 37 C. Roth, A. Appelhagen, N. Jobst and R. Ludwig, *Chemphyschem*, 2012, **13**, 1708–17.
- 38 A. Dolan, R. Atkin and G. G. Warr, *Chem. Sci.*, 2015, **6**, 6189–6198.
- 39 M. Liang, S. Khatun and E. W. J. Castner, *J. Chem. Phys.*, 2015, **142**, 121101.
- 40 M. Brehm, H. Weber, A. S. Pensado, A. Stark and B. Kirchner, *Zeitschrift fuer Phys. Chemie (Muenchen, Ger.)*, 2013, **227**, 177–203.
- 41 D. Martin, A. Weise and H.-J. Niclas, *Angew. Chemie Int. Ed. English*, 1967, **6**, 318–334.
- 42 X.-F. Wu and K. Natte, *Adv. Synth. Catal.*, 2016, **358**, 336–352.
- 43 I. I. Vaismant and M. L. Berkowitz, *J. Am. Chem. Soc.*, 1992, **21**, 1889–1896.
- 44 B. Kirchner and M. Reiher, *J. Am. Chem. Soc.*, 2002, **124**, 6206–15.
- 45 S. E. McLain, A. K. Soper and A. Luzar, *J. Chem. Phys.*, 2007, **127**, 174515.
- 46 A. P. MacKenzie and D. H. Rasmussen, *Nature*, 1968, **220**, 1315–1317.

- 47 J. M. G. Cowie and P. M. Toporowski, *Can. J. Chem.*, 1961, **39**, 2240–2243.
- 48 H. N. Bordallo, K. W. Herwig, B. M. Luther and N. E. Levinger, *J. Chem. Phys.*, 2004, **121**, 12457–12464.
- 49 A. K. Soper and A. Luzar, *J. Chem. Phys.*, 1992, **97**, 1320.
- 50 W. Jiang, Y. Wang and G. A. Voth, *J. Phys. Chem. B*, 2007, **111**, 4812–8.
- 51 U. Domańska and L. M. Casás, *J. Phys. Chem. B*, 2007, **111**, 4109–4115.
- 52 B. Fazio, A. Triolo and G. Di Marco, *J. Raman Spectrosc.*, 2008, **39**, 233–237.
- 53 M. A. Iglesias-Otero, J. Troncoso, E. Carballo and L. Romani, *J. Chem. Eng. Data*, 2008, **53**, 1298–1301.
- 54 C. Schröder, G. Neumayr and O. Steinhauser, *J. Chem. Phys.*, 2009, **130**, 194503.
- 55 B. Wu, Y. Liu, Y. Zhang and H. Wang, *Chemistry*, 2009, **15**, 6889–93.
- 56 Y. Litaeim and M. Dhahbi, *J. Mol. Liq.*, 2010, **155**, 42–50.
- 57 T. Chen, M. Chidambaram, Z. Liu, B. Smit and A. T. Bell, *J. Phys. Chem. B*, 2010, **114**, 5790–5794.
- 58 L. E. Ficke and J. F. Brennecke, *J. Phys. Chem. B*, 2010, **114**, 10496–10501.
- 59 M. Blesic, J. N. C. Lopes, M. F. C. Gomes and L. P. N. Rebelo, *Phys. Chem. Chem. Phys.*, 2010, **12**, 9685–9692.
- 60 S. Fendt, S. Padmanabhan, H. W. Blanch and J. M. Prausnitz, *J. Chem. Eng. Data*, 2011, **56**, 31–34.
- 61 J. A. Smith, G. B. Webber, G. G. Warr and R. Atkin, *J. Phys. Chem. B*, 2013, **117**, 13930–13935.
- 62 V. K. Sharma, S. Solanki, S. Bhagour and D. Sharma, *Thermochim. Acta*, 2013, **569**, 36–41.
- 63 B. Docampo-Álvarez, V. Gómez-González, T. Méndez-Morales, J. Carrete, J. R. Rodríguez, Ó. Cabeza, L. J. Gallego and L. M. Varela, *J. Chem. Phys.*, 2014, **140**, 214502.

- 64 T. Greaves and C. J. Drummond, *Chem. Rev.*, 2015, **115**, 11379–11448.
- 65 A. Chagnes, A. Tougui, B. Carr and N. Ranganathan, *J. Solution Chem.*, 2004, **33**, 247–255.
- 66 Y. Xu, B. Chen, W. Qian and H. Li, *J. Chem. Thermodyn.*, 2013, **58**, 449–459.
- 67 A. Jarosik, S. R. Krajewski, A. Lewandowski and P. Radzimski, *J. Mol. Liq.*, 2006, **123**, 43–50.
- 68 X. Song, H. Hamano, B. Minofar, R. Kanzaki, K. Fujii, Y. Kameda, S. Kohara, M. Watanabe, S. Ishiguro and Y. Umebayashi, *J. Phys. Chem. B*, 2012, **116**, 2801–13.
- 69 P. M. Mancini, G. G. Fortunato and L. R. Vottero, *Phys. Chem. Liq.*, 2004, **42**, 625–632.
- 70 G. Rai and A. Kumar, *J. Phys. Chem. B*, 2014, **118**, 4160–4168.
- 71 K. Fumino, P. Stange, V. Fossog, R. Hempelmann and R. Ludwig, *Angew. Chemie - Int. Ed.*, 2013, **52**, 12439–12442.
- 72 T. L. Greaves, D. F. Kennedy, A. Weerawardena, N. M. K. Tse, N. Kirby and C. J. Drummond, *J. Phys. Chem. B*, 2011, **115**, 2055–66.

Chapter IV: Unusual Binary Systems



*It is a popular fact that nine-tenths of the brain is not used and,
like most popular facts, it is wrong.*

[...]

*It **is** used.*

*And one of its functions is to make the miraculous seem ordinary
and turn the unusual into the usual.*

*(“**Small Gods**” - Sir Terry Pratchett)*

I. Micelles, clusters, or...?

The structure of ionic liquids has been thoroughly described in Chapter II. Dissolving a co-solvent into an IL may have a variety of effects depending on the nature of the salt and on the mixed compound¹⁻¹¹. Taking ethylammonium nitrate¹² as a prototype, there is a wide range of literature concerning the effects that mixing have on its structure¹³⁻²⁵. Recently it has been reported that the addition of n-alcohols to some ILs leads to an unexpected feature in the extreme low q region of the SAXS pattern^{11,26,27}, which from now on will be termed “Low q Excess” (LqE). Greaves *et al.*²⁸ observed that in some EAN-alcohol mixtures, some micellar-like structures could be found. A confirmation of this behaviour came from Jiang *et al.*²⁶ stating that when an alcohol is longer than twice the alkyl chain of the IL, then it is too big to be accommodated into the apolar domain thus forming a series of self-assembled structures where the cation acts as a co-surfactant. This interpretation cannot explain why the same effect is found in EAN-methanol mixtures, where one may expect a total mutual miscibility. For this system, when first observed by Triolo *et al.*^{11,14,29}, an explanation in terms of ionic liquid molecules clustering was proposed in order to explain the LqE¹¹. More recent findings, always by Triolo *et al.* on EAN+1-pentanol systems²⁷, suggest that the origin of the LqE is due to density and concentration fluctuations. In the last few months of my PhD, I have discovered that the LqE is much more common than one may believe, and it is not limited to protic ionic liquid + n-alcohols systems³⁰. Basing on my findings, the cause behind this unexpected feature in the SAXS patterns of some systems may be related to an incipient unmixing of the sample. So it is not a properly said “structural” feature, but a

physical state of the system. We have defined the LqE according to two criteria: i) the scattered intensity below 0.5 \AA^{-1} is higher of the sum of the scattered intensities of the two neat compounds weighted for their molar fractions, i.e. if the scattered intensity of the mixture does not fall in between the curves of both the pure compounds, and ii) if the first criterion is fulfilled, a mixture has an excess intensity if the diffracted intensity clearly shows a slope.

II. Janus Compounds

First I will expose my results on systems containing “dual” molecules, meaning that the compound has both a hydrophilic and a hydrophobic termination. I will take advantage from the Classical figure of Janus to better expose this duality. This kind of molecules have always attracted great



Figure 4.1: Janus

interest in the chemistry field³¹, due to their unique properties such as the ability to self-assemble³², the possibility to act as surfactants³³, the excellent solvent properties and a series of useful applications in synthesis.

II.1. EAN+methanol

This is the first system for which the LqE was ever reported in 2014 by Triolo *et al.*¹¹. At that time, his EPSR (reverse Monte Carlo) simulations suggested that the feature below 0.3 \AA^{-1} was generated by EAN clusters floating into a methanol sea. Such a rigid interpretation is unlikely to be invoked for a liquid homogenous phase. My molecular dynamics simulations²⁹, instead, suggested a much more flexible and fluctuant arrangement, where EAN-rich and methanol-rich regions were compenetrating.

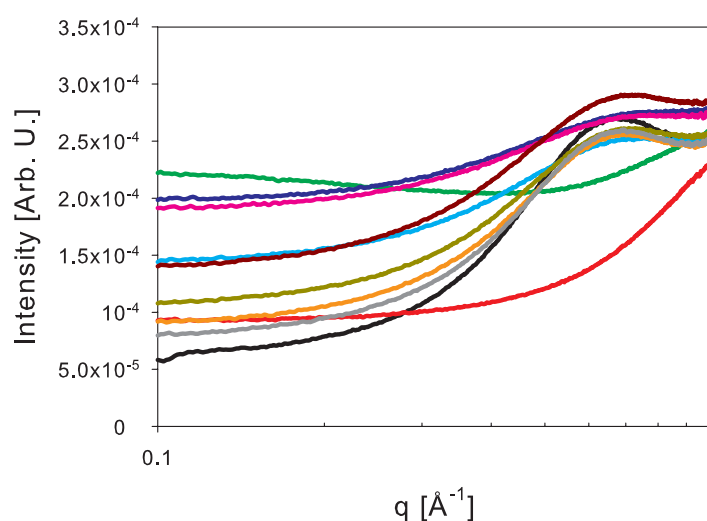


Figure 4.2: SAXS patterns for EAN+methanol systems. EAN (black); methanol (red); EM1 (green); EM2 (blue); EM3 (pink); EM4 (cyan); EM5 (brown); EM6 (gold); EM7 (orange); EM9 (grey).

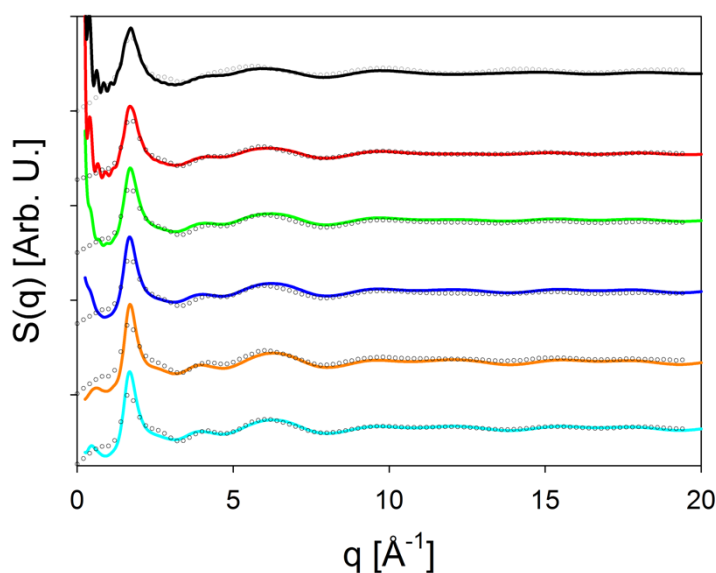


Figure 4.3: WAXS patterns for EAN+methanol systems. EM1 (black); EM2 (red); EM3 (green); EM5 (blue); EM7 (orange); EM9 (cyan). Symbols refers to experimental data, solid lines to the models.)

From figures 4.2 and 4.3 above, it is evident how at low EAN concentration the extreme low q region shows an intensity excess. From the Bragg law we can estimate that the *objects* which cause this phenomenon are larger than 60 Å in this case, but it is a strong underestimation because we cannot say the exact position of the maximum of the LqE. The volumetric analysis of this system shows similarities with the EAN-DMSO system.

System	χ_{EAN}	Density [g/ml]	Excess Molar Volume [ml/mol]
Methanol	0	0.792	0
EM05	0.05	0.84813	-0.6403
EM1	0.1	0.89232	-0.9183
EM2	0.2	0.96227	-1.1381
EM3	0.3	1.01679	-1.1849
EM4	0.4	1.06083	-1.1492
EM5	0.5	1.09781	-1.0987
EM6	0.6	1.12791	-0.9530
EM7	0.7	1.15299	-0.7487
EM8	0.8	1.17485	-0.5454
EM9	0.9	1.19372	-0.3179
EAN	1	1.2106	0

Table 4.1: EAN+methanol systems, composition, density and excess molar volume

In both cases the minimum is located at about 0.3 EAN molar fraction.

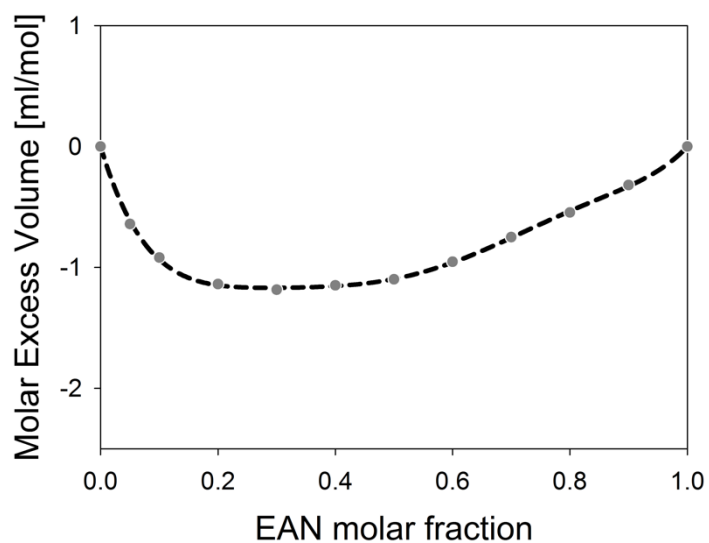


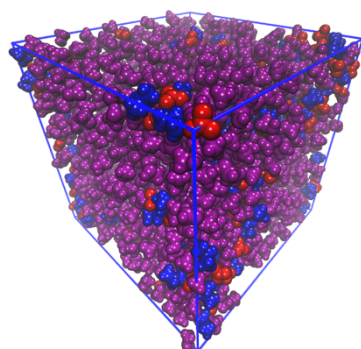
Figure 4.4: Excess molar volume for EAN+methanol systems at 25 °C

The MD simulations were always capable of finely reproducing the experimental densities.

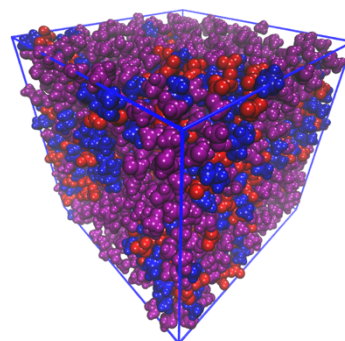
System	Exp. Density [g/ml]	Calc. Density [g/ml]
EM1	0.89232	0.8954
EM2	0.96227	0.9688
EM3	1.01679	1.0213
EM5	1.09781	1.1076
EM7	1.15299	1.1606
EM9	1.19372	1.2001

Table 4.2: Mass density comparison between experimental and computed data for EAN+methanol systems

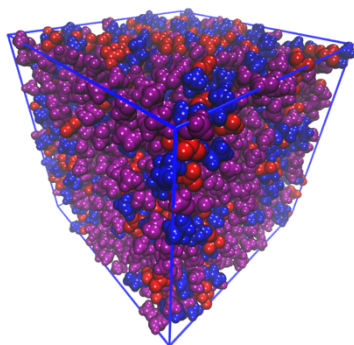
Nevertheless, to finely reproduce the LqE, in my simulations I had to use a box with an edge way larger than 120 Å. With the nowadays computational power such a simulation would last months, so I've performed some simulations using a box with a side of 80 Å, to check if I can achieve a qualitative agreement with the experiments. Visual inspection of the simulation boxes shows some kind of agglomeration when EAN is the minority compound (i.e. when LqE is observed).



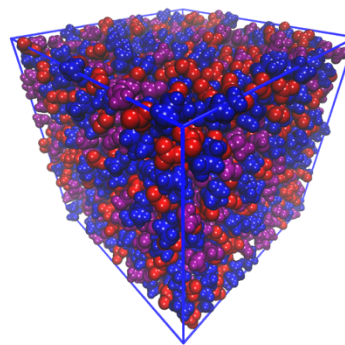
a



b



c



d

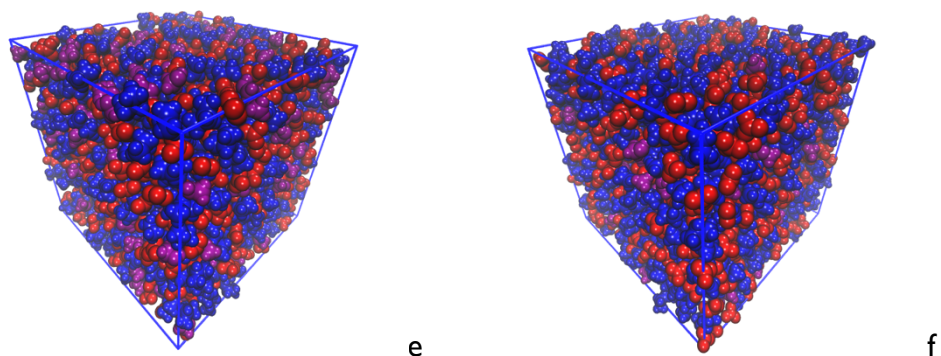
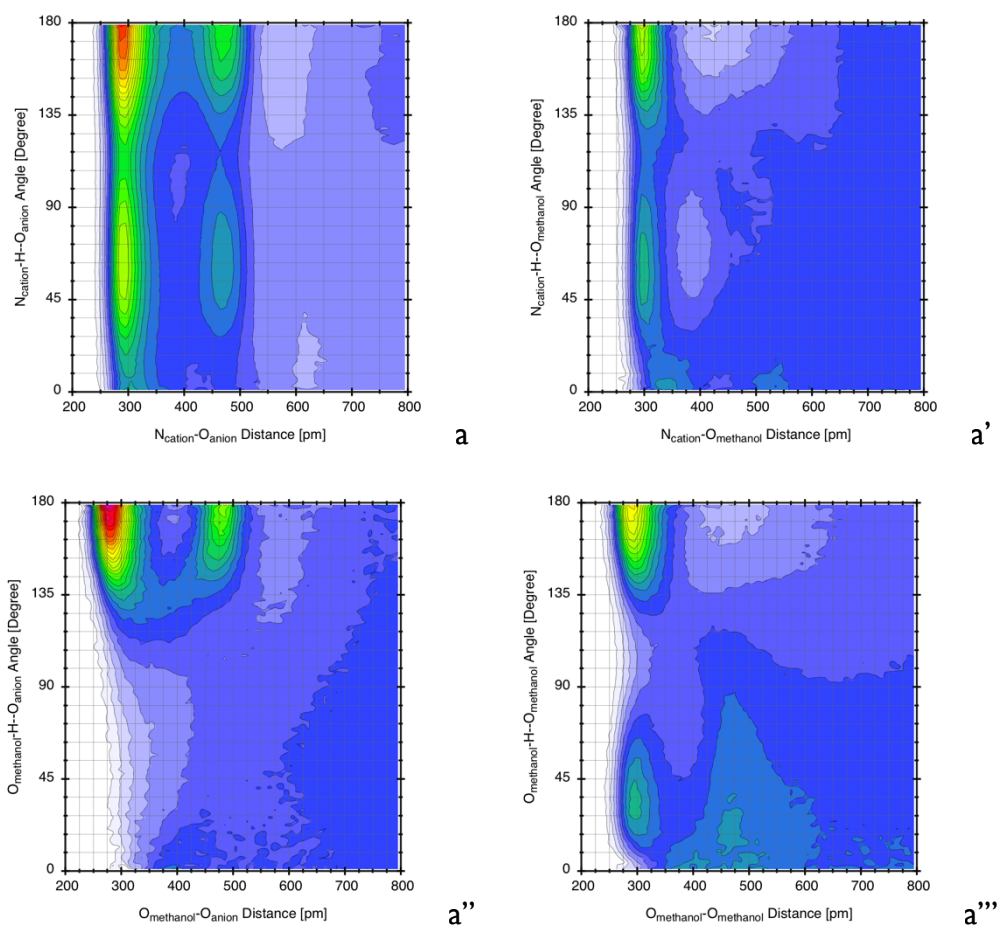
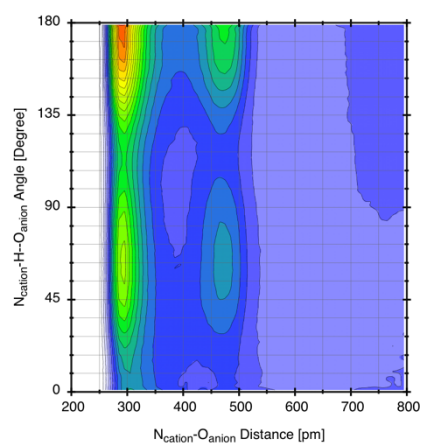


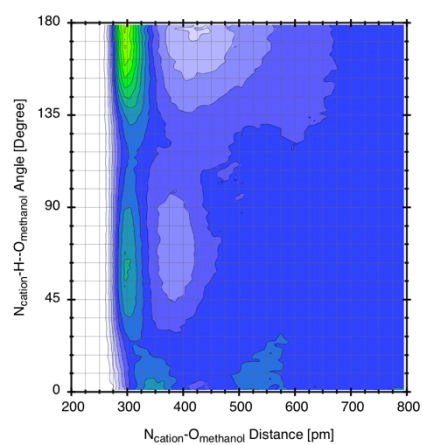
Figure 4.5: Snapshots of the simulation boxes for EAN+methanol systems. (a) EM1; (b) EM2; (c) EM3; (d) EM5; (e) EM7; (f) EM9. Cation (blue); anion (red); methanol (violet)

The analysis of the hydrogen bond geometry for this system is pretty complex because there are four different possible interactions: cation-anion, cation-methanol, anion-methanol and methanol-methanol.

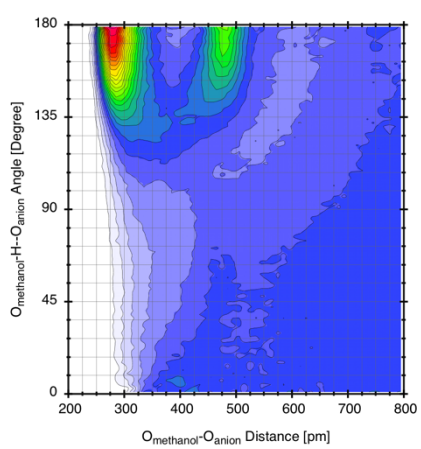




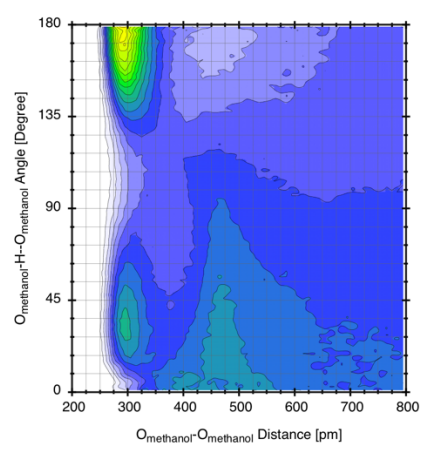
b



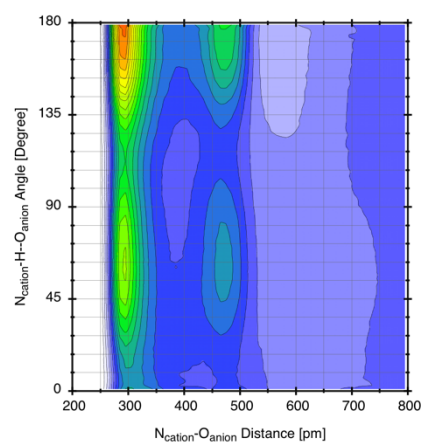
b'



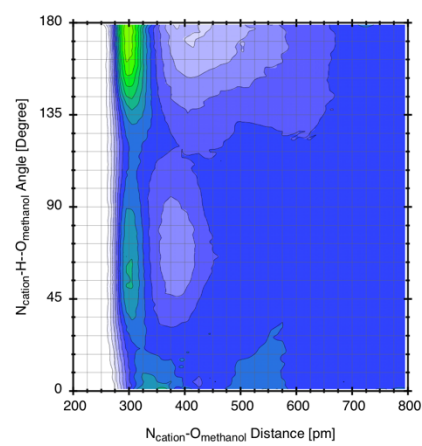
b''



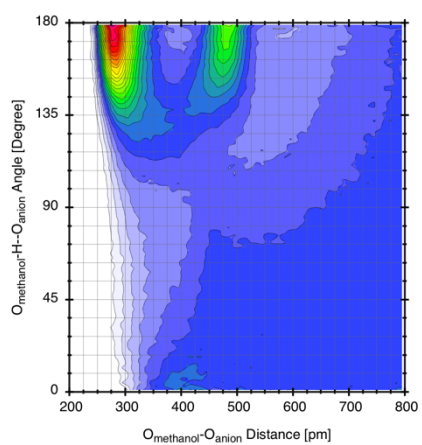
b'''



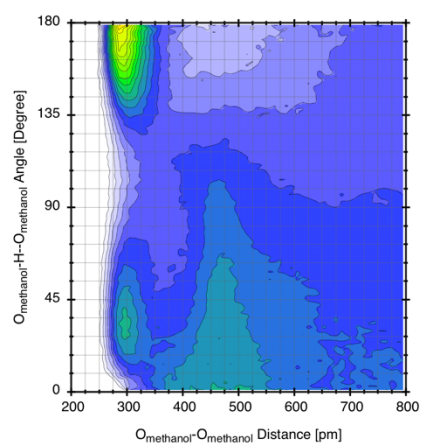
c



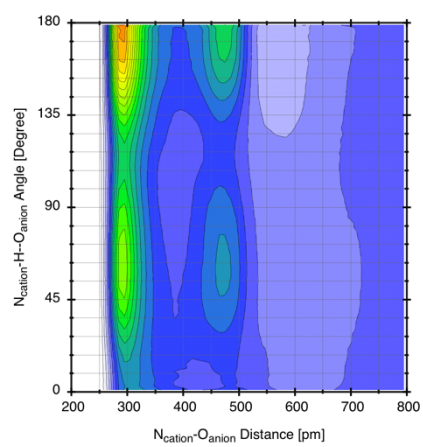
c'



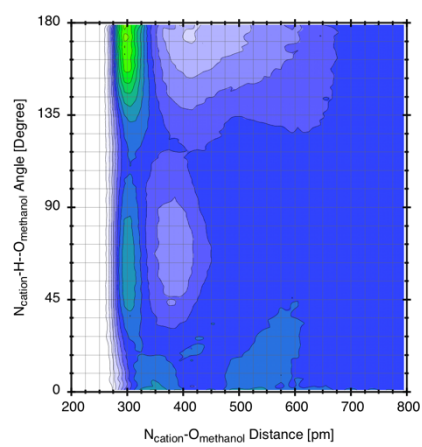
c''



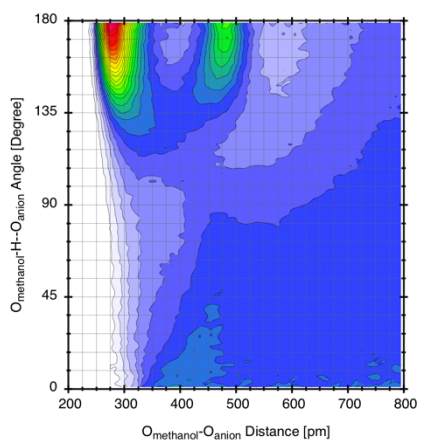
c'''



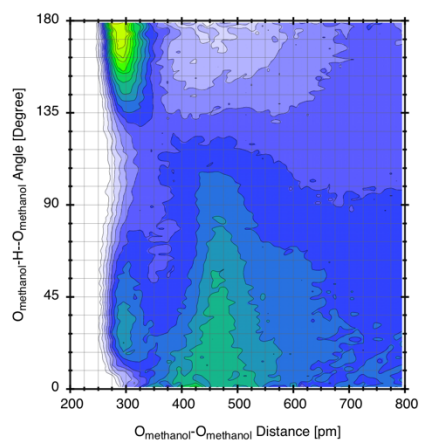
d



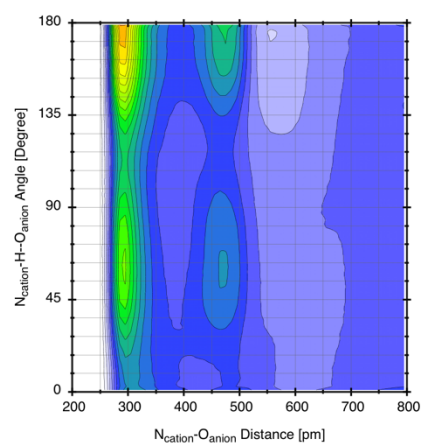
d'



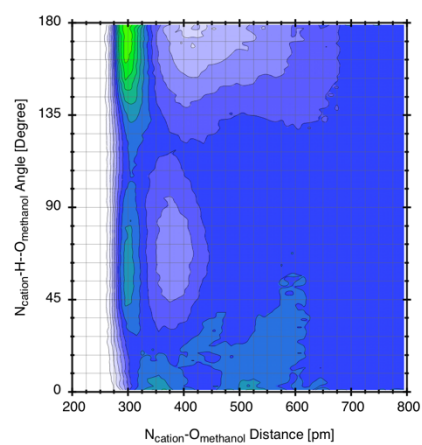
d''



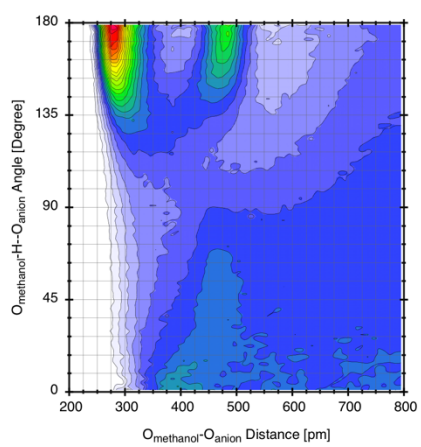
d'''



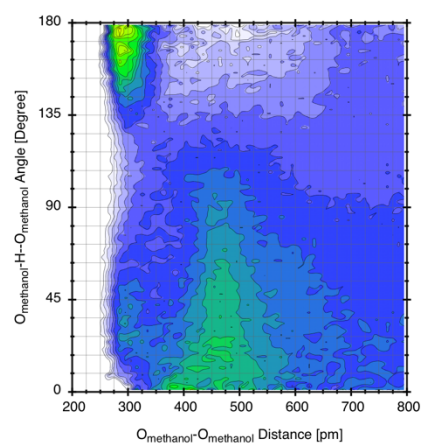
e



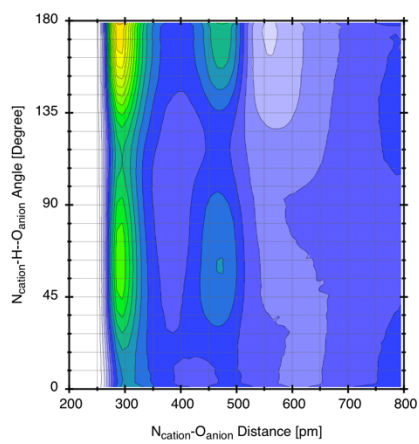
e'



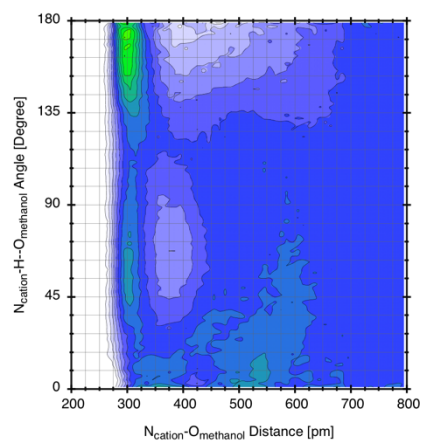
e''



e'''



f



f'

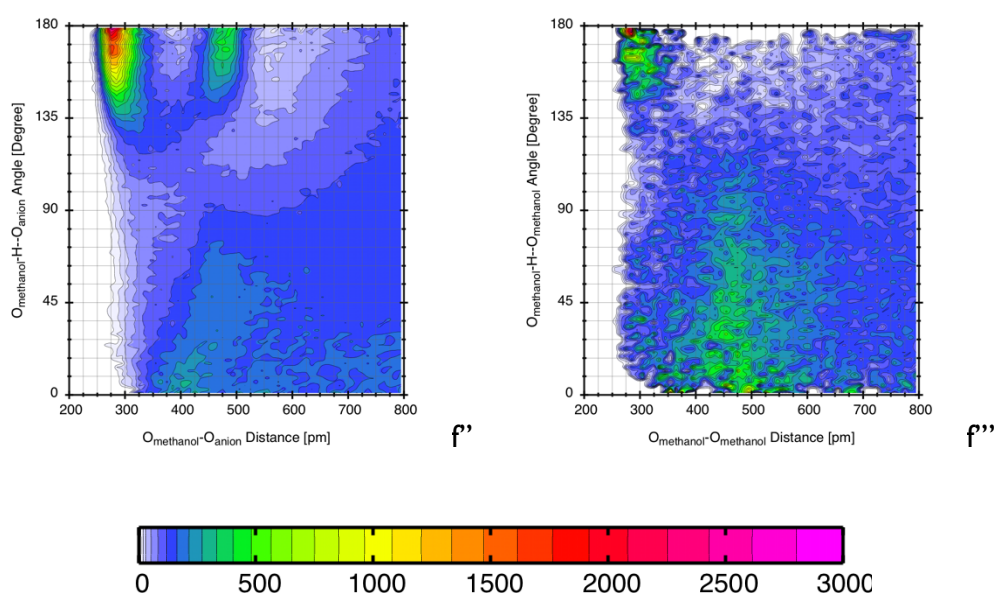
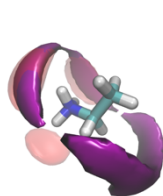
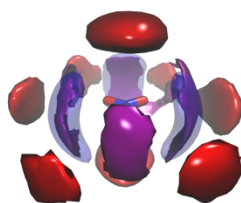


Figure 4.6: Combined radial-angular distribution functions for the various hydrogen bonds in the EAN+methanol systems. (a) EM1; (b) EM2; (c) EM3; (d) EM5; (e) EM7; (f) EM9. Plain letters refers to the NH₃-NO₃ interaction; single prime to NH₃-OH; double prime to OH-NO₃; triple prime to OH-OH.

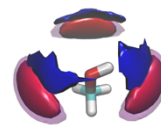
Two interesting observations can be made. The first is that the cation-anion interaction becomes stronger as methanol is added to EAN, reaching its maximum in the EM1 mixture. This could suggest that the cation prefers to interact with other ionic liquids fragments rather than methanol, originating EAN-rich regions where the alcohol is found in traces. The second one is that anion-methanol interaction is the strongest one independently of the mixture composition. To better understand the overall organization within this system, the SDF are probably the best instrument because of the pronounced anisotropy.



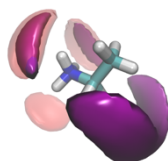
a



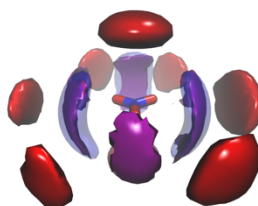
a'



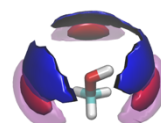
a''



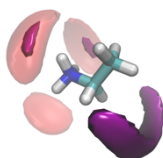
b



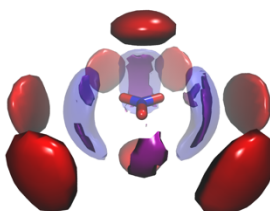
b'



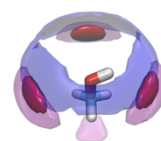
b''



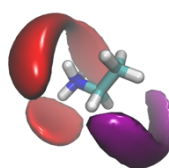
c



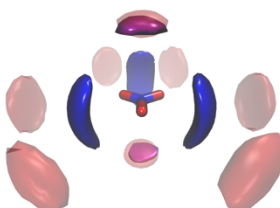
c'



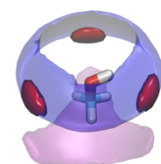
c''



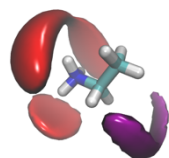
d



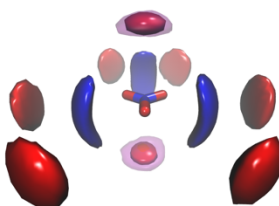
d'



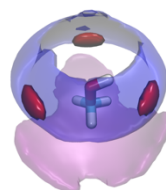
d''



e



e'



e''

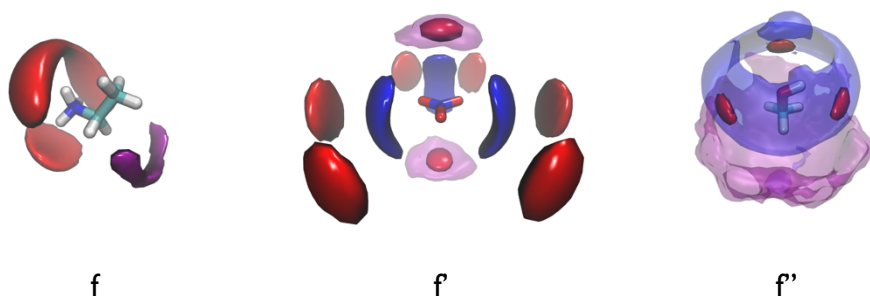


Figure 4.7: Spatial distribution functions for EAN+methanol systems. All the isosurfaces refer to 2 times the bulk density of the observed atom. (a) EM1; (b) EM2; (c) EM3; (d) EM5; (e) EM7; (f) EM9. Plain letters refer to cation environment; single prime to anion environment; double prime to methanol environment. Nitrogen of the cation (blue); oxygen of the anion (red); oxygen of the methanol (purple).

The results obtained with this analysis are outstanding and extremely clear. Looking at the coordination around the anion (central column), one may clearly see how the methanol is found in the equatorial positions in EM1, EM2 and EM3, while it swaps in axial positions in the systems containing more EAN. Simultaneously, the methanol-methanol coordination (right column) undergoes a transition at the same composition range. In methanol-rich systems, the alcohol coordinates itself around the hydroxyl group, while when EAN becomes important, it prefers to interact via the methyl group. This structural transition is pretty clear and corresponds to the experimental evidence: nitrate-methanol equatorial interaction and methanol-methanol hydroxyl coordination are found where the LqE is observed and suddenly vanish when there is no LqE in the SAXS pattern.

II.II. EAN+acetonitrile

Acetonitrile is a colourless liquid and is the simplest organic nitrile. It is a collateral product of the acrylonitrile manufacture. As a polar aprotic solvent it finds a wide range of applications in laboratory. It has a convenient liquid range and a high dielectric constant of 38.8. With a dipole moment of 3.92 D, acetonitrile dissolves a wide range of ionic and nonpolar compounds and is useful as a mobile phase in HPLC and LC-MS. The N-C-C skeleton is linear with a short C-N distance of 1.16 Å typical of a triple bond. Acetonitrile was first prepared in 1847 by the French chemist Jean-Baptiste Dumas. I have used this compound to check the differences with methanol, so highlighting the role of a hydrogen bond donor.

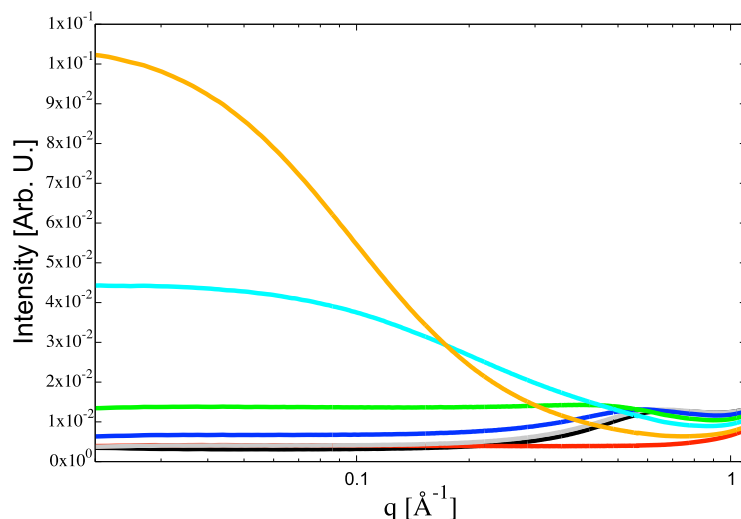


Figure 4.8: SAXS patterns for the EAN+acetonitrile systems. EAN (black); acetonitrile (red); ECN1 (orange); ECN3 (cyan); ECN5 (green); ECN7 (blue); ECN9 (grey)

Here the LqE is a lot higher than in the other mixtures and even higher than the main peak.

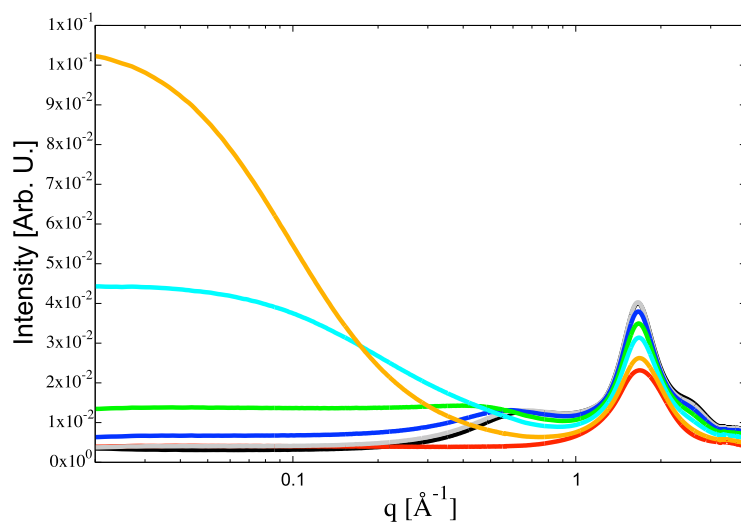


Figure 4.9: SWAXS patterns for the EAN+acetonitrile systems. EAN (black); acetonitrile (red); ECN1 (orange); ECN3 (cyan); ECN5 (green); ECN7 (blue); ECN9 (grey)

As in the case of EAN+methanol mixtures, the LqE has its maximum intensity at low EAN concentration, and decreases as the IL is added to the mixture. The entity of the LqE in this system, induced me to pay particular attention to it.

System	χ_{EAN}	Density [g/ml]	Excess Molar Volume [ml/mol]
Acetonitrile	0	0.7759	0
ECN1	0.1	0.85719	-0.8443
ECN3	0.3	0.98347	-1.6607
ECN5	0.5	1.07155	-1.5567
ECN7	0.7	1.13984	-1.2598
ECN9	0.9	1.18966	-0.5186
EAN	1	1.2106	0

Table 4.3: EAN+acetonitrile systems, composition, density and excess molar volume

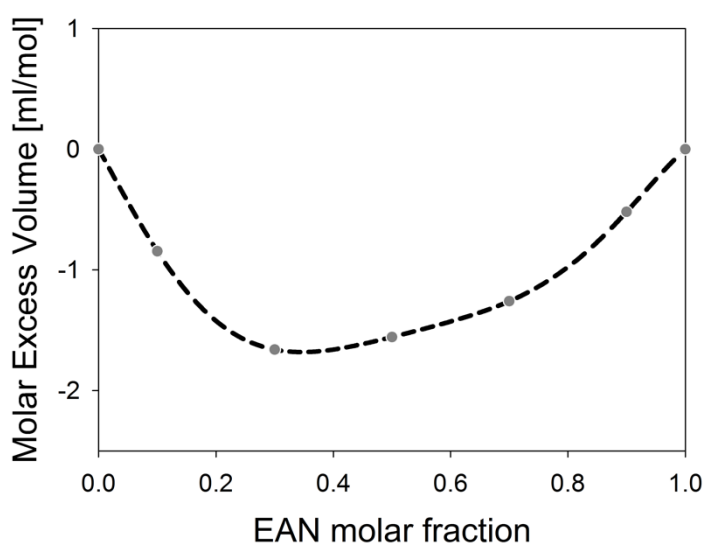


Figure 4.10: Excess molar volume for EAN+acetonitrile systems at 25 °C

This is the system where I've found the largest negative excess molar volume, meaning that the overall molecular interactions are strongly favourable. The minimum position is located again close to 0.3 EAN molar fraction.

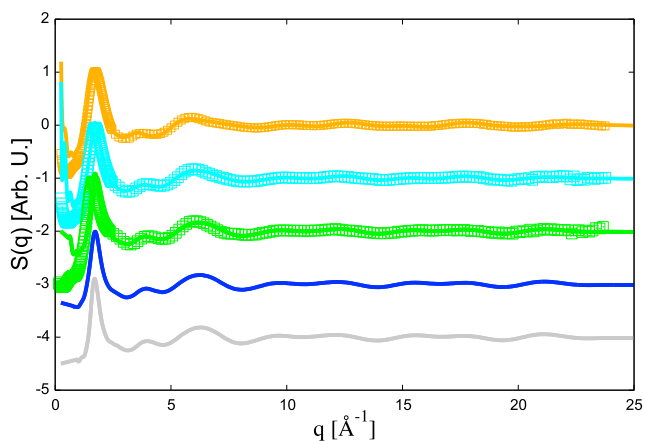


Figure 4.11: WAXS patterns for EAN+acetonitrile systems. ECN1 (orange); ECN3 (cyan); ECN5 (green); ECN7 (blue); ECN9 (grey). Symbols refer to experimental data; solid lines to the models

The models are able to reproduce the initial slope of the LqE when observable, while do not show such feature if the collected data lack it.

System	Exp. Density [g/ml]	Calc. Density [g/ml]
ECN1	0.85719	0.8576
ECN3	0.98347	0.9844
ECN5	1.07155	0.1068
ECN7	1.13984	1.1395
ECN9	1.18966	1.1901

Table 4.4: Mass density comparison between experimental and computed data for EAN+acetonitrile systems

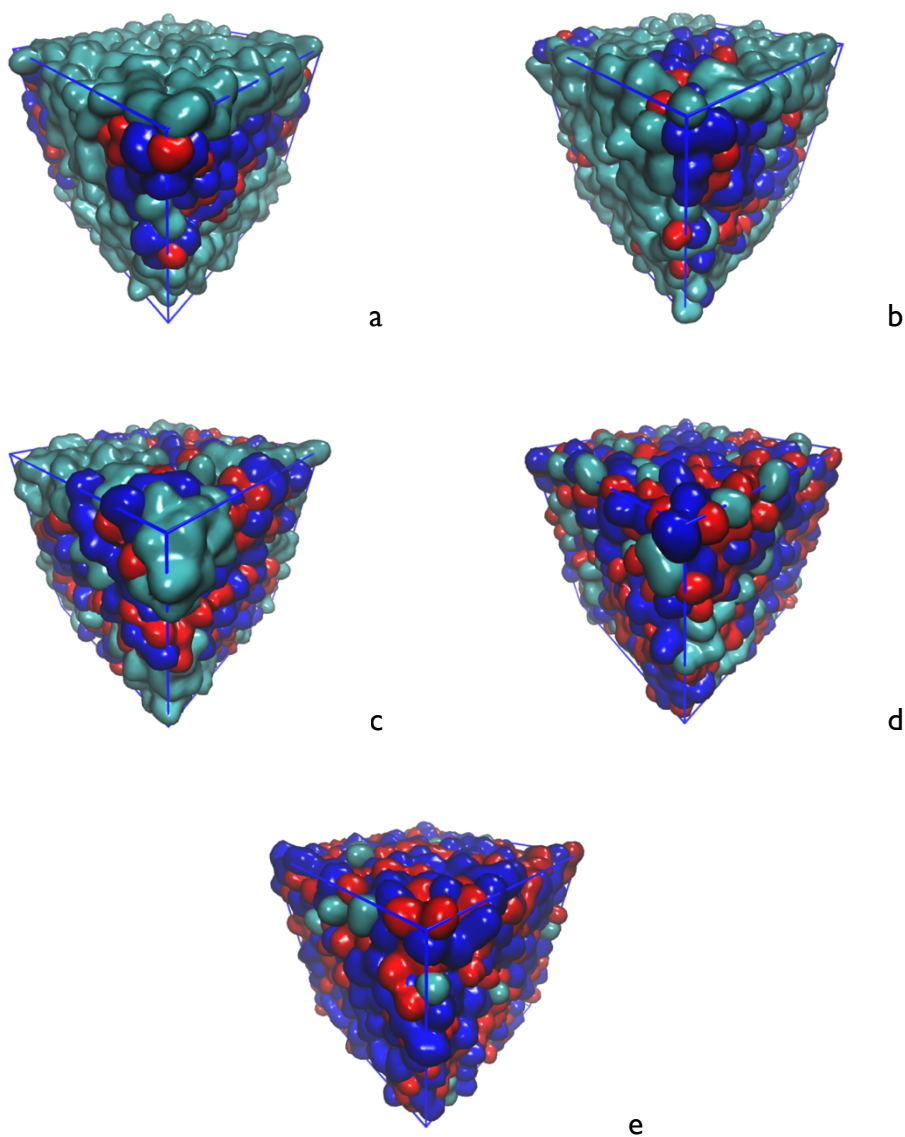


Figure 4.12: Snapshots of the simulation boxes for EAN+acetonitrile systems. (a) ECN1; (b) ECN3; (c) ECN5; (d) ECN7; (e) ECN9. Cation (blue); anion (red); acetonitrile (cyan)

The visual inspection of the simulation boxes shows clearly how ECN1, ECN3 and partially ECN5 are highly heterogeneous (it should be pointed out the all the mixtures are macroscopically homogeneous), *i.e.* the same systems for which the LqE is observable, suggesting a connection between nano phase-separation and this odd scattering feature. For this system I've also collected some viscosity data, which are shown in table 4.5 and figure 4.13.

χ_{EAN}	15 °C [cP]	20 °C [cP]	25 °C [cP]	30 °C [cP]	35 °C [cP]
0	0.4	0.37	0.35	0.32	0.3
0.1	0.792	0.737	0.685	0.647	0.615
0.3	3.05	2.765	2.451	2.354	2.262
0.5	8.299	7.358	6.37	6.038	5.66
0.7	20.13	17.22	14.73	12.19	10.3
0.9	39.46	33.07	27.58	24.12	20.16
1	42.59	35.77	32.69	29.6	25.83

Table 4.5: Viscosities for the EAN+acetonitrile systems as a function of temperature and composition.

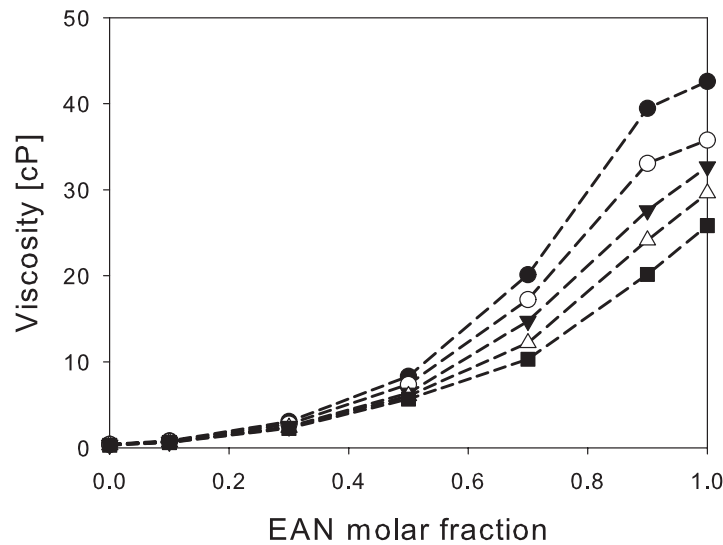


Figure 4.13: Viscosities for EAN+acetonitrile systems. 15 °C (black circles); 20 °C (white circles); 25 °C (black triangles); 30 °C (white triangles); 35 °C (black squares). Lines are a guide to the eye, not a fit.

It is convenient to plot the viscosity data in an Arrhenius-like plot, because following the formula

$$\eta = \eta_0 \cdot e^{-\frac{E_a}{RT}} \quad [4.1]$$

the linear regression of the points in that plot could yield some important observations.

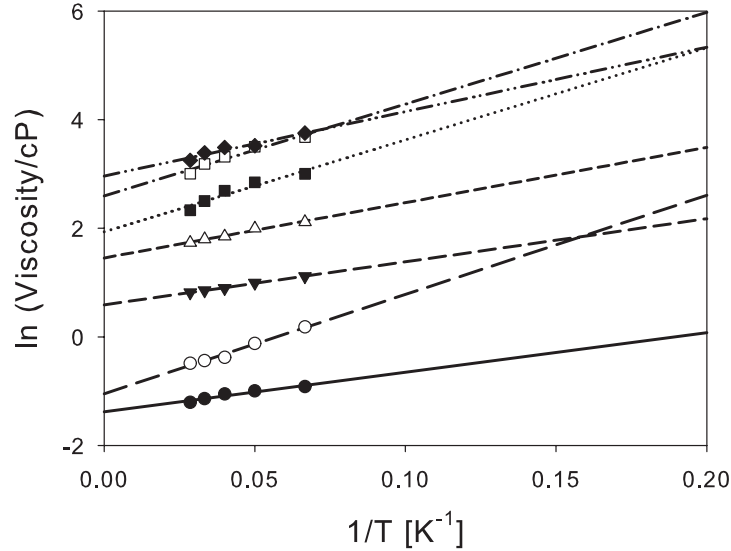


Figure 4.14: Viscosities for EAN+acetonitrile systems in an Arrhenius plot. EAN (black diamonds – dash double dotted line); ECN9 (white squares – dash single dotted line); ECN7 (black squares – dotted line); ECN5 (white triangles – short dashed line); ECN3 (black triangles – medium dashed line); ECN1 (white circles – long dashed line); acetonitrile (black circles – solid line)

	ACN	ECN1	ECN3	ECN5	ECN7	ECN9	EAN
η_0	0.2364	-1.0172	0.5892	1.4546	1.9190	2.5968	2.9613
$\frac{Ea}{RT}$	2.5534	17.9614	7.9292	10.1650	16.8479	16.8992	11.8556

Table 4.6: Fitting parameters for the EAN+acetonitrile systems viscosity

From the fit it is evident that there are no deviations from the Arrhenius Law. It is not trivial to rationalize these results, but the interpretation based on the excess viscosity (i.e. the analogue of the excess volume) it is often used to extract informations from this kind of data^{34–38}.

$$\eta^{ex} = \eta_{exp} - \chi_1 \eta_1 - \chi_2 \eta_2 \quad [4.2]$$

where η_{exp} is the experimental viscosity, χ_N is the molar fraction of component N and η_N is the viscosity of neat N at the same temperature.

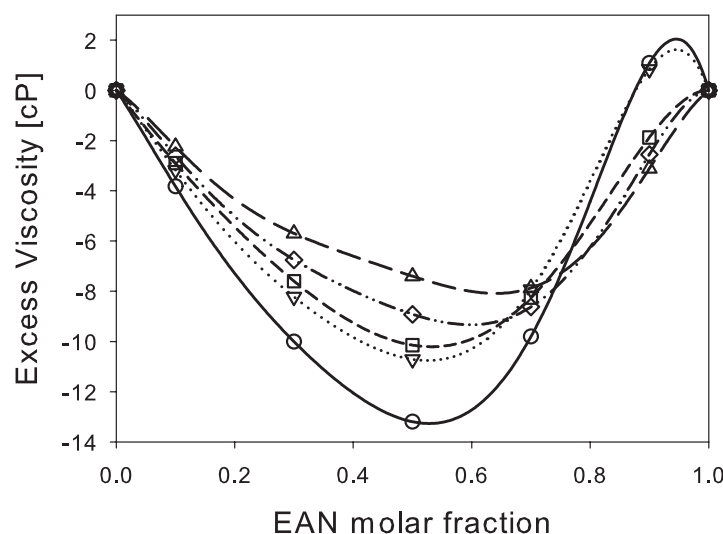


Figure 4.15: Excess viscosity for EAN+acetonitrile systems. 15 °C (circles – solid line); 20 °C (reverse triangles – dotted line); 25 °C (squares – short dashed line); 30 °C (diamonds – dash double dotted line); 35 °C (triangles – long dashed line)

The fitting parameters for the Redlich-Kister equation³⁹ are reported in table 4.6.

Parameter	15 °C	20 °C	25 °C	30 °C	35 °C
A₀	-52.7852	-42.8480	-40.6000	-35.6880	-29.6200
A₁	9.7614	6.9481	7.5823	15.0023	15.2192
A₂	27.2411	20.9649	16.3414	-11.3566	-22.3053
A₃	-68.5890	-54.4002	-22.9477	-23.9728	-14.2423
A₄	49.1613	40.2084	8.8226	34.9815	34.5347

Table 4.6: Fitting parameters for EAN+acetonitrile systems excess viscosity

Excess viscosity is a probe of the molecular interaction, negative values meaning that the interactions are less strong than one could expect, and *viceversa* for positive deviations. The lines relative to the highest temperatures (i.e. 35 °C, 30 °C and 25 °C) in figure 4.15 always show a negative deviation from the ideal behaviour, whereas at 15 °C and 20 °C a positive deviation is found from ~ 0.9 EAN molar fraction onward. This could mean that when acetonitrile is added to the IL, at relatively low temperature a strong favourable interaction is established, that is lost warming the system and/or adding further acetonitrile. Another notable fact is that the minimum position is located slightly higher than 0.5 EAN molar fraction and remains approximately constant at that value at 15 °C, 20 °C and 25 °C. For higher temperatures the minimum is shifted towards the EAN-rich region. This mean that at relatively high temperatures, acetonitrile induces a

steep decrease in the IL viscosity even in small amounts, while it is less effective lowering the temperature. The last observation is that the largest deviation is found at the lowest temperature, meaning that the system behaves more and more as an ideal one as the temperature is raised. For this system I have collected also data for another quantity strictly related to viscosity, the diffusion constant D . The latter was determined by means of NMR DOSY experiments⁴⁰, by following separately the diffusion of the two components of the mixture. This was possible because in the ^1H -NMR spectrum the signals from EAN and the signal from acetonitrile were well separated. As an example here the spectra of the 1:1 mixture is reported.

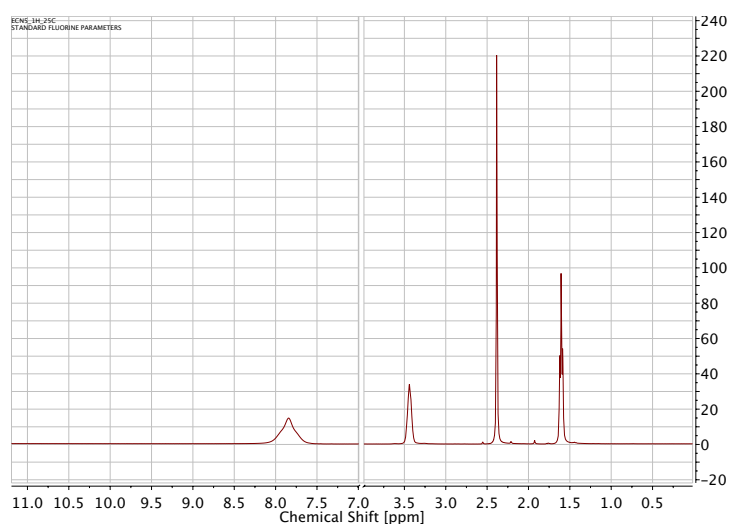


Figure 4.16: ECN5 ^1H NMR spectrum

All the chemical shifts for each system studied are reported in table 4.7

	$\text{N}\equiv\text{CH}_3$	$\text{H}_3\text{C}-\overset{\text{H}_2}{\underset{\text{NH}_3}{\text{C}}}^+$	$\text{H}_3\text{C}-\overset{\text{H}_2}{\underset{\text{NH}_3}{\text{C}}}^+$	$\text{H}_3\text{C}-\overset{\text{H}_2}{\underset{\text{NH}_3}{\text{C}}}^+$
ACN	2.67	--	--	--
ECN1	2.59	1.85	3.65	8.01
ECN3	2.49	1.73	3.55	7.93
ECN5	2.39	1.60	3.43	7.84
ECN7	2.36	1.57	3.42	7.84
ECN9	2.29	1.53	3.38	7.80
EAN	--	1.48	3.34	7.76

Table 4.7: ^1H NMR chemical shifts for EAN+acetonitrile systems

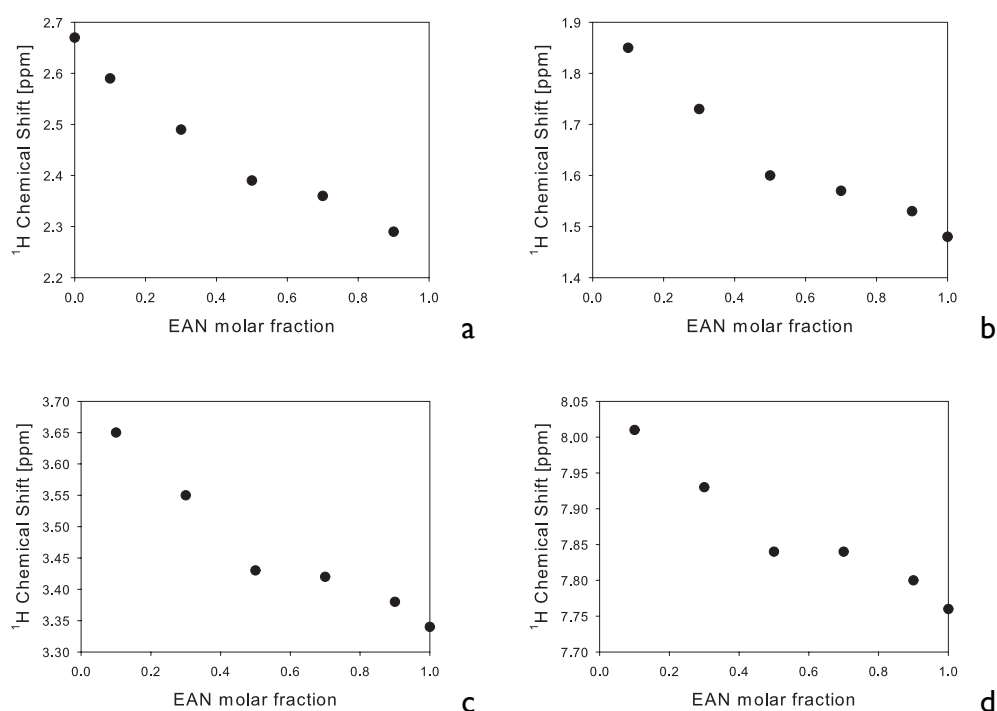


Figure 4.17: ^1H NMR chemical shifts for EAN+acetonitrile systems. (a) acetonitrile methyl group; (b) cation methyl group; (c) cation methylene group; (d) cation ammonium group

Upon EAN addition, all the signals appear to be shifted towards smaller values, indicating a progressive shielding of all the signals. It is interesting how two well defined and different trends are observed for all the shifts. In fact the mixtures at 0.5 and 0.7 EAN molar fractions always show similar chemical shifts, while steep, almost parallel slopes are found after 0.7 and before 0.5, indicating once more the transition between two well defined states, the nano-heterogeneous (EAN molar fraction ≤ 0.5) and the homogeneous (EAN molar fraction ≥ 0.7). The analysis of the DOSY spectra also supports this interpretation. The classical approach of fitting the integral value of a characteristic NMR signal using a three parameters exponential decay function

$$Y = A + B \cdot e^{-C \cdot x} \quad [4.3]$$

returns directly the diffusion constant of the examined molecule as the C parameter. Results for ECN systems are shown in table 4.8 and figure 4.18.

System	Diffusion Constant [10 ⁻¹¹ *m ² s ⁻¹]	
	Cation	Acetonitrile
ACN	--	432.57
ECN1	79.90	245.00
ECN3	28.20	125.00
ECN5	18.30	51.00
ECN7	16.20	32.00
ECN9	15.20	4.52
EAN	3.80	--

Table 4.8: Diffusion constant for EAN+acetonitrile systems

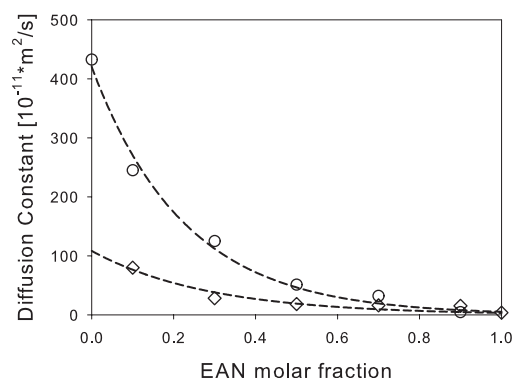


Figure 4.18: Diffusion constant for EAN+acetonitrile systems. Acetonitrile (circles); cation (diamonds)

On further analysis, applying the Bayesian method⁴¹ to the DOSY spectra, the picture appears more complicated than the simple fit could figure out.

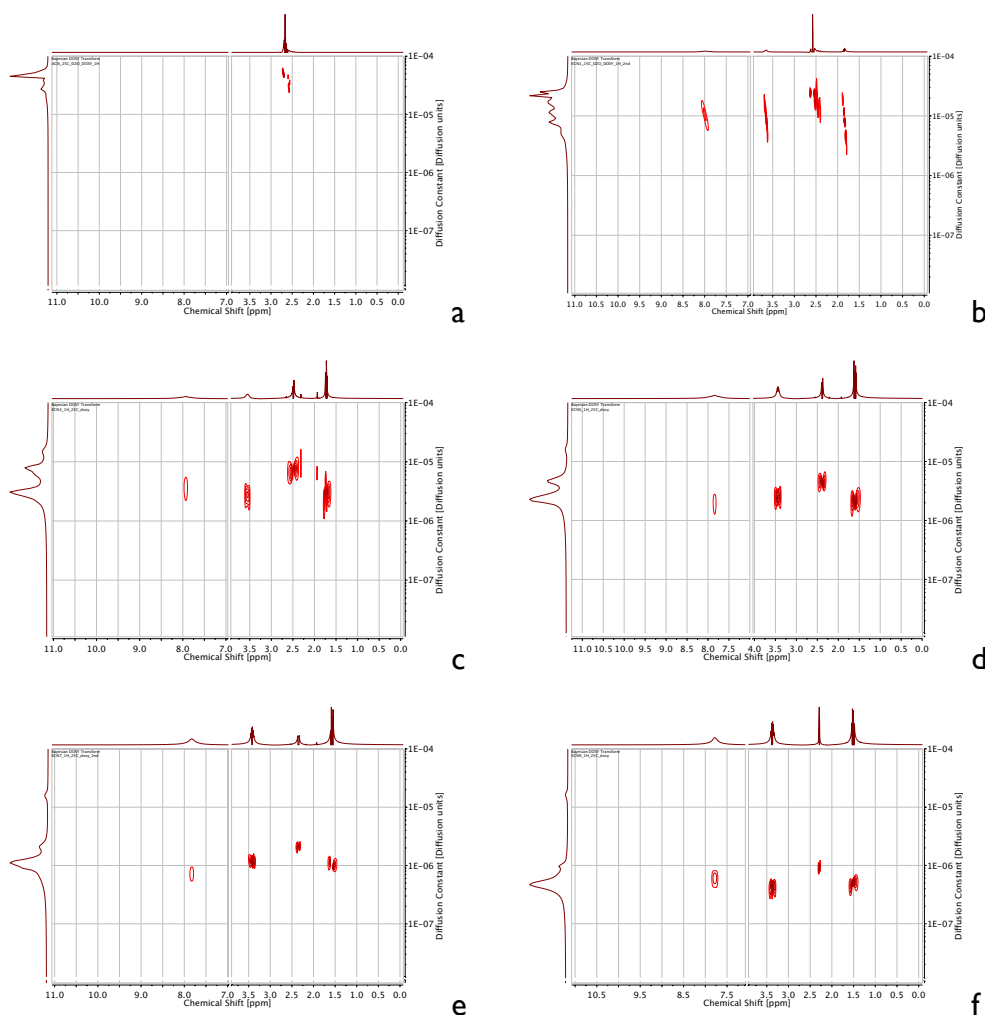
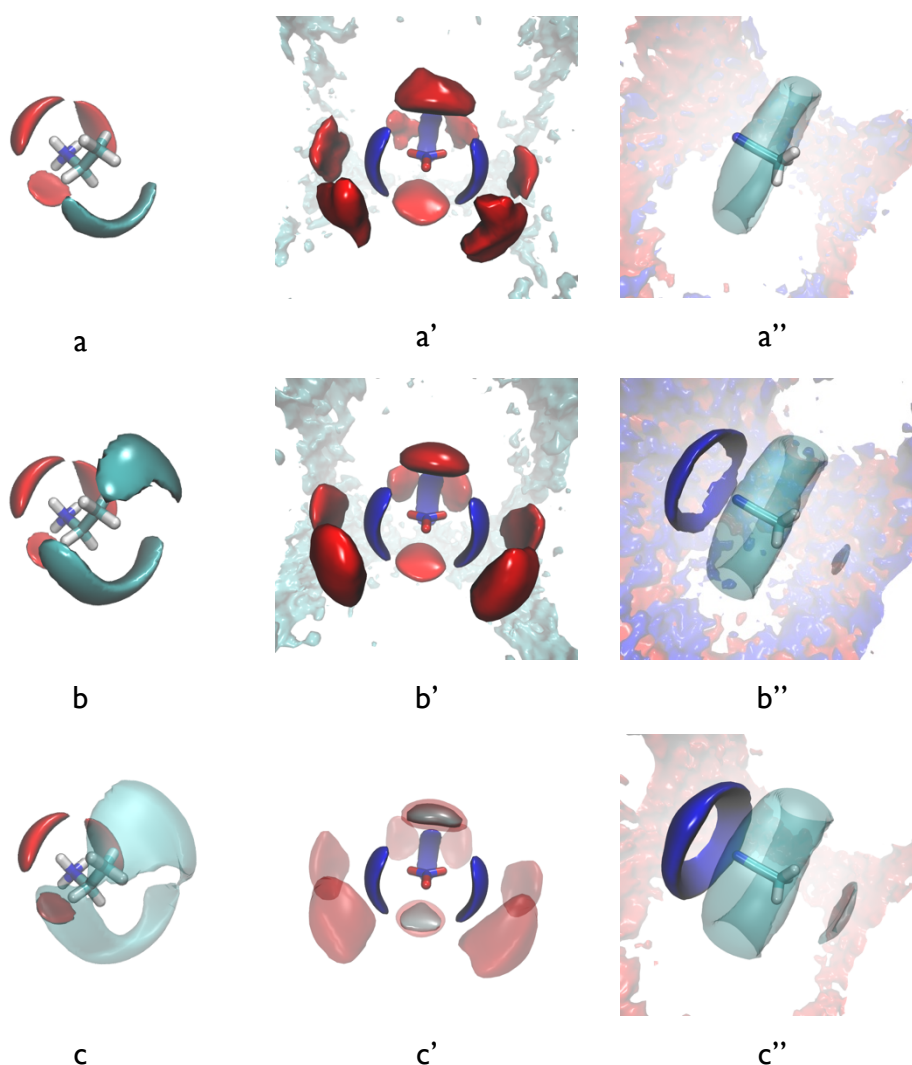


Figure 4.19: Bayesian plots of ¹H NMR DOSY for EAN+acetonitrile systems. (a) acetonitrile; (b) ECN1; (c) ECN3; (d) ECN5; (e) ECN7; (f) ECN9

While in the EAN-rich systems (*i.e.* ECN9, ECN7 and partially ECN5) the *spots* relative to the cation are small and defined, in ECN1 and ECN3 (and partially ECN5) they are very broad. This lends to a wide variety in the values of the diffusion constant, as appears clear from the shape of their distribution that does not appear like a Gaussian-like curve. This means that there are identical molecules (the cations) in the mixture, moving differently because their environment is very different and so experience various interactions. Once again this observation supports our interpretation of local unmixing in the EAN-poor regime. Finally, from the models I have extracted the spatial distribution functions.



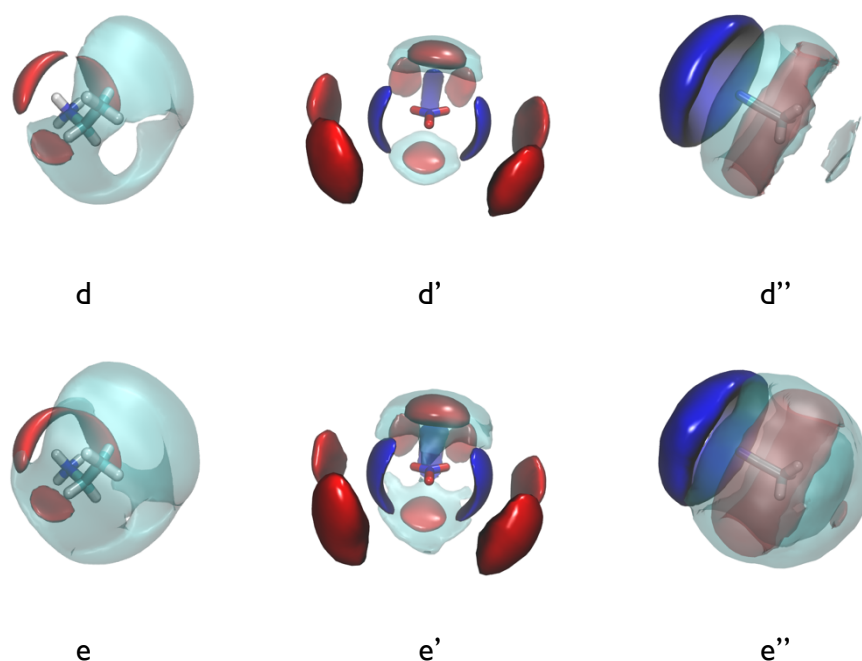


Figure 4.20: Spatial distribution functions for EAN+acetonitrile systems. All the isosurfaces refer to 2 times the bulk density of the observed atom. (a) ECN1; (b) ECN3; (c) ECN5; (d) ECN7; (e) ECN9. Plain letters refer to cation environment; single prime to anion environment; double prime to methanol environment. Nitrogen of the cation (blue); oxygen of the anion (red); nitrogen of the acetonitrile (cyan).

The cation surrounding evolves straightforward from ECN1 to ECN9. Acetonitrile does not compete with the nitrate to hydrogen-bond the ammonium head, but it prefers to interact with the central methylene and (less) with the terminal methyl group. The anion environment shows a clear evolving picture that complies finely with all other observations. ECN1 and ECN3 show clearly that there are absolutely no correlations between acetonitrile and nitrate and a neat transition is observed in ECN5 where acetonitrile starts coordinating the anion in the axial positions, competing with other anions. Also the acetonitrile surrounding relates nicely with the observations, in fact ECN1, ECN3 and ECN5 show that the nitrate does not correlate with the acetonitrile while the cation starts interacting with it in very poorly in ECN3 and meaningfully in ECN5. The structural heterogeneity in ECN1, ECN3 and partially in ECN5 seems to be strongly related with the LqE in the SAXS patterns.

III. Symmetric Compounds

Here the situation is much different, because the co-solvent is not *dual*, that is the molecular structure does not show defined hydrophilic and hydrophobic regions. This prevents the self-assembly of the co-solute, thus removing a variable in the complex understanding of the LqE.



Figure 4.21: Piazza del Popolo, Rome-ITALY

The first observation of such feature in mixtures containing symmetrical compounds, was taken by me during an experiment at the SAXS beamline at ESRF (Grenoble-France). There I have found³⁰ that this behaviour is much more common and general than one might think, and a wider definition and interpretation is needed.

III.1. EAN+ 1,2-dimethoxy ethane and EAN+ 1,4-diaminobutane

1,2-dimethoxyethane (DME), also known as dimethyl glycol or glyme, is a common solvent which is widely used in electrochemistry.

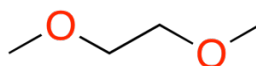


Figure 4.22: 1,2-dimethoxy ethane

Although DME is miscible with water in any proportion at room conditions⁴², we observed that while a $\chi_{\text{EAN}}=0.4$ mixture is macroscopically homogenous, the $\chi_{\text{EAN}}=0.3$ mixture is clearly separated into two liquid phases, so here we take into account mixtures with χ_{EAN} down to 0.4 and not lower. A similar behaviour is observed in EAN:n-Octanol mixtures where critical unmixing happens at high alcohol concentrations^{15,43,44}. This observation plays a central role in the model that I am going to propose for the explanation of the experimental evidences. In the following figure the SAXS patterns of the EAN+ 1,2-dimethoxyethane mixtures are reported.

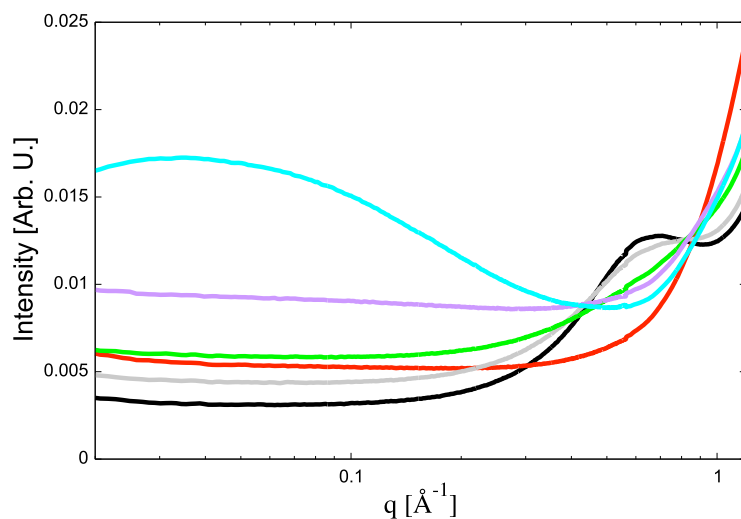


Figure 4.23: SAXS patterns for EAN+1,2-dimethoxy ethane systems. EAN (black); 1,2-dimethoxy ethane (red); EDME4 (cyan); EDME5 (purple); EDME7 (green); EDME9 (gray)

System	χ_{EAN}	Density [g/ml]	Excess Molar Volume [ml/mol]
DME	0	0.86824	0
EDME4	0.4	0.98456	0.8312
EDME5	0.5	1.02047	0.5623
EDME7	0.7	1.11859	-1.8484
EDME9	0.9	1.17938	-0.6380
EAN	1	1.2106	0

Table 4.9: EAN+1,2-dimethoxy ethane systems, composition, density and excess molar volume

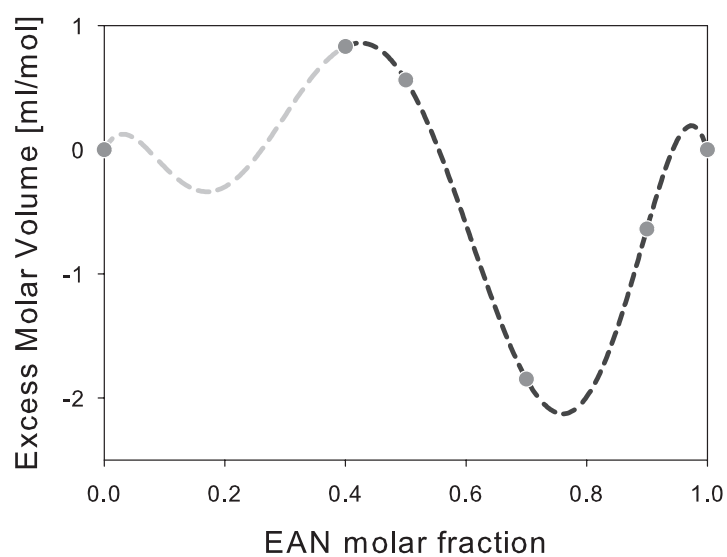


Figure 4.24: Excess molar volume for EAN+1,2-dimethoxy ethane systems at 25 °C

A broad, intense feature spanning from 0.4 Å⁻¹ down to the limit of detection is clearly observable for the EDME4 mixture. Also EDME5 shows an unusual high intensity in the same region, but it may be argued that there is no slope indicating the presence of something resembling a peak. 1,4-diaminobutane (DAB) is a bad-smelling low melting solid also known as *putrescine*⁴⁵. In nature is produced by the breakdown of the amino acids when an organism is dead. This compound, together with *cadaverine* (1,5-diaminopentane), is the main cause of the unpleasant odour of dead animals.

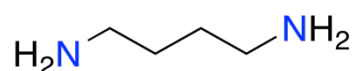
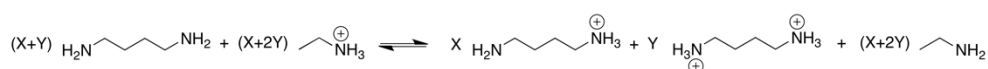


Figure 4.25: 1,4-diaminobutane

It is completely miscible in both water and EAN and shares also exactly the same pKa (10.8) with the ethylammonium cation. We have observed that EAN+DMA solutions turn bright yellow after few days after the preparation, indicating the speciation of the molecules in the system according to the equilibrium



Scheme 4.1: Equilibrium in EAN+1,4-diaminobutane systems

For this reason, the mixtures were prepared and measured within two minutes, to minimize the speciation. The collected data are reported below.

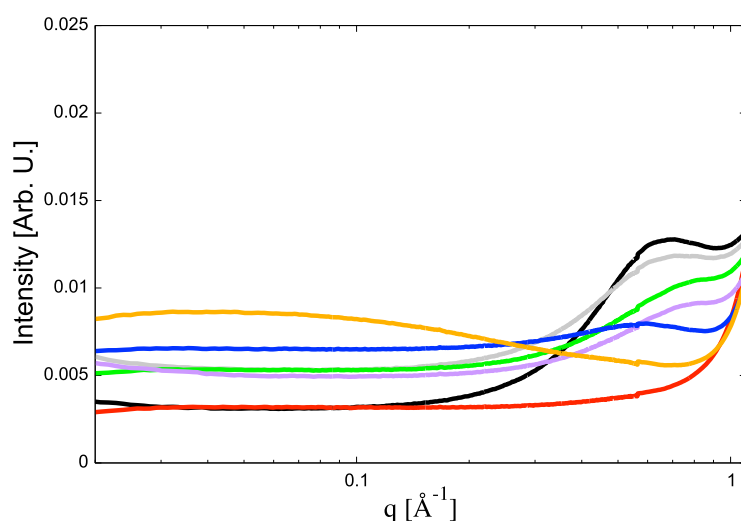
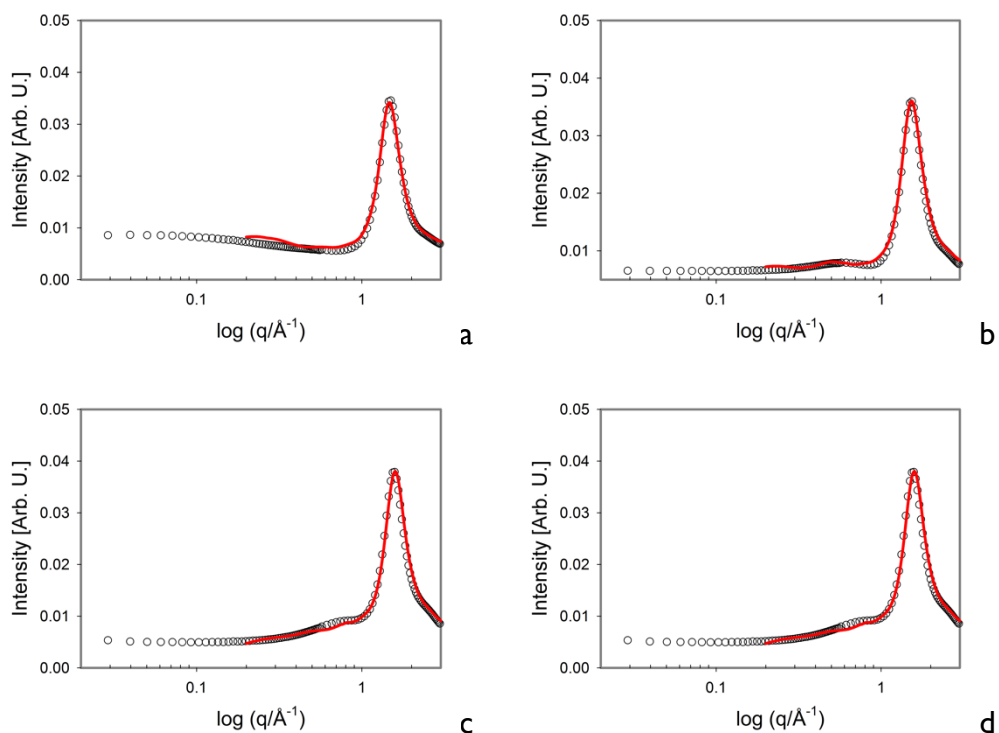


Figure 4.26: SAXS patterns for EAN+1,4-diaminobutane systems. EAN (black); 1,4-diaminobutane (red); EPI (orange); EP3 (blue); EP5 (purple); EP7 (green); EP9 (gray)

System	χ_{EAN}	Exp. Density [g/ml]	Calc. Density [g/ml]
DAB	0	0.87745 (30 °C)	0.8725
EPI	0.1	0.92465	0.9247
EP3	0.3	0.99922	0.9996
EP5	0.5	1.06510	1.0640
EP7	0.7	1.13531	1.1321
EP9	0.9	1.19684	1.1955
EAN	1	1.2106	1.2143

Table 4.10: Mass density comparison between experimental and computed data for EAN+1,4-diaminobutane systems

Although it is pretty small, an unusual slope is observable for the EPI system in the same q range of the one in EDME4. The agreement between experimental and computed SAXS patterns is almost quantitative in the q region accessible to the models.



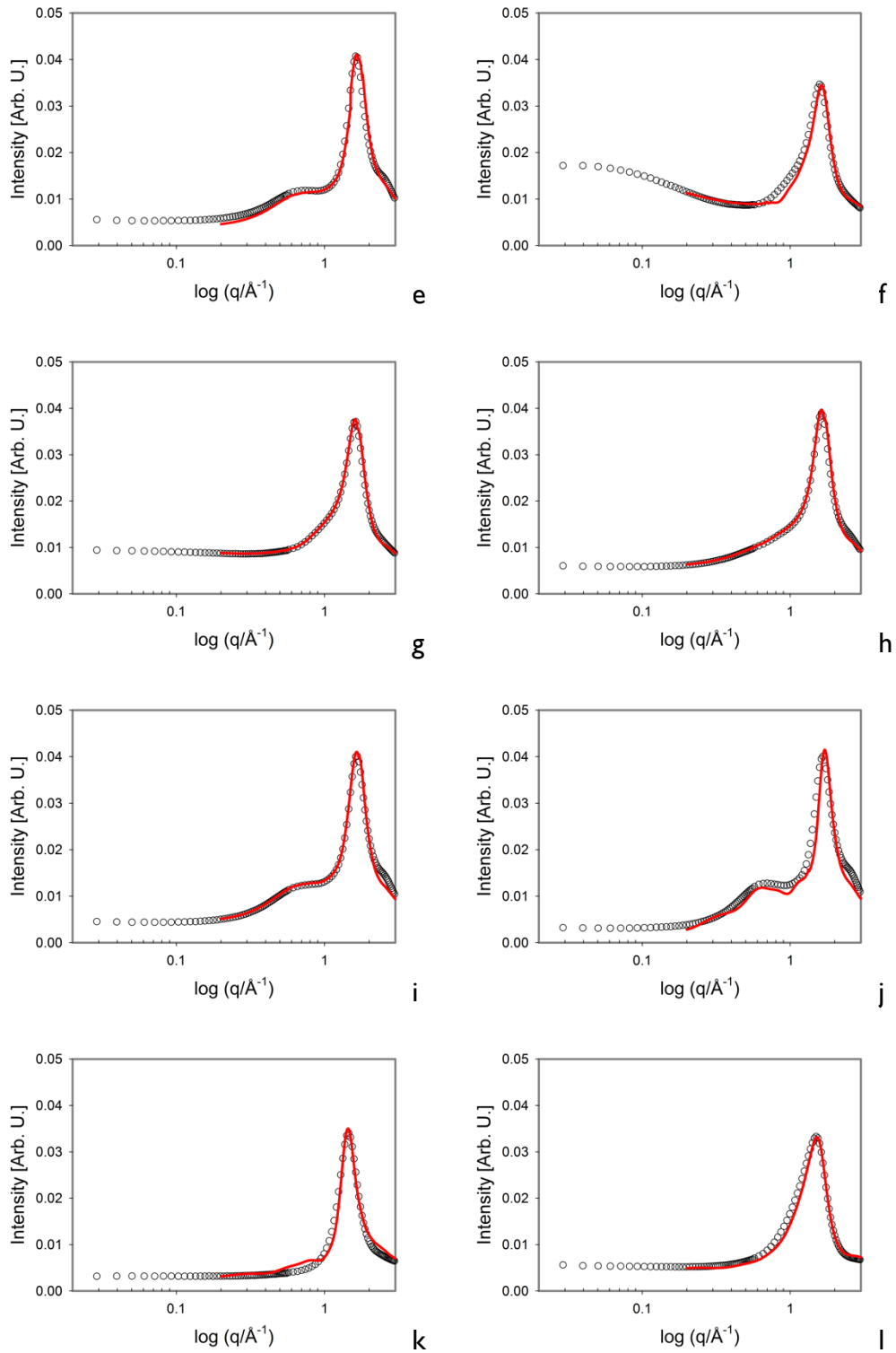


Figure 4.27: SWAXS patterns for EAN+1,2-dimethoxy ethane and EAN+1,4-diaminobutane systems. (a) EPI; (b) EP3; (c) EP5; (d) EP7; (e) EP9; (f) EDME4; (g) EDME5; (h) EDME7; (i) EDME9; (j) EAN; (k) 1,4-diaminobutane; (l) 1,2-dimethoxy ethane. Symbols refer to experimental data; solid lines to the models

Albeit the models cannot reach the same low q , the initial slope of the LqE is finely reproduced by the simulations when the latter is experimentally observed.

This suggests that the simulations are a reliable model to interpret the complex structure of these systems. A useful tool for the analysis of EDME and EP systems is the computation of the 2D density maps, *i.e.* a two dimensional graphic representation of the mass density within the system. In figure 4.28 the results obtained with the GROMACS⁴⁶ utility `g_densmap` are reported.

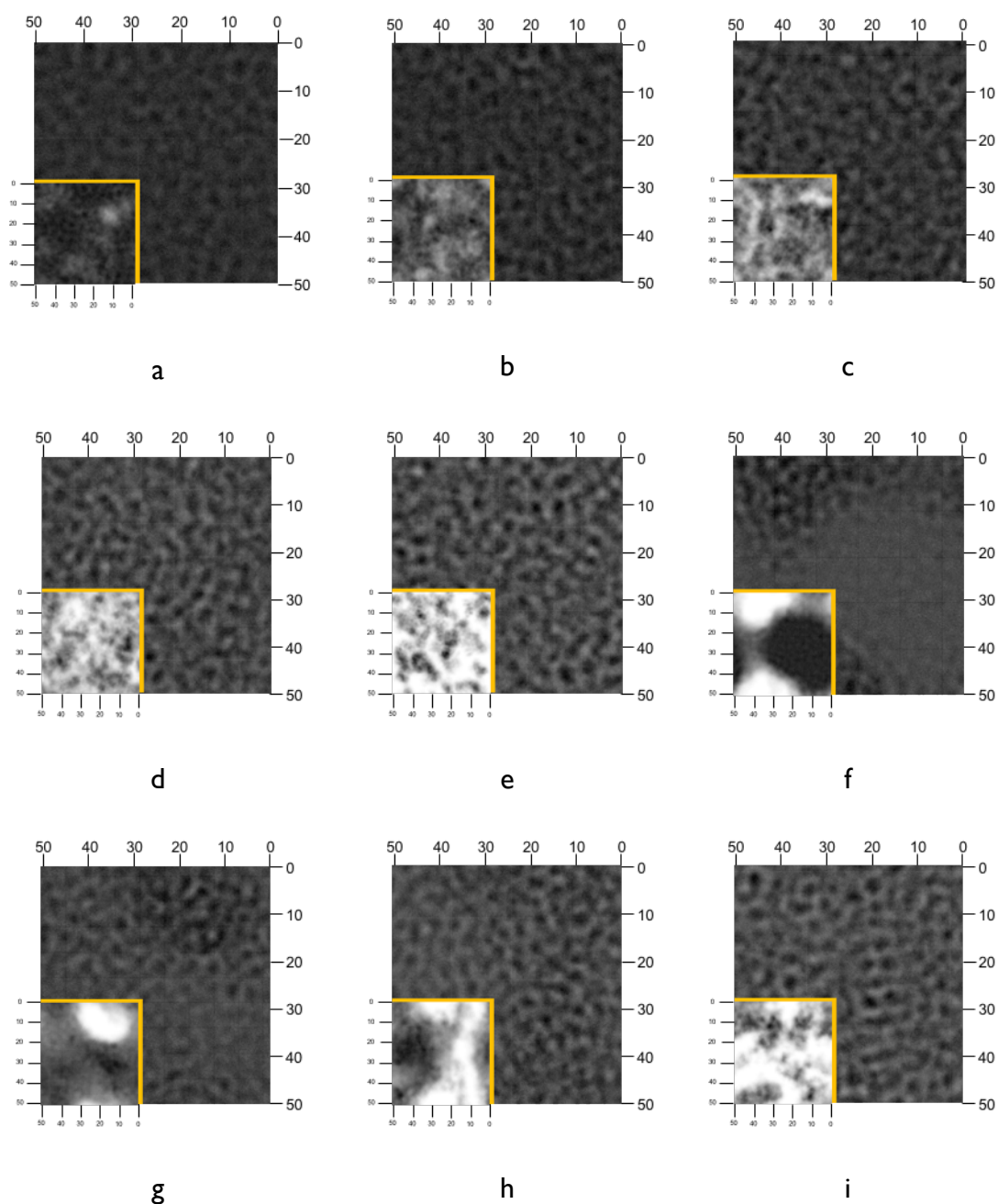


Figure 4.28: 2D density maps obtained from the molecular dynamics simulations of the mixtures in this work. For each system two maps are shown: total mass density, thus considering each molecule in the system; in the inset is shown the contribution of DAB/DME only. Darker parts mean higher densities. (a) EP1; (b) EP3; (c) EP5; (d) EP7; (e) EP9; (f) EDME4; (g) EDME5; (h) EDME7; (i) EDME9

It is quite evident from the total density maps how the sponge-like structure characteristic of some ionic liquids is practically intact for both the systems when EAN percentage is 90%. With DAB, the dilution of EAN leads to progressive vanishing of this organization (and, consequently, the LqP disappears)^{47,48}. Considering only the contribution of putrescine, it is notable how its progressive addition causes a little, but evident, fluctuation in the density maps. At 10% EAN some clear spots are easily individuated suggesting the beginning of the incipient unmixing process discussed above. With DME the scenario is more definite. At equimolar composition the embryonic unmixing is quite strong and exhibits a white spot in the DME-density map indicating ether absence in that region. The 40% EAN mixture shows an even enhanced solvophobic effect. All these observations are perfectly compliant with the experimental observations, indicating that the density fluctuations are responsible for the LqE in the SAXS patterns. I have searched for the origin of these density fluctuations in the thermodynamics of the systems. On the basis that the highest LqE is observed in EDME4 (*i.e.* the last homogenous mixture before phase separation), I have speculated that molecular affinity could play an important role. To check my hypothesis, I have extracted from the simulations two thermodynamic quantities strongly linked to molecular affinity, namely the enthalpy of vaporization (of the molecular compound) and the enthalpy of mixing. The first one is a measure of how *comfortable* a molecule is in the solution, and was calculated according to the formula⁴⁹

$$\Delta_{vap}H = -(E^{int} + \chi_{EAN} \cdot E^{EAN}) + RT \quad [4.4]$$

where E^{int} is the total internal energy per molecule of the system, χ_{EAN} is the EAN mole fraction, and E^{EAN} is the internal energy of the ideal gas EAN, obtained simulating a single ion pair at the same temperature as the other simulations in a box large enough in order to resemble the isolated state neglecting the intermolecular contributions. In our case the box has a side of 100 Å and the resulting E^{EAN} is -131.83 kJ mol⁻¹. The results are plotted in figure 4.29.

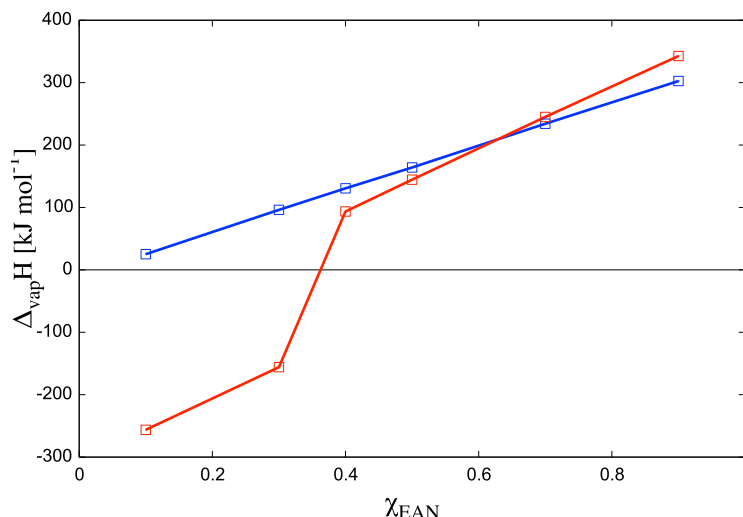


Figure 4.29: Enthalpy of vaporization of the molecular compound for EAN+1,2-dimethoxy ethane (red) and EAN+1,4-diaminobutane (blue). Lines are a guide to the eye, not a fit

It is evident how the vaporization of the neutral co-solvent becomes progressively easier when the same is added to the mixture, meaning that the molecular affinity decreases upon the addition of the molecular liquid. This is true for both DME and DAB, but the ether shows a marked step when the ionic liquid molar fraction goes from 0.4 to 0.3, showing a negative enthalpy of vaporization, that could suggest spontaneous vaporization of DME. Indeed, a critical unmixing is experimentally observed when DME is added to a solution of 0.4 EAN molar fraction. The second probe we used to check the molecular affinity is the enthalpy of mixing, obtained from the simulations through the following equation⁵⁰

$$\Delta_{\text{mix}} H = P \cdot V^{\text{Ex}} + E^{\text{int}} - \sum \chi_i \cdot E_i \quad [4.5]$$

where P is the pressure (1 bar), V^{Ex} is the excess volume and E_i is the internal energy of the pure liquids per molecule, obtained performing a simulation for each compound at the same temperature. As seen in figure 4.30

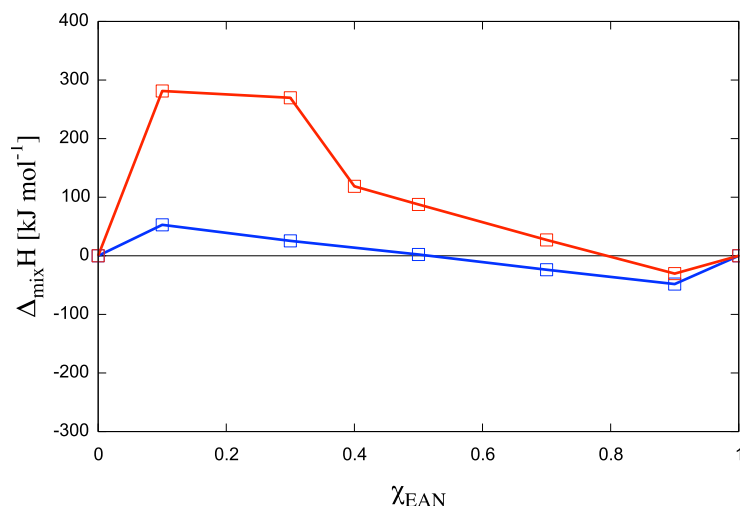


Figure 4.30: Enthalpy of mixing for EAN+1,2-dimethoxy ethane (red) and EAN+1,4-diaminobutane (blue). Lines are a guide to the eye, not a fit

the reverse of vaporization enthalpy is seen for $\Delta_{\text{mix}} H$ which increases with molecular liquid concentration indicating, once more, that the molecular affinity is weakened when EAN is the minority component. A marked step in DME curve below $\chi_{\text{EAN}}=0.4$ composition ratio demonstrates once more the tendency of the system to go towards the unmixed state. To have a quantitative picture of the thermodynamics underlying our observation, one should use Gibbs free energy instead of simply enthalpy considerations, but the computation of the entropic effects is not trivial from molecular dynamics simulations and it is often affected by considerable errors. Experimentally we know that DAB is miscible with EAN in all proportions, therefore the mixing enthalpy for the mixture at 0.1 EAN molar fraction (46.84 kJ mol⁻¹), must be “paid for” by entropic effects. For larger values, as for the high-DME-containing mixtures (~300 kJ mol⁻¹), entropy cannot play a decisive role.

IV. Contextualization

I have shown how some EAN-molecular compound binary mixtures exhibit a broad feature in the extreme low-q region of the SAXS pattern, thus suggesting the presence of nanoscale objects in the system. This kind of behaviour is generally found in soft matter systems consisting in aqueous solutions of macromolecules (proteins, DNA, polymers) or disperse nanoparticle. It is also

possible to find it in some mixture of water with some surfactants, in that case the objects responsible for the feature are some self-assembled structures, such as micelles, worms, rods, tubes or vesicles. To date, only five papers^{11,14,26,27,30} deal with this observation in systems containing ionic liquids, trying to give an explanation on this phenomenon. My contribution in this manuscript (and in ref 43) is to clarify that this behaviour is much more common than thought before, in fact I have observed the existence of the LqE for a variety of different systems. In table 4.1 I the system analysed and the main characteristics at the basis of its choice are shown.

System	Reason
EAN+methanol	The first system in which LqE was observed.
EAN+acetonitrile	Acetonitrile is structurally similar to methanol, but it is unable to donate hydrogen bonds, so it is the perfect candidate to assess if hydrogen bonds have a role in the LqE.
EAN+1,2-dimethoxyethane	DME is part of the “glycol series” in Chapter III, finding the LqE in this system was unexpected because of its symmetry. This is a case of serendipity.
EAN+1,4-diamonobutane	After discover the LqE in EDME systems, I have chosen DAB because it has similar size as DME, same symmetry but both the terminations are polar, unlike DME.

Table 4.1 I: Systems discussed in this Chapter

My findings shed a light on what generates the LqE in this kind of systems. By now there are three theories that try to explain the phenomenon underlying the LqE:

- Clusters of IL molecules. These clusters would form because of the solvophobic effect induced by the amphiphilicity of the solvent, i.e. EAN prefers to expose as little area as it can to methanol and on the surface of those clusters the favourable hydrogen bonding interaction take place. This was the original explanation made from Triolo and me on the EAN-methanol system in 2014¹¹.

- Self-assembled structures. Atkin *et al.* suggested²⁶ that the IL could act as a co-surfactant in mixtures of IL-alcohols, specifying that LqE appears only when the alcohol tail is shorter than two times the tail of the IL.
- Density fluctuations. Triolo suggested²⁷ that strong density fluctuations in the system EAN+n-Pentanol could give rise to the LqE, being the seed of an incipient demixing of the system.

While all the three theories suggested until now can easily explain the observation of LqE in systems containing ionic liquids and amphiphilic liquids (albeit the hypothesis of Atkin could not explain EAN-methanol nor EAN-acetonitrile), the first two fail for EDME and EP systems, because 1,2-dimethoxyethane and 1,4-diaminobutane are symmetric (so they cannot self-assemble nor act as co-surfactants), and one has polar terminations and the other apolar (thus excluding solvophobic effects). Nevertheless, the third hypothesis is able to explain all the observation. My contribution intends to clarify why these density fluctuations take place. All the data that I have collected, both experimental and theoretical, strongly support the incipient demixing interpretation. All the systems show the LqE in the EAN-poor regime, suggesting that is the ionic liquid that *wants* to segregate. The spatial distribution functions for the EM system show a clear transition from EM3 to EM4. Same thing for the ECN systems, where the transition happens more gradually at ECN3 and ECN5, exactly the threshold where the LqE disappears. The anion environment seems to have a central role here, as for the LqP. While structural considerations are of great importance, the main role is played by thermodynamics. The molecular affinity, in terms of enthalpy of mixing and enthalpy of vaporization (of the molecular compound), shows a clear correlation with the LqE. A mixture that is approaching the unmixing (*i.e.* its enthalpy of mixing is much higher than zero) undergoes large scale density fluctuations that generate the odd feature observed in SAXS. Obviously it is possible that for some systems the LqE is originated by self-assembly, but for other systems it cannot be.

V. Summary

In this chapter I have presented my findings on the Low q Excess. Summarizing:

- The LqE may be found in much more systems than one may expect.
- Amphiphilicity of the co-solvent is not strictly required.
- Systems that shows the LqE are highly heterogeneous.
- The molecular affinity plays the main role for this phenomenon.

VI. References

- 1 P. M. Mancini, G. G. Fortunato and L. R. Vottero, *Phys. Chem. Liq.*, 2004, **42**, 625–632.
- 2 M. Deetlefs, C. Hardacre, M. Nieuwenhuyzen, O. Sheppard and A. K. Soper, *J. Phys. Chem. B*, 2005, **109**, 1593–8.
- 3 A. Jarosik, S. R. Krajewski, A. Lewandowski and P. Radzimski, *J. Mol. Liq.*, 2006, **123**, 43–50.
- 4 A. A. H. Pádua, M. F. Costa Gomes and J. N. A. Canongia Lopes, *Acc. Chem. Res.*, 2007, **40**, 1087–96.
- 5 S. Thomaier and W. Kunz, *J. Mol. Liq.*, 2007, **130**, 104–107.
- 6 B. Fazio, A. Triolo and G. Di Marco, *J. Raman Spectrosc.*, 2008, **39**, 233–237.
- 7 Y. Kohno and H. Ohno, *Chem. Commun. (Camb.)*, 2012, **48**, 7119–30.
- 8 R. Hayes, S. Imberti, G. G. Warr and R. Atkin, *Angew. Chem. Int. Ed. Engl.*, 2012, **51**, 7468–71.
- 9 M. Piana, J. Wandt, S. Meini, I. Buchberger, N. Tsiouvaras and H. a. Gasteiger, *J. Electrochem. Soc.*, 2014, **161**, 1992–2001.
- 10 S. Omar, J. Lemus, E. Ruiz, V. R. Ferro, J. Ortega and J. Palomar, *J. Phys. Chem. B*, 2014, **118**, 2442–50.
- 11 O. Russina, A. Sferrazza, R. Caminiti and A. Triolo, *J. Phys. Chem. Lett.*, 2014, **5**, 1738–1742.

- 12 P. Walden, *Bull. Acad. Imper. Sci St. Petersburg.*, 1914, **8**, 405–422.
- 13 R. Hayes, S. Imberti, G. G. Warr and R. Atkin, *Phys. Chem. Chem. Phys.*, 2011, **13**, 3237–47.
- 14 O. Russina, A. Mariani, R. Caminiti and A. Triolo, *J. Solution Chem.*, 2015, **44**, 699–685.
- 15 A. Oleinikova and M. Bonetti, *J. Chem. Phys.*, 1996, **104**, 3111.
- 16 I. Boumalham, P. Letellier, A. Mayaffre and M. Turmine, *J. Chem. Thermodyn.*, 2007, **39**, 1132–1143.
- 17 R. Kanzaki, K. Uchida, X. Song, Y. Umebayashi and S. Ishiguro, *Anal. Sci.*, 2008, **24**, 1347–9.
- 18 M. U. Araos and G. G. Warr, *Langmuir*, 2008, **24**, 9354–9360.
- 19 R. Zarrougui and M. Dhahbi, *J. Solution Chem.*, 2010, **39**, 1531–1548.
- 20 T. L. Greaves, D. F. Kennedy, N. Kirby and C. J. Drummond, *Phys. Chem. Chem. Phys.*, 2011, **13**, 13501–9.
- 21 C. R. López-Barrón, D. Li, L. Derita, M. G. Basavaraj and N. J. Wagner, *J. Am. Chem. Soc.*, 2012, **134**, 20728–20732.
- 22 J. A. Smith, G. B. Webber, G. G. Warr and R. Atkin, *J. Phys. Chem. B*, 2013, **117**, 13930–13935.
- 23 B. Docampo-Álvarez, V. Gómez-González, T. Méndez-Morales, J. Carrete, J. R. Rodríguez, Ó. Cabeza, L. J. Gallego and L. M. Varela, *J. Chem. Phys.*, 2014, **140**, 214502.
- 24 O. Russina, M. Macchiagodena, B. Kirchner, A. Mariani, B. Aoun, M. Russina, R. Caminiti and A. Triolo, *J. Non. Cryst. Solids*, 2015, **407**, 333–338.
- 25 R. Zarrougui, M. Dhahbi and D. Lemordant, *J. Solution Chem.*, 2015, **44**, 686–702.
- 26 H. J. Jiang, P. A. FitzGerald, A. Dolan, R. Atkin and G. G. Warr, *J. Phys. Chem. B*, 2014, **118**, 9983–90.

- 27 A. Triolo, W. H. Schroer and O. Russina, *J. Phys. Chem. B*, 2016, **9**, 2638–2643.
- 28 T. L. Greaves and C. J. Drummond, *Chem. Soc. Rev.*, 2013, **42**, 1096–120.
- 29 A. Mariani, O. Russina, R. Caminiti and A. Triolo, *J. Mol. Liq.*, 2015, **212**, 947–956.
- 30 A. Mariani, R. Dattani, R. Caminiti and L. Gontrani, *J. Phys. Chem. B*, 2016.
10.1021/acs.jpcb.6b07295
- 31 R. Böhmer, C. Gainaru and R. Richert, *Phys. Rep.*, 2014, **545**, 125–195.
- 32 L. Dougan, J. Crain, J. L. Finney and A. K. Soper, *Phys. Chem. Chem. Phys.*, 2010,
12, 10221–9.
- 33 I. E. Franco, P. Lorchat, J.-P. Lamps, M. Schmutz, A. Schröder, J.-M. Catala, J. Combet and F. Schosseler, *Langmuir*, 2012, **28**, 4815–28.
- 34 A. Heintz, D. Klasen and J. K. Lehmann, *J. Solution Chem.*, 2002, **31**, 467–476.
- 35 A. Chagnes, A. Tougui, B. Carr and N. Ranganathan, *J. Solution Chem.*, 2004, **33**,
247–255.
- 36 B. Mokhtarani, A. Sharifi, H. R. Mortaheb, M. Mirzaei, M. Mafi and F. Sadeghian, *J. Chem. Thermodyn.*, 2009, **41**, 1432–1438.
- 37 D. Das, A. Messaâdi, Z. Barhoumi and N. Ouerfelli, *J. Solution Chem.*, 2012, **41**,
1555–1574.
- 38 A. R. Mahajan and S. R. Mirgane, *J. Thermodyn.*, 2013, **1**.
- 39 O. Redlich and A. T. Kister, *Ind. Eng. Chem.*, 1948, **40**, 345–348.
- 40 C. S. Johnson Jr., *Prog. Nucl. Magn. Reson. Spectrosc.*, 1999, **34**, 203–256.
- 41 G. L. Bretthorst, *J. Magn. Reson.*, 1990, **88**, 533–551.
- 42 S. Hezaveh, S. Samanta, G. Milano and D. Roccatano, *J. Chem. Phys.*, 2011, **135**.
- 43 T. Heimburg, S. Z. Mirzaev and U. Kaatz, *Phys. Rev. E*, 2000, **62**, 4963–4967.
- 44 A. Oleinikova and M. Bonetti, *J. Solution Chem.*, 2002, **31**, 397–413.
- 45 K. Bryson and R. J. Greenall, *Faraday Transit.*, 1996, **92**, 913–919.

- 46 S. Pronk, S. Páll, R. Schulz, P. Larsson, P. Bjelkmar, R. Apostolov, M. R. Shirts, J. C. Smith, P. M. Kasson, D. Van Der Spoel, B. Hess and E. Lindahl, *Bioinformatics*, 2013, **29**, 845–854.
- 47 K. Shimizu, C. E. S. Bernardes, A. Triolo and J. N. Canongia Lopes, *Phys. Chem. Chem. Phys.*, 2013, **15**, 16256–62.
- 48 A. Mariani, R. Caminiti, M. Campetella and L. Gontrani, *Phys. Chem. Chem. Phys.*, 2016, **18**, 2297–2302.
- 49 X. Wu, Z. Liu, S. Huang and W. Wang, *Phys. Chem. Chem. Phys.*, 2005, **7**, 2771–9.
- 50 J. Dai, X. Li, L. Zhao and H. Sun, *Fluid Phase Equilib.*, 2010, **289**, 156–165.

Chapter V: Conclusions



"All right," said Susan. "I'm not stupid. You're saying humans need... fantasies to make life bearable."

REALLY? AS IF IT WAS SOME KIND OF PINK PILL? NO. HUMANS NEED FANTASY TO BE HUMAN. TO BE THE PLACE WHERE THE FALLING ANGEL MEETS THE RISING APE.

"Tooth fairies? Hogfathers? Little—"

YES. AS PRACTICE. YOU HAVE TO START OUT LEARNING TO BELIEVE THE LITTLE LIES.

"So we can believe the big ones?"

YES. JUSTICE. MERCY. DUTY. THAT SORT OF THING.

"They're not the same at all!"

YOU THINK SO? THEN TAKE THE UNIVERSE AND GRIND IT DOWN TO THE FINEST POWDER AND SIEVE IT THROUGH THE FINEST SIEVE AND THEN SHOW ME ONE ATOM OF JUSTICE, ONE MOLECULE OF MERCY. AND YET—

Death waved a hand.

AND YET YOU ACT AS IF THERE IS SOME IDEAL ORDER IN THE WORLD, AS IF THERE IS SOME... SOME RIGHTNESS IN THE UNIVERSE BY WHICH IT MAY BE JUDGED.

"Yes, but people have got to believe that, or what's the point—"

MY POINT EXACTLY."

(Death and Susan – "The Hogfathers" – Sir Terry Pratchett)

I. Final Considerations

During my PhD I have extensively studied how a series of molecular compounds, chosen for their physical and chemical properties, interacts with ethylammonium nitrate. I have taken EAN as a prototype for the class of protic ionic liquids. My studies were focused mainly on the structure that the molecules exhibit as a function of the ionic liquid concentration. To achieve the most complete picture possible, I have used a series of complementary techniques, such as Wide Angle X-ray Scattering, Small Angle X-ray Scattering, NMR spectroscopy, densimetry and viscosimetry. All the experimental data were interpreted with the help of models obtained by classical Molecular Dynamics simulations, carried out using AMBER (versions 11 to 14) with the GAFF force field (details on the computational method can be found in Chapter I). To start, I have explored the structural and dynamical properties of the three simplest monoalkylammonium nitrates ionic liquids, EAN, PAN and BAN. I have basically confirmed the literature results stating that despite their short alkyl tail, they show a mesoscopic

defined organization consisting of nano-segregation of polar/apolar domains, thus assuming the characteristic *sponge-like* structure. The grade of ordering goes as $\text{EAN} < \text{PAN} < \text{BAN}$, simply because a longer chain has more segregation effectiveness. While the density decreases going from EAN to BAN, viscosity becomes larger due to the larger contact surface.

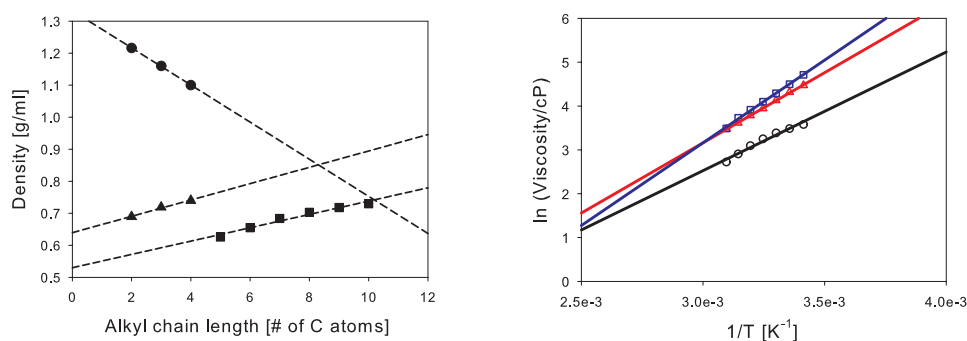


Figure 5.1: (left) Density trend as a function of alkyl tail length for monoalkylammonium nitrate ionic liquids (circles); monoalkylamines (triangles); n-alkanes (squares). Lines refer to linear fit. (right) Arrhenius plot for the viscosities of EAN (black), PAN (red) and BAN (blue). Symbols refer to experimental data, solid lines to the fit

In figure 5.1 are reported also the density values for some liquid n-Alkanes and the parent amines of the analysed PILs. It is interesting to note that unlike ILs, the densities of both amines and n-alkanes increase linearly with the alkyl tail. The discrepancy of the trends may be simply explained considering that the weight of the nitrate anion becomes less and less important as methylene groups are added to the chain; for EAN the nitrate accounts for the 57% of the mass, for PAN is 51% and 46% for BAN, so the difference between PILs and amines becomes smaller and smaller and the density approaches the value of the amines. On the other hand, lengthening the chain of amines and alkanes increases both the molecular weight and the packing efficiency, resulting in higher and higher densities. By contrast the viscosity trend follows the alkyl tail length, because of the enhanced surface contact of the molecules. In this manuscript I have presented a quantity useful to estimate the strength of the hydrogen bonds taking into account the viscosity of the liquid. This quantity, named C_{HB} is simply the ratio between the hydrogen bond free energy, calculated by the Eyring equation on the basis of the lifetime of the interaction between donor and acceptor, and the activation energy of the viscous flow calculated by the Arrhenius law. C_{HB} appears to be consistent if applied to EAN, PAN and BAN. Being the considered

interaction always between the ammonium head and the nitrate anion, one would expect a similar strength for the interaction, as it is found, indeed. The alkyl tail length also strongly influences the pressure response of these compounds. When the pressure is raised to 1 GPa, the cations assume a shrunk, coiled conformation that is more pronounced the longer is the chain, confirming and expanding the theory made so far. Figure 5.2 below shows the schematic arrangement of the molecules within EAN, as a prototype of all the three PILs under consideration.

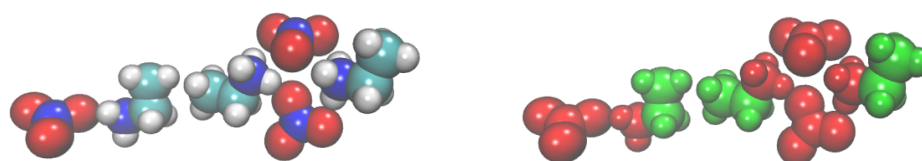


Figure 5.2: Minimal model of the nanosegregation in EAN. Right side highlights the polar (red) and apolar (green) domains

Once understood the properties of the neat PILs, I have proceeded to study the binary mixtures with some molecular compounds. In Chapter III I have discussed four systems, namely EAN+DMSO/ethylene glycol/2-methoxy-1-ethanol/2-amino-1-ethanol, while Chapter IV deals with some unusual behaviour of EAN+methanol/acetonitrile/1,4-diaminobutane/1,2-dimethoxyethane. The ED system was found to show a behaviour similar to the DMSO+water system. Albeit I have not measured the experimental melting point of the mixtures, I have stored them at -20 °C for two days without observing solidification. It should be noted that EAN has a melting point of 13 °C and DMSO of 19 °C. This is due to the strong association of the co-solvent with the cation, mediated by the high dipole of the S-O bond. Our findings suggest the formation of a stoichiometric stable complex, structured like in figure 5.3.a. This is analogous to the DMSO+water system, as shown in figure 5.3.b.

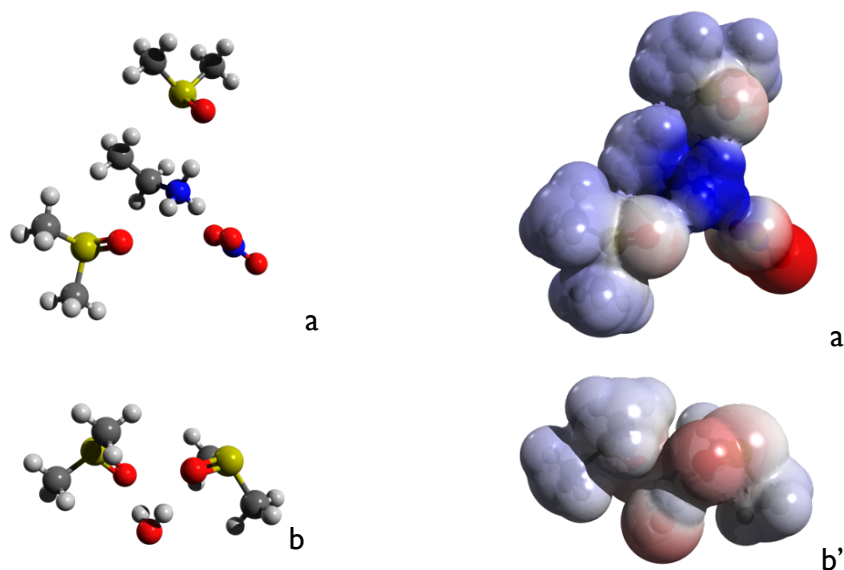


Figure 5.3: (a) EAN+DMDO 1:2 complex; (b) water+DMSO 1:2 complex. Plain letters refer to simple models, primes to electrostatic potential surfaces.

The EAN+ethylene glycol mixtures show a high degree of ideality. They have null enthalpy of mixing and the smaller excess molar volume of all the studied systems. While the ED system is standing alone, a homologous series consisting of 1,2-ethanediol, 2-methoxy-1-ethanol and 1,2-dimethoxyethane was used to check the importance of the hydrogen bond in PILs+molecular liquids mixtures.

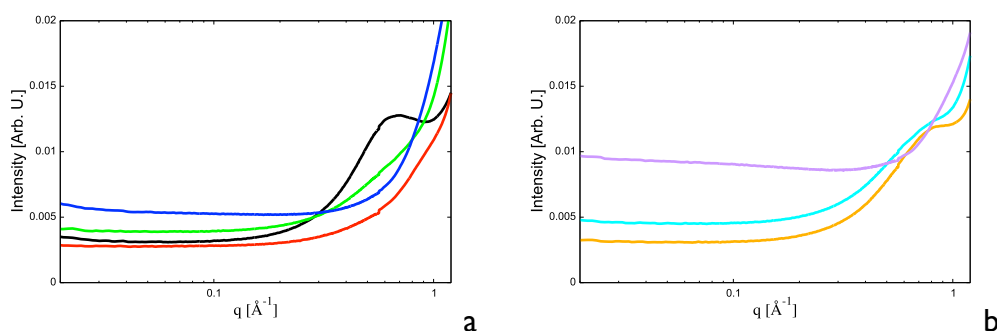


Figure 5.4: SAXS patterns for EAN+"glycol series". (a) neat compounds, EAN (black); ethylene glycol (green); 2-methoxy-1-ethanol (blue); 1,2-dimethoxy ethane (red). (b) 1:1 mixtures, EG5 (orange); EMEOS (cyan); EDMES (purple)

Looking at the extreme low q region of figure 5.4 it is evident how the hydrogen bond seems to have an important role in the LqE. While with the ethylene glycol the curve relative to the system is flat and falls between the curves of the two neat compounds, with methyl-glycol is also flat but its intensity is slightly higher

than the most intense of its components (*i.e.* MEO). This effect is way more pronounced with 1,2-dimethoxyethane, thus suggesting that the solvent properties of EAN are strongly linked to its hydrogen bond network and how it interacts with the host co-solvent. But the hydrogen bond interaction cannot be the only reason behind the LqE because also systems containing methanol, acetonitrile and 1,4-diamonobutane exhibit this feature. Basing on my findings the main property responsible of the LqE is the molecular affinity.

Acknowledgements



Thank you for coming to see me. Don't hesitate to leave.
(“Guards! Guards!” – Sir Terry Pratchett)

Ten years. It has been ten years since my first step in the Chemistry Department at La Sapienza University of Rome. In this period, I have met a lot of people: teachers, researcher, students and other employees. All of them, with no exceptions, have contributed to my growing as a man and, as a side effect, as a scientist. For this reason, I want to thank:

Prof. Ruggero Caminiti, my supervisor, head of the EDXD group at La Sapienza. Thank you for welcoming me into the group, for teaching me new things every day and for the emails at 3.00 a.m..

Dr. Lorenzo Gontrani. Thank you for everything. There are simply no words capable to express my gratitude for you. I won't be here without your effort.

Dr. Luigi Bencivenni. Thank you for the wise counsel. Thank you for introducing me in the Physical Chemistry world.

Prof. Claudia Sadun. Thank you for the explanations, and for the blueberries.

Prof. Enrico Bodo. Thank you for the insightful discussions.

Prof. Dimitrios Fessas, Prof. Alberto Schiraldi and Dr. Marco Signorelli from the DeFENS department of University of Milan. Thank you for the kind hospitality.

Prof. Edward W. Castner Jr., and all his group at CCB department at Rutgers University. Thank you for welcoming me, for the great science done with you and for all the effort in helping me in the last few months of my PhD fellowship.

The research groups of Prof. Paolo Postorino, Prof. Stefano Lupi, Dr. Alessandro Nucara, Prof. Giancarlo Masci, Dr. Francesca Leonelli. Thank you all for the collaboration. My work would be pointless without your contributions.

The ESRF and the RAL. Thank you for granting me beamtime.

My parents Lucia and Giacomo. Thank you for supporting me, no matter what.

My sister Samanta. Thank you for being someone to be proud of.

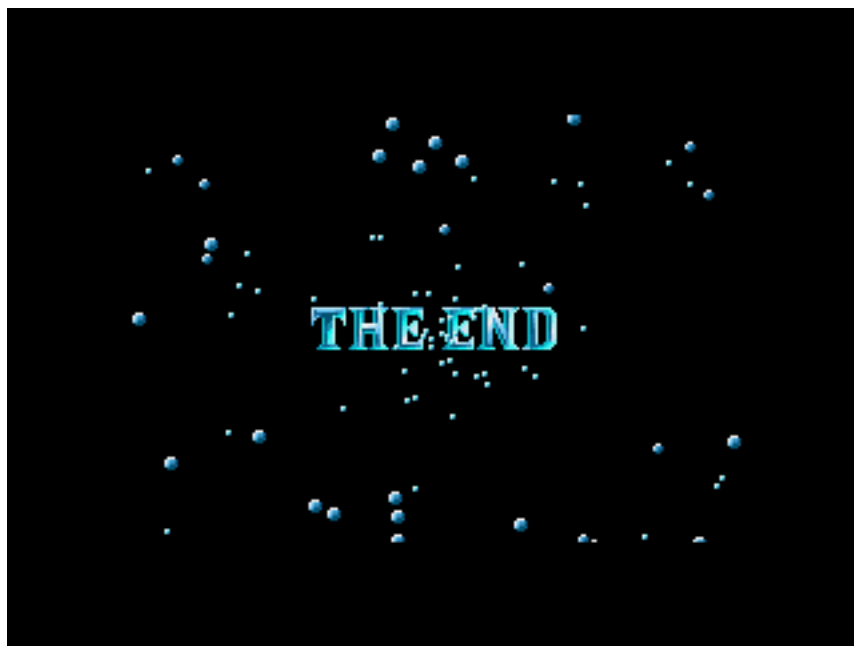
My brother Giangiacomo. Thank you for my childhood.

Chiara. For being the one that I was looking for, for being the person that I need.

Gioggio, Gatto, La Bionda, Scotch, K', il Vecchio, Dalmah, N'd'gio, Valentina, Federica, Eleonora e Arianna. Thank you for making every day a special one.

Prof. Virgilio Ciampani and Prof. Alessandra D'Orazio. Thank you for three of the best years in my life.

... and all the Final Fantasy fans



Appendix A: Materials

*“... one book could be a library, if it was a book that made a big enough dimple in L-space.
A book with a title like ‘100 ways with Broccoli’
was unlikely to be one such, whereas
‘The Relationship Between Capital and Labour’
might be, especially if it had an appendix on making explosives”
(Sir Terry Pratchett)*

I. Consumables

Ethylammonium Nitrate and Propylammonium Nitrate were purchased at IoLiTec at the highest available purity ($\geq 98\%$). They were pumped under high vacuum at slight warming ($50\text{ }^{\circ}\text{C}$) overnight to remove residual water. The final moisture was checked using ^1H NMR and water was undetectable. Butylammonium Nitrate was prepared titrating 1-butylamine (Sigma Aldrich, $\geq 99\%$) with nitric acid (Sigma Aldrich, $\geq 90\%$). Once prepared, BAN was dehydrated in a rotary evaporator and then treated as EAN and PAN to remove residual water. DMSO (Sigma Aldrich, 99.9%) was treated with molecular sieves ($4\text{ }\text{\AA}$) to remove residual water. All other chemicals were purchased at Sigma Aldrich at the highest available purity and used as are (ethylene glycol 99.8%; 2-amino-1-ethanol 99.5%; 2-methoxy-1-ethanol 99.5%; methanol 99.9%; acetonitrile 99.8%; 1,2-dimethoxyethane 99.9%; 1,4-diaminobutane 99%).